University of Alberta

Inhibiting submicron and nanoscale copper powder agglomeration with the addition of propylamine, butylamine, benzenethiol and polyacrylic acid

by

Martina Elena Rusnacik

A thesis submitted to the Faculty of Graduate Studies and Research in partial fulfillment of the

requirements for the degree of *Master of Science*

in

Chemical Engineering

Department of *Chemical and Materials Engineering*

Edmonton, Alberta

Spring 2006

Library and Archives Canada

Published Heritage Branch

395 Wellington Street
Ottawa ON K1A 0N4
Canada

Bibliothèque et Archives Canada

Direction du Patrimoine de l'édition

395, rue Wellington
Ottawa ON K1A 0N4
Canada

Your file Votre référence
ISBN: 0-494-13879-3
Our file Notre référence
ISBN: 0-494-13879-3

NOTICE:
The author has granted a non-exclusive license allowing Library and Archives Canada to reproduce, publish, archive, preserve, conserve, communicate to the public by telecommunication or on the Internet, loan, distribute and sell theses worldwide, for commercial or non-commercial purposes, in microform, paper, electronic and/or any other formats.

The author retains copyright ownership and moral rights in this thesis. Neither the thesis nor substantial extracts from it may be printed or otherwise reproduced without the author's permission.

AVIS:
L'auteur a accordé une licence non exclusive permettant à la Bibliothèque et Archives Canada de reproduire, publier, archiver, sauvegarder, conserver, transmettre au public par télécommunication ou par l'Internet, prêter, distribuer et vendre des thèses partout dans le monde, à des fins commerciales ou autres, sur support microforme, papier, électronique et/ou autres formats.

L'auteur conserve la propriété du droit d'auteur et des droits moraux qui protège cette thèse. Ni la thèse ni des extraits substantiels de celle-ci ne doivent être imprimés ou autrement reproduits sans son autorisation.

In compliance with the Canadian Privacy Act some supporting forms may have been removed from this thesis.

While these forms may be included in the document page count, their removal does not represent any loss of content from the thesis.

Conformément à la loi canadienne sur la protection de la vie privée, quelques formulaires secondaires ont été enlevés de cette thèse.

Bien que ces formulaires aient inclus dans la pagination, il n'y aura aucun contenu manquant.

Canada

To my parents, Katarina and Jozef Rusnacik and my brother, David

ABSTRACT

Preventing agglomeration of metallic particles is a concern in the preparation of micrometer and nanometer powders by means of the liquid-phase method. Irregular agglomerates formed during the drying process pose difficulties for material characterization, and ultimately lead to flaws in the final product. As the spherical diameter decreases, the individual particles exhibit substantial inter-particle attractions due to electrostatic and van der Waals forces. These forces result in particle agglomeration and growth, and eventually facilitate the formation of hard agglomerates during particulate drying.

In order to suggest a possible mechanism of copper powder agglomeration, a fundamental understanding of the surface chemistry and morphology of the agglomerates was required. To minimize the propensity to form hard agglomerates, organic media such as propylamine, butylamine, benzenethiol or polyacrylic acid was used to coat the surface of the dispersed particles prior to drying. It was found that propylamine and butylamine were suitable surfactants to disperse the copper particles. Benzenethiol and polyacrylic acid were poor surfactants as the copper particles were not dispersed and agglomeration was not prevented.

ACKNOWLEDGEMENTS

I am extremely grateful for the support, understanding, love, patience and advice from my parents, Jozef and Katarina Rusnacik and my brother, David. I would also like to acknowledge Dr. Alan E. Nelson for all of his advice, help, encouragement and for presenting me with countless challenges.

I am also grateful to Wa'el Abdallah for teaching me how to use all of the instruments that I needed, for all of his time spent aiding me with data analysis, advice and for being such a great supportive friend. Mingyong Sun has also been a great friend. I am thankful for the assistance that was provided by Tina Barker, Andree Koenig, Walter Boddez, Dimitre Karpuzov and the staff at the Alberta Centre for Surface Engineering and Science (ACSES).

I would also like to acknowledge Umicore Canada Ltd. and NSERC for their funding.

TABLE OF CONTENTS

CHAPTER 1: INTRODUCTION

1.1 Nanoparticles and the effect of particle size..... 1

1.2 Overview of this study and hypothesis..... 2

CHAPTER 2: LITERATURE REVIEW

2.1 Introduction..... 4

2.2 Copper Powders: Preparation and Applications

2.2.1 Commercial Preparation Methods..... 4

2.2.2 Properties of Fine Copper Particles..... 6

2.2.3 Applications of Copper Powder

2.2.3.1 General Applications..... 7

2.2.3.2 Superconductors..... 8

2.2.3.3 Computer Memory..... 9

2.2.3.4 Electronic Devices..... 9

2.2.4 Current Industrial Limitations..... 9

2.3 Mechanisms of Particle Agglomeration

2.3.1 Agglomeration Phenomena..... 10

2.3.2 Mechanisms of Agglomeration..... 11

2.4 Approaches to Minimize Agglomeration

2.4.1 Introduction..... 14

2.4.2 Organics as Surfactants..... 14

2.4.3 Polymers as Surfactants..... 15

2.5 Micro- and Nano-scale Analysis of Fine Particles

2.5.1 Enabling Characterization Instrumentation..... 16

2.5.2 Surface Structure and Surface Composition..... 17

2.6 Summary..... 18

CHAPTER 3: EXPERIMENTAL METHODS

3.1 Introduction..... 19

3.2 Surfactant Studies

3.2.1 Materials..... 19

3.2.2 Experimental Procedure..... 20

3.3 X-Ray Photoelectron Spectroscopy (XPS)

3.3.1 Introduction..... 25

3.3.2 Sample Preparation..... 27

3.3.3 Experimental Method..... 27

3.3.4 Chemicals Used as Standards..... 29

3.3.5 Analysis Conditions..... 30

3.4 Scanning Electron Microscopy (SEM) and Energy Dispersive Spectroscopy (EDS)

3.4.1 Introduction..... 33

3.4.2 Sample Preparation..... 34

3.4.3 Experimental Method..... 37

3.4.4 Analysis Conditions..... 37

3.5 Infrared Spectroscopy

3.5.1 Introduction..... 38

3.5.2 Sample Preparation..... 39

3.5.3 Experimental Method..... 39

3.5.4 Experimental Parameters..... 41

3.6 Differential Scanning Calorimetry (DSC) and Thermogravimetric Analysis (TGA)

3.6.1 Introduction..... 43

3.6.2 Sample Preparation..... 44

3.6.3 Experimental Method..... 44

3.6.4 Analysis Conditions..... 46

3.7 Particle Size Distribution Analysis..... 46

CHAPTER 4: RESULTS

4.1 Introduction..... 47

4.2 Overview of the Commercial Process..... 48

4.3 XPS Analysis of the Copper Powders

4.3.1 Analysis of Copper Standards by XPS..... 49

4.3.2 Characterization of Commercial Copper Powders..... 51

4.3.3 Characterization of Propylamine ($CH_3CH_2CH_2NH_2$) Addition..... 55

4.3.4 Characterization of Butylamine ($CH_3CH_2CH_2CH_2NH_2$) Addition.. 56

4.3.5 Characterization of Benzenethiol (C_6H_6S) Addition..... 62

4.3.6 Characterization of Polyacrylic Acid ($C_3H_4O_2$) Addition..... 65

4.4 Infrared Spectroscopy and Thermogravimetric Analysis of Copper Powders

4.4.1 Characterization of Propylamine ($CH_3CH_2CH_2NH_2$) Addition..... 68

4.4.2 Characterization of Butylamine ($CH_3CH_2CH_2CH_2NH_2$) Addition.. 72

4.4.3 Characterization of Benzenethiol (C_6H_6S) Addition..... 76

4.4.4. Characterization of Polyacrylic Acid ($C_3H_4O_2$) Addition..... 80

4.5 SEM/EDS Analysis and Particle Size Distribution of the Copper Powders

4.5.1 Characterization of Commercial Copper Powders..... 82

4.5.2 Characterization of Propylamine ($CH_3CH_2CH_2NH_2$) Addition..... 83

4.5.3 Characterization of Butylamine ($CH_3CH_2CH_2CH_2NH_2$) Addition. 85

4.5.4 Characterization of Benzenethiol (C_6H_6S) Addition..... 87

4.5.4 Characterization of Polyacrylic Acid ($C_3H_4O_2$) Addition..... 89

4.6 Summary..... 91

CHAPTER 5: DISCUSSION

5.1 Introduction..... 92

5.2 Characterization of the copper process by x-ray photoelectron spectroscopy (XPS) and secondary electron microscopy (SEM)..... 93

5.3 Copper Coated with Propylamine..... 94

5.4 Copper Coated with Butylamine..... 98

5.5 Copper coated with Benzenethiol..... 100

5.6 Copper coated with Polyacrylic Acid..... 103

5.7 Comparison of Organic Surfactants..... 104

CHAPTER 6: CONCLUSION AND FUTURE WORK

6.1 Conclusion..... 107

6.2 Future Work

6.2.1 Additional Copper Studies..... 108

6.2.2 Preliminary Work on Nickel

6.2.2.1 Introduction..... 109

6.2.2.2 Nickel Standards..... 109

6.2.2.3 Characterization of the Nickel Process..... 110

REFERENCES..... 115

APPENDIX A..... 119

LIST OF TABLES

CHAPTER 3

Table 3.1	Chemicals used for the preparation of surfactants.....	20
Table 3.2	Chemicals used for the preparation of standards.....	30
Table 3.3	Analysis conditions for the copper and nickel standards and the samples studied in the copper production process.....	31
Table 3.4	Analysis conditions for the samples obtained in nickel production.....	31
Table 3.5	Analysis conditions for the copper samples coated with propylamine, butylamine, benzenethiol and polyacrylic acid.....	32
Table 3.6	Charge neutralizer operating parameters.....	32
Table 3.7	IR operating parameters for copper analysis.....	42

CHAPTER 4

Table 4.1	Summary of spectral features for copper standards.....	50
Table 4.2	Summary of spectral features from XPS for the copper process samples.....	54
Table 4.3	Summary of spectral features for the copper-propylamine samples.....	58
Table 4.4	Chemical composition of the copper – propylamine samples.....	59
Table 4.5	Summary of spectral features for the copper-butylamine samples	60
Table 4.6	Chemical composition of the copper – butylamine samples.....	61
Table 4.7	Summary of spectral features for the copper-benzenethiol samples.....	63
Table 4.8	Chemical composition of the copper – benzenethiol samples.....	64
Table 4.9	Summary of spectral features for the copper-polyacrylic acid samples.....	66
Table 4.10	Chemical composition of the copper – polyacrylic acid samples..	67
Table 4.11	Results from infrared spectroscopy: copper coated with propylamine.....	70

Table 4.12 Results from infrared spectroscopy: copper coated with butylamine..... 74
Table 4.13 Results from infrared spectroscopy: copper coated with benzenethiol..... 78
Table 4.14 Results from infrared spectroscopy: copper coated with polyacrylic acid..... 81
Table 4.15 Particle size distribution results..... 84
Table 4.16 Particle size distribution results..... 86
Table 4.17 Particle size distribution results..... 88
Table 4.18 Particle size distribution results..... 90

CHAPTER 6

Table 6.1 Summary of spectral features for nickel standards..... 112

APPENDIX A

Table A.1 Summary of spectral features obtained by XPS (Nickel process samples)..... 130
Table A.2 Composition of the nickel samples in various stages in the production process..... 131

LIST OF FIGURES

CHAPTER 2

Figure 2.1 Simplified flow sheet for the production of copper powders..... 5

Figure 2.2 Binding mechanisms of particle agglomeration..... 13

CHAPTER 3

Figure 3.1 Schematic of the experimental procedure used in the surfactant studies..... 21

Figure 3.2 Fisher ultrasonic bath..... 24

Figure 3.3 Millipore 47mm all glass vacuum filter holder..... 24

Figure 3.4 The photoemission process..... 26

Figure 3.5 Kratos Axis His 165 System..... 28

Figure 3.6 The scanning electron microscope..... 35

Figure 3.7 Energy dispersive spectroscopy..... 36

Figure 3.8 Schematic diagram for a typical IR system..... 40

Figure 3.9 Schematic diagram of the thermo-gravimetric system..... 45

CHAPTER 4

Figure 4.1 Simplified flow sheet for the production of copper powders..... 48

Figure 4.2 Copper flow diagram – changes in oxidation state and morphology..... 53

Figure 4.3 Comparing the binding energy of Cu 2p in the various copper propylamine samples..... 59

Figure 4.4 Comparing the binding energy of Cu 2p in the various copper butylamine samples..... 61

Figure 4.5 Comparing the binding energy of Cu 2p in the various copper benzenethiol samples..... 63

Figure 4.6 Comparing the binding energy of Cu 2p in the various copper polyacrylic acid samples..... 66

Figure 4.7 Rate of mass change as a function of temperature copper-propylamine..... 71

Figure 4.8 Rate of mass change as a function of temperature: copper-butylamine..... 75
Figure 4.9 Rate of mass change as a function of temperature: copper-benzenethiol..... 79
Figure 4.10 Rate of mass change as a function of temperature: copper-polyacrylic acid..... 81
Figure 4.11 Categories of agglomeration and representative images from SEM: copper-propylamine..... 84
Figure 4.12 Categories of agglomeration and representative images from SEM: copper- butylamine..... 86
Figure 4.13 Categories of agglomeration and representative images from SEM: copper-benzenethiol..... 88
Figure 4.14 Categories of agglomeration and representative images from SEM: copper-polyacrylic acid..... 90

CHAPTER 6

Figure 6.1 Nickel flow diagram – changes in oxidation state..... 113
Figure 6.2 Changes in particle morphology along nickel production..... 114

APPENDIX A

Figure A.1a Survey scan for Cu^0..... 119
Figure A.1b Narrow scan for Cu^0..... 119
Figure A.2a Survey scan for Cu^{+2}..... 119
Figure A.2b Narrow scan for Cu^{+2}..... 119
Figure A.3a Survey scan of the copper control..... 120
Figure A.3b Narrow scan of Cu 2p (copper control)..... 120
Figure A.4a Survey scan of Cu coated with 10 vol% propylamine..... 120
Figure A.4b Narrow scan of Cu 2p (Cu coated with 10 vol% propylamine).. 120
Figure A.5 IR spectrum of the copper 121
Figure A.6 IR spectrum of copper coated with 10 vol% propylamine..... 121

Figure A.7	IR spectrum of copper coated with 10 vol% propylamine after TGA analysis.....	121
Figure A.8	Particle size distribution for the copper control.....	122
Figure A.9	Particle size distribution for copper-1 vol% propylamine.....	122
Figure A.10	Particle size distribution for copper-2 vol% propylamine.....	122
Figure A.11	Particle size distribution for copper-5 vol% propylamine.....	122
Figure A.12	Particle size distribution for copper-10 vol% propylamine.....	122
Figure A.13	IR spectrum of copper coated with 10 vol% butylamine.....	123
Figure A.14	IR spectrum of copper coated with 10 vol% butylamine after TGA analysis.....	123
Figure A.15	Particle size distribution for copper-1 vol% butylamine.....	124
Figure A.16	Particle size distribution for copper-2 vol% butylamine.....	124
Figure A.17	Particle size distribution for copper-5 vol% butylamine.....	124
Figure A.18	Particle size distribution for copper-10 vol% butylamine.....	124
Figure A.19	IR spectrum of copper coated with 10 vol% benzenethiol	125
Figure A.20	IR spectrum of copper coated with 10 vol% benzenethiol (post TGA analysis).....	125
Figure A.21	Particle size distribution for copper coated with 1 vol% benzenethiol.....	126
Figure A.22	Particle size distribution for copper coated with 2 vol% benzenethiol.....	126
Figure A.23	Particle size distribution for copper coated with 5 vol% benzenethiol.....	126
Figure A.24	Particle size distribution for copper coated with 10 vol% benzenethiol.....	126
Figure A.25	IR spectrum of copper coated with 10 M polyacrylic acid.....	127
Figure A.26	IR spectrum of copper coated with 10 M polyacrylic acid (after TGA analysis).....	127
Figure A.27	Particle size distribution for copper coated with 0.5 M polyacrylic acid.....	128
Figure A.28	Particle size distribution for copper coated with 1.0 M	

polyacrylic acid..... 128
Figure A.29a Survey scan for Ni^0..... 129
Figure A.29b Narrow scan for Ni^0..... 129
Figure A.30a Survey scan for Ni^{+2}..... 129
Figure A.30b Narrow scan for Ni^{+2}..... 129
Figure A.31a Survey scan for Ni black (contains Ni^{+3}) 129
Figure A.31b Narrow scan for Ni black..... 129

ABBREVIATIONS

AES	Auger Electron Spectroscopy
BSC	Benzeneselonal
BT	Benzenethiol
DFT	Density Functional Theory
DSC	Differential Scanning Calorimetry
EDX	Energy Dispersive X-Ray Analysis
FTIR	Diffuse Reflectance Infrared Fourier Transform Spectroscopy
HREELS	High-Resolution Electron Energy Loss Spectroscopy
HTS	High Temperature Superconductor
IR	Infrared Spectrocopy
LEED	Low-Energy Diffraction
Mono	Monochromatic
PVD	Physical Vapour Deposition
SAM	Self-Assembled Monolayers
SEM	Scanning Electron Microscopy
TGA	Thermal Gravimetric Analysis
XPS	X-ray Photoelectron Spectroscopy

UNITS

A	Amps
eV	Electron volts
cm^{-1}	Inverse centimetre (wavenumber)
V	Volts

GREEK SYMBOLS

γ	bending vibration
η	bonds to
υ	stretching vibration

CHAPTER 1: INTRODUCTION

1.1 Nanoparticles and the effect of particle size

Nanoparticles are defined as a collection of 10 to 1000 atoms, and this particular cluster of atoms has physical, chemical, optical, and electronic properties that are highly size dependent (Pietsch, 1991). In technological applications, these properties are of significant importance in contrast to the properties of bulk solid-state materials. To tailor the properties, the size of the individual particles can be manipulated. However, in disperse systems, adhesion arising from inter-particle forces becomes an issue with decreasing particle size. This phenomenon promotes aggregation, agglomeration, coating and caking (Pietsch, 1991).

As particle size decreases, the characteristics that are used to describe the quality of a single particle improves greatly. For example, all solid materials have imperfections in their structure (Pietsch, 1991). When the loading stress concentration increases, the material has a tendency to break. However, by decreasing the size of the particles in the material, the likelihood of defects in the material decreases significantly (Pietsch, 1991). In other words, by decreasing the agglomeration nature of the powder, it is possible to increase the strength of the metal.

With current developments in nanotechnology, nanoparticles have been generated by solution-phase methods, gas phase methods, and vacuum synthesis techniques. With the solution phase method, preventing agglomeration of metallic particles is highly desired. Irregular agglomerates that form during the drying process present difficulties for material characterization, and ultimately produce flaws in the final product (Messing et al., 1982). This problem becomes increasingly difficult as the particle diameter decreases to the nanometer region (Voogt et al., 1996). Electrostatic and van der Waals forces contribute to inter-particle attraction. As the spherical diameter decreases, the particles become attracted to one another (Voogt et al., 1996). These forces contribute to particle agglomeration and growth, and eventually facilitate the formation of hard agglomerates during particulate drying (Messing et al., 1982). The mechanical strength of the agglomerates depends on the nature of the binding forces at coordination points between individual particles, at interfaces between the liquid matrix and the solid particles, and/or

through liquid bridges between the individual particles (Pietsch, 1991). In order to generate dispersed ultra fine metal powers (< 500 nm) for the ceramic and capacitor industry, the mechanisms of metal particle agglomeration must be better understood.

1.2 Overview of this study and hypothesis

In order to determine the mechanism of copper powder agglomeration, a fundamental understanding of the surface chemistry and morphology of the particle agglomerates is required. A detailed study of copper particles and agglomerates was conducted using x-ray photoelectron spectroscopy (XPS) and scanning electron microscopy (SEM). These techniques, available though the Alberta Centre for Surface Engineering and Science (ACSES), provide the spectroscopic resolution required to characterize the surface chemistry and morphology of the agglomerates. XPS and SEM provide accurate quantitative (i.e., elemental identification and oxidation state) and qualitative (i.e., visual) analysis of the agglomerate particle size and shape, the presence or lack thereof of hard bridges, and the extent of surface oxidation.

Following the determination of the prevalent agglomeration mechanism(s), a suitable strategy was developed to minimize the propensity to form hard agglomerates. Several strategies can be suggested on the basis of previously studied systems. If oxide layer formation is a contributing factor for the formation of agglomerates, organic media, such as, propylamine, butylamine, benzenethiol, and polyacrylic acid, can be used to coat the surface of the dispersed particles prior to drying. The oxidized agglomerates (copper powders) can be re-dispersed in an organic medium where they are subjected to ultrasonic irradiation (Suslick et al., 1999). If the agglomeration mechanism is caused by the formation of hard bridges between particles, the ionic strength of the liquid matrix and the drying temperature can be adjusted to prevent condensation of salt bridges (Pietsch, 1991).

To ensure that the organic coating was applied to the surface of the copper particles, SEM was used to determine the morphology of the particles. By comparing the samples to a control group, it was possible to determine if the organic coating was effective to suppress agglomeration. Thermogravimetric analysis (TGA) was further used to determine the thermodynamic stability of the coating. It is important to coat the particles

with a material that can be easily removed. Furthermore, infrared spectroscopy (IR) was used to study the behaviour of bonds between atoms. IR was also used to determine which functional groups are still evident following heating in the thermogravimetric analysis. Consequently, characterization of particle surface chemistry and morphology through this research will allow effective selection strategies for particle stabilization.

Following the introduction of nanoparticles and the objective of this work, Chapter 2 describes in more detail the properties of copper, how copper powders are commercially prepared, and applications of the final end product. In this chapter, nanotechnology and its application in semiconductors, computer memory, and electronics is also given. The discussion continues with the definition of agglomeration, properties of fine particles and the phenomena and mechanisms of agglomeration. Chapter 2 concludes with suggestions used to minimize or prevent agglomerate formation. Various experimental methods such as x-ray photoelectron spectrometry (XPS), scanning electron microscopy (SEM), infrared spectroscopy (IR), thermal gravimetric analysis (TGA), and particle size distribution analysis are discussed in Chapter 3. The procedure for adding a surfactant to the copper particles is also described in this chapter. The results for characterizing the copper powder generated by Umicore Canada Ltd. and the results from adding a surfactant to the copper powder are described in Chapter 4. Chapter 5 is devoted to a discussion of the obtained results, while Chapter 6 exemplifies a brief conclusion of the entire study and suggestions for future work. Some initial characterization was completed on samples obtained along the nickel production process, and preliminary results from the characterization of standards are also demonstrated in this chapter.

CHAPTER 2: LITERATURE REVIEW

2.1 Introduction

Recently, considerable progress has been made to synthesize and characterize well-defined nanoparticles and their dispersions. In this chapter, the preparation and applications of copper powder are discussed. For most of the applications mentioned, a dispersion of uniform, non-agglomerated nanoparticles is preferred. The chapter continues with an analysis of the mechanisms of agglomeration and approaches to minimize agglomeration. The chapter concludes with an introduction of the techniques that can be used to analyze fine particles.

2.2 Copper Powders: Preparation and Applications

2.2.1 Commercial Preparation Methods

Copper metal is prepared using numerous methods. Most commonly, the floatation process is used to concentrate the copper (Greenwood, 1998). Initially, copper sulfide ores contain 1 % to 2 % copper, but through the floatation process, the concentration of the metals increases to 20 % to 40 %. In the froth-floatation process, the crude ore is ground to form a fine powder and mixed with frothing reagents, water and collecting reagents. The next stage in the process consists of blowing air through the mixture. In turn, mineral particles bind to the bubbles and froth is generated on the surface. The froth is then collected, distilled and a clean concentrate is collected. The concentrated slurry is further heated to remove the sulfur and other impurities. A blast furnace is used to smelt the mixture with iron oxide to produce a copper matte, which is a molten solution of copper sulfide and iron sulfide. The matte is transferred to a converter where it is treated by blowing air to remove sulfur and iron. The sulfur is removed as sulfur dioxide and the iron is removed as a slag of ferrous oxide. The resulting copper is 98 to 99 % pure.

Electrolysis is used to further purify the copper. The copper produced by the above process is cast into anodes, which are suspended in an acidic solution of $CuSO_4$ and H_2SO_4. Thin sheets of pure copper are used as the cathode. During electrolysis, the anode is dissolved in the electrolyte and pure copper metal is deposited on the cathode. Solid impurities consisting of silver, gold, and precious metals, remain in the electrolytic solution.

The above copper preparation method can be described by the following reactions:

$$2FeS + 3O_2 \rightarrow 2FeO + 2SO_2 \quad (1)$$

$$2Cu_2S + 3O_2 \rightarrow 2Cu_2O + 2SO_2 \quad (2)$$

$$2Cu_2O + Cu_2S \rightarrow 6Cu + SO_2 \quad (3)$$

Umicore Canada Ltd. produces high quality coating materials using a unique chemical process, as illustrated in Figure 2.1. A copper solution, water, organic additives, ammonium hydroxide and a reducing agent are added to a batch reactor held at 40 °C. A slurry consisting of copper suspended in an aqueous phase is generated. When the copper particles precipitate out, they are washed with water, and spray dried at 100 °C. Spray drying is highly suited for the continuous production of dry solids. The operating conditions and dryer design are selected such that the end product achieves the desired particle size distribution, moisture content, and particle shape. In essence, the copper solution is sprayed from the nozzle onto a heated wall and the particles dry upon contact. The final step in the chemical process involves classification of the particles according to size.

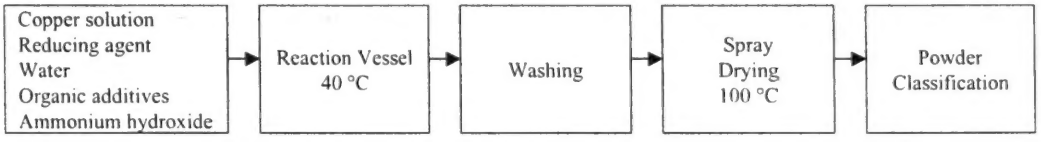

Figure 2.1 Simplified flow sheet for the production of copper powders.

The chemistry of copper relies on its oxidation-reduction characteristics. Copper (II) in solution can be reduced to metallic copper with the addition of a strong reducing agent, such as hydrazine (N_2H_4). However, the oxidation products of hydrazine are strongly dependent on the pH of the solution, the temperature, the oxidizing agent used and whether impurities are present in the solution.

It is known that in the presence of an acid, a copper ammonia sulfate complex reacts to form Cu_2O. Nitric acid and sulfuric acid are two possibilities for acids (Chang, 2002). Cu_2O is relatively unstable and in the presence of a strong reducing agent, such as hydrazine, and metallic copper is formed (Equation 7).

$$Cu^0(s) + 2NH_3 + (NH_4)_2SO_4 + 1/2O_2 \rightarrow [Cu(NH_3)_4SO_4] + H_2O \quad (4)$$

$$Cu^0(s) + Cu(NH_3)_4SO_4 \rightarrow [Cu(NH_3)_2]_2SO_4 \quad (5)$$

$$H_2SO_4 + H_2O + [Cu(NH_3)_2]_2SO_4 \rightarrow Cu_2O + 2(NH_4)_2SO_4 \quad (6)$$

$$2Cu_2O + N_2H_4 \rightarrow 4Cu^0(s) + 2H_2O + N_2 \quad (7)$$

Since the copper process at Umicore Canada Ltd. is proprietary, specific solution chemistry details are not known.

2.2.2 Properties of Fine Copper Particles

Copper is a metallic element with an atomic number of 29 and a molecular weight of 63.546 amu. The metal has melting point of 1083.4 °C and a boiling point of 1567 °C. It has three common valence states, 0, +1 or +2. Copper can be described as reddish metal with a face centered cubic crystalline structure (Greenwood, 1998).

The most important properties of copper in terms of industrial and commercial applications include malleability, ductility, heat and electrical conductivity. The transition metal also has a low chemical reactivity (Greenwood, 1998). Upon exposure to moist air, a greenish protective film forms on the surface, and this layer ensures that the metal does not endure further oxidation or degradation. It is only possible to dissolve copper in hot solutions of concentrated sulfuric acid, hydrochloric acid, and concentrated nitric acid (Chang, 2002).

As particles decrease in size, the characteristics that describe quality improve significantly. For example, improvements are evident in solubility, reactivity, particle homogeneity, strength, and optical characteristics. When particles decrease in size, there is a decreased probability in which imperfections are evident and there is a reduced risk of breakage. Conversely, irreversible deformation occurs in particles that decrease in size.

However, mechanical processing and handling become difficult, as the particles have a tendency to stick to one another. Particle agglomerates have the following properties: flow through pores becomes difficult, a resistance to fluid flow is evident, and separation becomes difficult (Pietsch, 1991).

In disperse systems, adhesion becomes an area of concern in the production and processing of small solid matter. Decreasing the size of particles beyond the critical size of 100 μm is associated with agglomeration, aggregation and caking (Pietsch, 1991).

2.2.3 Applications of Copper Powder

2.2.3.1 General Applications

Copper is the most plentiful metal and is used in every aspect of our daily lives (Carmony, 1990) and approximately 3,000,000 tones of copper are used in American industries. What makes copper unique from various other elements, is that it is used extensively in all engineering applications and it is not used exclusively for a single product. In pure form, copper can be drawn into wires or cables for power transmission, building wiring, motor and transformer wiring, wiring in commercial and commercial electronics, telecommunication cables, plumbing, heating, air conditioner tubing, applications in construction and electroplated undercoats for nickel, chrome and zinc (Carmony, 1990). Copper compounds are also used extensively in agriculture for the production of insecticides, fungicides and prevent algal development in water reservoirs (Carmony, 1990). Copper can also be used as an alloy with zinc and lead (Guy, 1960 and Hosford, 2005). In a cast form, the alloy is used in commercial tubing, electrical contacts, automotive and machine parts, coinage and decorative hardware (Pinner, 1962).

With advances in technology, industry is focusing on the development of copper thin film products. The products involve a wide range of effective evaporation materials,

sputtering targets, accessories for electronics and semi-conductors, optics, optical data storage, coatings, and solar cells.

Nickel and copper powders are base metal powders that are used in electronics and circuitry. The market for these powders is rapidly growing due to expanding applications in multi-layer capacitors, polymer ink conductive traces, circuit board surge protection devices, and non-linear resistors. The thin film materials produced are used to coat these products. Two requirements of the coatings include that the material must be reflective and corrosion resistant, and it must be possible to tailor metal powder properties in order to achieve the stringent requirements of the electronic industry.

2.2.3.2 Superconductors

Over the past decade, there has been a focus on the production of high temperature superconductors (HTS). The discovery of HTS exhibiting superconductivity above liquid nitrogen temperature has led to the development of special purpose electronics (Khare, 2003). It has been claimed that the development of HTS will have significant advantages over conventional conductors. The superconductor electronics specifications include higher speed and lower power consumption. In normal conductors, such as copper wire, the atoms in the wire impede the free flow of electrons. As a result, the current energy is released as heat. These characteristics have several advantages in communication technology, computers, high frequency electronics and magnetic field measurements.

Electrical components are becoming smaller and smaller. The present concern is that the circuitry will become so small that it will be unable to carry electricity using the current methods that are employed today (Plunkett, 2004). There is a general agreement among researchers that nanotechnology may offer a solution to this particular problem. Current production methods generate electrical components out of materials without manipulating the atomic structure. When the material is observed at an atomic level, it becomes evident that the molecules and atoms are disorganized. Thus, by manipulating the structure of these materials it will be possible to construct miniaturized computer chips and electronics (Plunkett, 2004).

Currently, semiconductors used in computers are approximately 90 nm in diameter. If semi-conductors consisting of carbon nano-tubes, which were coated with a thin film of

copper were developed, this would revolutionize the computer industry. Computers would become very small and fast. Similarly, cell phones have the potential of becoming a personalized compact computer. Manufacturing this particular technology on a commercial level is several years away but with current advances it is possible.

2.2.3.3 Computer memory

The goal of major computer companies is to develop computer memory on the basis of nanotechnology. IBM's major focus has been on memory chips that have a theoretical storage capacity of one terabyte per square inch. Other companies are trying to develop a RAM chip that can match the storage capacity of a hard drive (Plunkett, 2004). Furthermore, in the future, it may be possible to turn a computer on instantly as they will no longer require traditional booting up.

The objective of using nanotechnology in these advancing fields is to use smaller molecules in the development of small and compact components that can store large quantities of information.

2.2.3.4 Electronic Devices

To date, nanotechnology will have considerable impact in electronics. A drive is evident to develop smaller computers, cell phone and electronic components. However, smaller objects are prone to heat and radiation damage (Chow and Gonsalves, 1996). For all of the applications previous mentioned, non-agglomerated nanoparticles are necessary. These nano-particle dispersions should be free of any by products and excess surface free agents that would interfere in the generation of thin films (Shi et al., 2005). In other words, if the copper particles are coated to prevent agglomeration, the coating must be easily removed from the surface prior to thin film generation.

2.2.4 Current Industrial Limitations

Nanotechnology comprises of all developments in technology that are used to create structures with sizes below 100 nm (Chow and Gonsalves, 1996). Through time, nanotechnology will interface with technologies such as electronics, biotechnology, chemistry, and robotics (Plunkett, 2004). New methods will be developed to generate

products that use micro-components. Since nanotechnology is such a new development, it is also the least understood. One of the greatest problems in this field includes defining the boundary between optimistic claims, practical capabilities and the feasible development of products (Plunkett, 2004).

Nano-sized particles are the smallest possible particles, as this scale approaches the molecular and atomic length scales. This area is difficult to understand at this point in time because materials on the nano-scale behave differently in contrast to macro-scale materials (Plunkett, 2004). Gravity and friction have different effects on extremely small particles, and consequently when studying nano-scale materials it is critical to consider atomic forces, chemical bonds and quantum mechanics.

Despite the interest in nanotechnology, it is not feasible to construct every imaginable material into a nano-sized item. It is important to consider investigating basic structures with promising properties (Plunkett, 2004). For instance, we can consider nano-tubes and nano-wires. These nano-structured materials can be synthesized with a high level of definition (Shi et al., 2005) and the properties of nanoparticles can be tailored by size manipulation (Husein et al., 2004). Nano-tubes and nano-wires have wide applications in lithography, atomic layer deposition and molecular vapor deposition. Dispersions consisting of oxide nanoparticles are used to prepare nano-structured oxide coatings, sensors, inorganic membranes, transparent thin films, and thin electrolytes that are used in solid oxide fuel cells (Shi., et al., 2005). Once basic materials are understood, it is easier to begin to understand complex devices.

2.3 Mechanisms of Particle Agglomeration

2.3.1 Agglomeration Phenomena

Agglomeration refers to the process by which particulate matter is gathered into a agglomerate. During changes in particle size, adhesion forces become effective (Pietsch, 2001). The adhesion forces tend to result in increased particle size and changes in the shape of the particles.

Adhesion of fine particles occurs during all operation of production. Particle adhesion during mechanical grinding is undesirable as it lengthens the grinding time and increases

the energy requirement. Agglomerated particles are also unwanted during analytical separation.

Adhesion and agglomeration of fine particles becomes a problem in transportation and storage, as conglomerates are often clogged in feeders and prevent discharge into silos. Thus, it is pertinent to understand how agglomeration occurs and a means to prevent the formation of agglomerated particles (Pietsch, 1991).

Adhesion of individual particles is a result of the competition between surface and volume forces (Pietsch, 1991). In order for adhesion to occur, the environmental forces such as gravity, inertia, and drag must be smaller in comparison to the forces of attraction. Adhesion tendency, T_A, is the ratio of all binding forces ($B_i(x)$) and the sum of the environmental forces, ($F_{jy}(x)$), as determined by Equation 8.

$$T_A = \frac{\sum_i B_i(x)}{\sum_i F_{jy}(x)} > 1 \qquad (8)$$

The attraction and environmental forces are highly dependent on the size of the powder particles. When $T_A > 1$, adhesion is evident.

It is known that the forces of attraction are characteristic of short-range forces. When the distance between particles is increased, the magnitude of the attraction forces decreases. Decreasing the particle size is desired because there is a lower probability of agglomerate formation.

2.3.2 Mechanisms of Agglomeration

The possible mechanisms of agglomeration can be divided into several key groups, including (1) short range van der Waals and electrostatic attraction forces between particles, (2) solid bridge formation or sintering, (3) interfacial forces and capillary pressure, (4) adhesion and cohesion forces, and (5) physical interlocking (Pietsch, 1991). These mechanisms are depicted in Figure 2.2 (interlocking is not shown).

Attraction forces (van der Waals forces) between solids (Figure 2.2A) also causes unwanted agglomeration. At extremely small distances the force of attraction is relatively

large; however, the strength diminishes with increasing distance between the particles (Pietsch, 1991). The van der Waals forces have a short-range character.

Solid bridges or sintered bridges, as shown in Figure 2.2B, form if the temperature of the system rises above two-thirds of the melting temperature of the solids (Pietsch, 1991). As a result, diffusion of molecules from one particle to another is evident and bonding occurs at points of contact. The diffusion velocity is dependent on temperature, pressure and the contact surface area (Voogt and Mens, 1996).

Most finely divided solids have the ability to attract free atoms and molecules from the atmosphere. As a result, adsorption layers (Figure 2.2C) with a thickness of < 3 nm can form (Pietsch, 1991). The forces in this layer are sufficient to deform particles at the contact points, which results in larger contact areas and higher bond strengths (Voogt and Mens, 1996).

One of the most common agglomeration mechanisms in wet phases is that of liquid bridges. The bridges (Figure 2.2D) form at coordination points between particles and form agglomerates. The liquid bridges develop from free water and condensation of capillaries (Pietsch, 1991).

The mechanism of agglomeration relies on several factors, including the ionic strength of the liquid matrix, the concentration of dissolved salts, drying temperature, and oxygen concentration (Pietsch, 1991). These factors will determine whether molecular interactions, liquid/solid bridges, sintered bridges, or chemical reaction (oxidation) agglomeration mechanisms are prevalent in the hard agglomerate. Indeed, the mechanism of agglomeration may include one or more of the aforementioned mechanisms. Accurate knowledge of the agglomeration mechanism will facilitate the next stage in nano-scale production. The primary focus of this research is not determining the exact mechanism of copper powder agglomeration, rather the focus consists of methods that can be used to inhibit agglomerate formation.

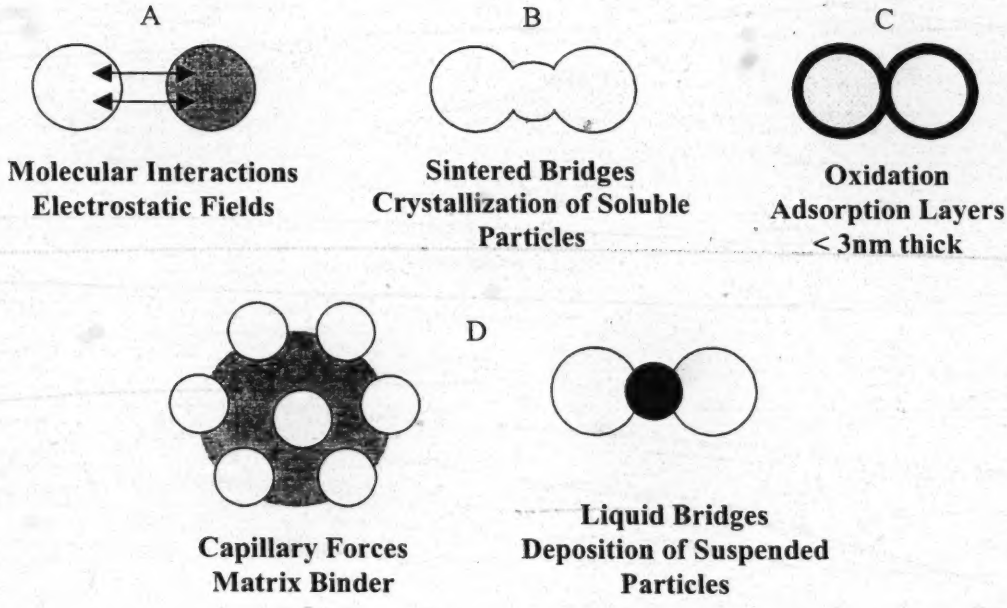

Figure 2.2 Binding mechanisms of particle agglomeration. Adapted from Pietsch. W. (1991). *Size Enlargement by Agglomeration*. Wiley, New York, NJ.

2.4 Approaches to Minimize Agglomeration

2.4.1 Introduction

Surfactant adsorption and surface solubilization are being studied on an on-going basis, and are employed in a variety of technologies. For example, surfactants are used in detergency, emulsification, dispersion of agglomerates, floatation, coating, recovery of petroleum and adhesion (Sharma, 1995). These examples depend on the ability of the surfactant to adsorb on an interface (solid-liquid, liquid-liquid, liquid-vapour) and their ability to solubilize hydrocarbon materials in micelles.

Surfactants are classified according to the type of group on the head of the micelle. Surfactants that contain a negatively charged head group are referred to as anionic surfactants. This category of surfactants consists of carboxylic acids, salts and alkyl benzene sulfonates. Quaternary ammonium salts and amines are called cationic surfactants. They possess a positively charged head group. Non-ionic surfactants have a hydrophilic head group that is not charged. Ethers and esters fall within this category (Sharma, 1995).

2.4.2 Organics as surfactants

Amines bind strongly to surfaces of metals. Bowe et al. (2003) studied the extraction of heavy metals by amines adsorbed onto silica. In their study, they used saturated, straight chain primary amines as coordinating ligands in the removal of copper (II) from aqueous solutions. It was found that smaller amine chains, such as propylamine, are very stable and the surfactant binds to the surface of copper through nitrogen atom. Nitrogen behaves as the coordination donor (Bowe et al., 2003).

Butylamine, like propylamine, has a hydrophobic head (Sharma, 1995). Butylamine was also chosen as a surfactant because amines bind strongly to surfaces of metals and the compound has a low boiling point of 70 °C. An optimistic claim for these experiments is butylamine will behave better as a surfactant to hinder agglomerate growth due to its longer hydrocarbon chain, and upon heating the coating will be removed. It is expected that the longer hydrophobic tail will repel the particles away from one another.

The use of a surfactant counter ion as a reactant is a new approach to develop nanoparticles in an emulsion. Husein et al. (2003) studied the formation of silver chloride nanoparticles in micro-emulsions by direct precipitation with a surfactant counter ion. Benzenethiol was chemisorbed on the surface of silver as benzenethiolate. It was found that benzenethiol adsorbs readily onto a metallic surface. Upon bonding to the surface, the metal binds to the sulfur and the benzene ring of benzenethiol is titled at 25° from the substrate normal (Woo Han et al., 2001).

Temperature dependent DRIFTS (Diffuse Reflectance Infrared Fourier Transform Spectroscopy) spectra indicated that the copper benzenethiol bonds are weakened with heating. The vibrational peaks of the benzenethiolate species were observed up to 458 K, however, at 418 K the bonds were weakened (Woo Han et al., 2001). It was also determined that benzenethiolate does not undergo any structural changes during heating. In other words, the benzene ring does not undergo fragmentation during heating.

Most of the thiol compounds that are investigated as particle aggregates contain a long hydrophobic tail (Woo Han et al., 2001) that form micelles. The coating acts to repel each of the particles away from one another. In essence, there is a reduction in the force of attraction between the copper particles.

2.4.3 Polymers as Surfactants

Production of fine particles that are easily handled and coated is fairly difficult. The development of the smallest and finest particles is determined by the efficiency of the dispersants used during the production process (Phillips and Skuse, 2004). Sodium polyacrylate is used readily in the production of fine particle size calcium carbonate and kaolin slurries that are used in paper coating technology (Phillips and Skuse, 2004). The use of this surfactant results in the development of the highest possible solids content and minimizes drying costs. Sodium polyacrylate is a flexible long chain surfactant that has lateral chain-chain interactions (Sharma, 2005). If the hydrophobic tails of the surfactant will interact with one another, it is anticipated that the electrostatic interactions between the copper particles will decrease. In turn, the particles will repel from one another.

A disadvantage of using this particular surfactant includes that the boiling point of polyacrylic acid is approximately 800 °C (Sharma, 2005). By the time the polymer is removed from the particles, decomposition of copper oxide will occur.

Therefore, in the present study, polyacrylic acid was employed as a surfactant to minimize the propensity of copper to form solid agglomerates. Polyacrylic acid will be utilized as the reagent is readily available and is relatively inexpensive.

2.5 Micron- and Nano-scale Analysis of Fine Particles

2.5.1 Enabling Characterization Instrumentation

Scanning probe microscopy is an important experimental technique that is used to characterize and synthesize nano-materials. Atomic force microscopes and scanning tunneling microscopes can be used to observe the surface and determine how the atoms move around (Chow and Gonsalves, 1996). These instruments are immensely useful in understanding atomic behavior. In the future, they will have the potential to manipulate nano-scale objects.

Manipulating nano-sized particles involves fabrication and self-assembly. Fabrication consists of changing the atomic structure of a material (Plunkett, 2004). Atoms can be pushed, pulled or lifted by tiny scanning arms while AFMs and electronic bombardment tools can be used to write on atomic surfaces. These methods are very difficult to employ at the industrial level because the development of significant quantities of a given atom is time consuming process.

Physical and chemical vapor deposition devices are another important innovation. These devices are used to spread a thin layer of a substance over a given area (Plunkett, 2004). The copper powder is coated onto electronic and semiconductor components using the physical vapor deposition method. Vapor deposition refers to any process in which materials in the vapor state is condensed through chemical reaction, condensation or conversion to form a solid material (Khare, 2003). These processes are used to form coatings to alter the optical, corrosion resistance, mechanical, electrical and wear properties of a material (Plunkett, 2004).

Self-assembly is a promising technique that can be used in commercial and industrial processes, as it relies on chemical processes or natural forces to alter the atomic structure.

This particular technique consists of polymerization and crystal growth. Crystalline growth involves the replication of a prototype structure. Polymerization involves the development of long molecules by either heating, mixing or running electric current through the chemicals. This technique relies heavily on the chemical and electric attraction between elements.

2.5.2 Surface Structure and Surface Composition

It is well known that nanoscale materials often have chemical and physical properties that differ largely from similar compositions in the bulk (Hills et al., 2003), and recent studies of surfaces and atoms have gained a large interest in the scientific community. Nanoscale materials have complex structural and chemical properties. As a result, there is a drive to fully develop the relationships that exist amongst composition, size and structure.

To accomplish detailed structural characterization, researchers take advantage of the improvements that have been made in analytical techniques.

Scanning electron microscopy is a very powerful tool used to characterize small metal particles. Current instruments are capable of atomic resolution. With this in mind, it is possible to examine supported nanoparticles.

Hills et al. (2003) used a collection of analytical techniques to study Pt, Ru, and Pt-Ru nanoparticles. X-ray photon spectroscopy (XPS), scanning transmission electron microscopy (STEM), energy dispersive x-ray analysis (EDX) and electron nano-diffraction are used to determine elemental composition, size distributions and microstructures of the powdered particles.

By studying the precursors, supports and the alloying reactions that occur on the surface of metal particles, it is possible to determine the effect that the experimental conditions have on the cluster assembly and on particle growth.

2.6 Summary

Consequently, there is a drive to develop nanometer sized metal particles for use in microelectronics, optics, computers and superconductors. Since these components are becoming smaller and smaller, it is necessary to ensure that the metallic particles are as small as possible. The copper powder developed by the process shown in Figure 2.1 is heavily agglomerated. The particles are very large in size and cluster formation is dominant. Research has suggested that one approach to minimize agglomeration is to add a surfactant to the raw copper powder. Surfactants are used in detergency, emulsification, and dispersion of agglomerates (Sharma, 1995). In this study, propylamine, butylamine, benzenethiol and polyacrylic acid will be employed to determine whether agglomeration of copper powder could be minimized or prevented, and if so which surfactant loading achieves the best possible results. Once the coating is adsorbed onto the surface of the copper particles, it is just as important to determine whether it can be easily removed. To accomplish detailed structural characterization surface science techniques such as XPS, SEM, EDS, IR and TGA will be used. Chapter 3 provides full detail of experimental methods used in the agglomeration study.

CHAPTER THREE: EXPERIMENTAL METHODS

3.1 Introduction

The main objective of this research is to characterize the surface chemistry of copper powders, and copper powders re-dispersed in different aqueous media to prevent agglomeration. To accomplish the detailed compositional analysis of the copper powders, several analytical techniques for materials characterization are used. The techniques of primary importance include x-ray photoelectron spectroscopy (XPS), secondary electron microscopy (SEM), energy dispersive x-ray analysis (EDS), infrared spectroscopy (IR), and thermogravimetric analysis (TGA). These techniques and specific operating conditions are discussed in the following sections.

3.2 Surfactant Studies

3.2.1 Materials

Four individual studies were carried out on the raw copper powder supplied by Umicore Canada Ltd. Details on the development of the raw copper powder were given in Chapter 2. The powder that is used in the surfactant studies was collected from the reactor in an aqueous phase. It was not treated, purified or dried prior to addition of the surfactant.

In one study copper was coated with propylamine in ethanol. The other studies consist of coating copper with sec-butylamine in ethanol, benzenethiol in ethanol and polyacrylic acid in nanopure water. Table 3.1 presents the details of the chemicals used in the experiments.

Table 3.1 Chemicals used for the preparation of surfactants

Compound	Molecular Formula	Purity	CAS#	MW (g/mol	BP (°C)	Supplier
Propylamine	C_3H_9N	99+ %	107-10-8	59.11	48.0 at 760 mmHg	Aldrich
Butylamine	$C_4H_{11}N$	99 %	1395284-6	73.14	63.0 at 760 mmHg	Aldrich
Benzenethiol	C_6H_6S	99+ %	108-98-5	110.18	169.0	Aldrich
90% Ethanol, 5% Methanol, 5% 2-Propanol	CH_3CH_2OH					Fisher Scientific
Sodium Polyacrylate	$C_3H_3NaO_2$		900304-07	94.04		Aldrich
Copper (raw) Powder						Umicore

3.2.2 Experimental Procedure

Two sets of samples were prepared under the identical conditions to ensure that the results were consistent with one another. In addition, a control copper sample was also prepared (propylamine, butylamine, benzenethiol, polyacrylic acid were not added to the powder). The control was used as a source of comparison to determine the effect and degree of agglomeration after a surfactant was added to the powder (Figure 3.1).

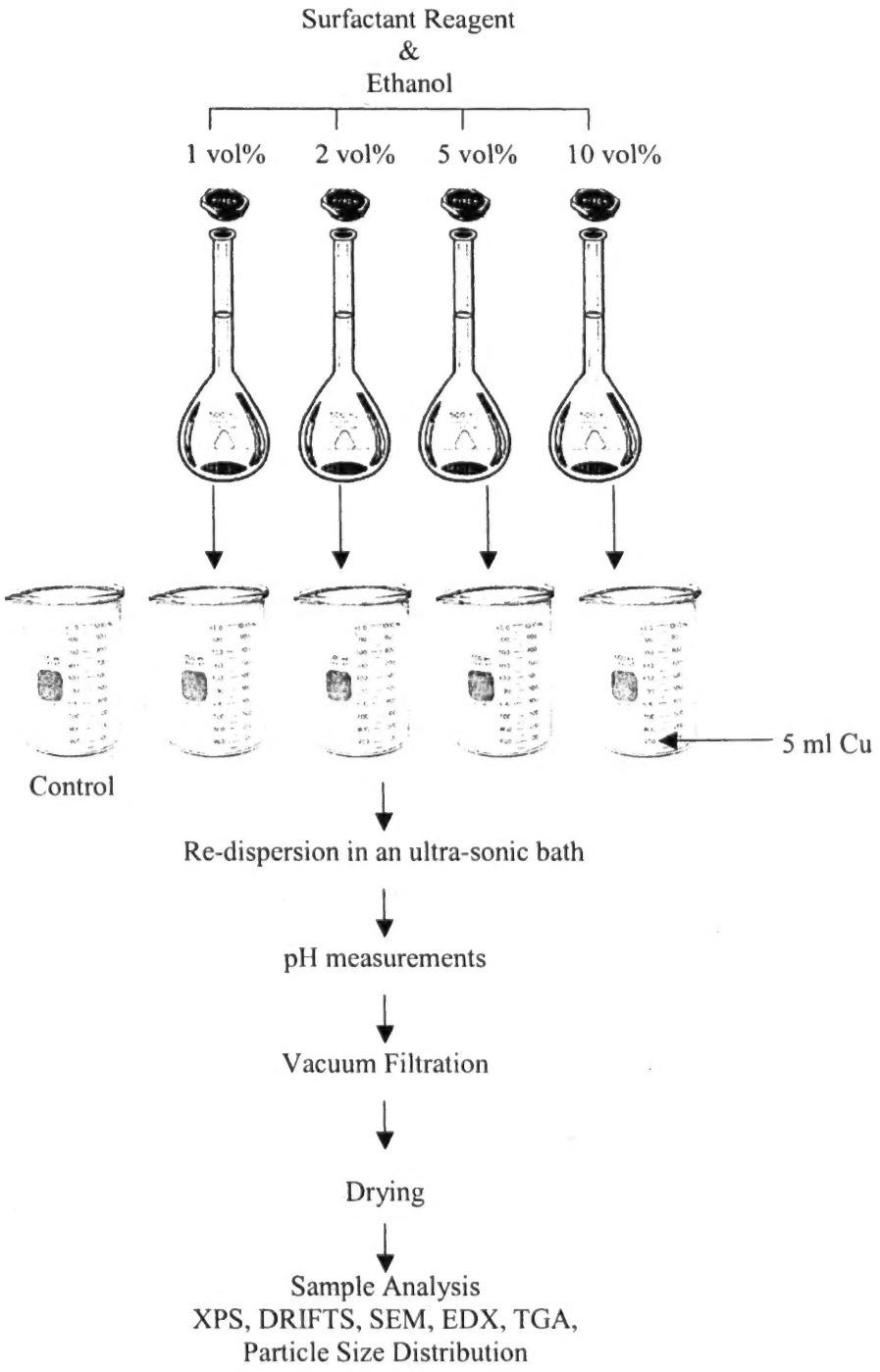

Figure 3.1 Schematic of the experimental procedure used in the surfactant studies

To prepare the copper powder with the propylamine surfactant, the following experimental procedure was used (Figure 3.1):

1. Wash all glassware with acetone, nanopure water and dry in an oven at 400 °C overnight.
2. Prepare surfactant solutions containing 1 vol%, 2 vol%, 5 vol% and 10 vol% propylamine.
   a. 1 vol% Surfactant Solution: Using a 1 ml volumetric pipette, measure 1 ml propylamine (Aldrich, Table 3.1) and insert into a 100 ml volumetric flask. Dilute to volume with ethanol (Fisher Scientific, Table 3.1). Mix thoroughly.
   b. 2 vol% Surfactant Solution: Using a 2 ml volumetric pipette, measure 2 ml propylamine (Aldrich, Table 3.1) and insert into a 100 ml volumetric flask. Dilute to volume with ethanol (Fisher Scientific, Table 3.1). Mix thoroughly.
   c. 5 vol% Surfactant Solution: Using a 5 ml volumetric pipette, measure 5 ml propylamine (Aldrich, Table 3.1) and insert into a 100 ml volumetric flask. Dilute to volume with ethanol (Fisher Scientific, Table 3.1). Mix thoroughly.
   d. 10 vol% Surfactant Solution: Using a 10 ml volumetric pipette, measure 10 ml propylamine (Aldrich, Table 3.1) and insert into a 100 ml volumetric flask. Dilute to volume with ethanol (Fisher Scientific, Table 3.1). Mix thoroughly.
3. Label 5 beakers: control, 1 vol% propylamine, 2 vol% propylamine, 5 vol% propylamine and 10 vol% propylamine
4. Measure 5 ml of copper powder and obtained from Umicore with a 10 ml graduated cylinder. The powder was contained in an aqueous water phase. This batch was necessary such that the powder was not exposed to prior washing, drying and classification steps. Thus, any changes in the morphology of the samples were due to the respectable surfactant.

5. Place the copper slurry into a 100 ml beaker. Rinse the graduated cylinder with nanopure water.
6. Add 30 ml (excess) of the respectable surfactant solution into the beaker.
7. Place each of the beakers into the heated ultrasonic bath for 30 minutes ($T_{water} = 40\ ^{\circ}C$) (Figure 3.2).
8. Stir occasionally.
9. Measure the pH of each of the samples.
10. Filter the mixture under vacuum filtration (Figure 3.3).
11. Rinse the beaker with distilled water.
12. Place the residue in the muffle oven at 100 °C for 30 minutes.
13. Place the powder samples into well-labeled vials (air-tight) for surface characterization analysis.

The above procedure was also used to prepare the copper powder samples using butylamine and benzenethiol as surfactants.

To prepare the copper powder coated with polyacrylic acid the following procedure was used:

1. Wash all glassware with acetone, nanopure water and dry in an oven at 400 °C overnight.
2. Prepare surfactant solutions containing 0.5 M and 1.0 M polyacrylate acid.
    a. 0.5 M Surfactant Solution: Dissolve 4.7 g of sodium polyacrylate (Aldrich, Table 3.1) in 25 ml of nanopure water. When dissolved, transfer the solution to a 100 ml volumetric flask. Dilute to volume with nanopure water and mix thoroughly.
    b. 1.0 M Surfactant Solution: Dissolve 9.4 g of sodium polyacrylate (Aldrich, Table 3.1) in 25 ml of nanopure water. When dissolved, transfer the solution to a 100 ml volumetric flask. Dilute to volume with nanopure water and mix thoroughly.
3. Label 3 beakers: control, 0.5 M and 1.0 M polyacrylic acid
4. Repeat steps 4 to 13 on pages 22 and 23.

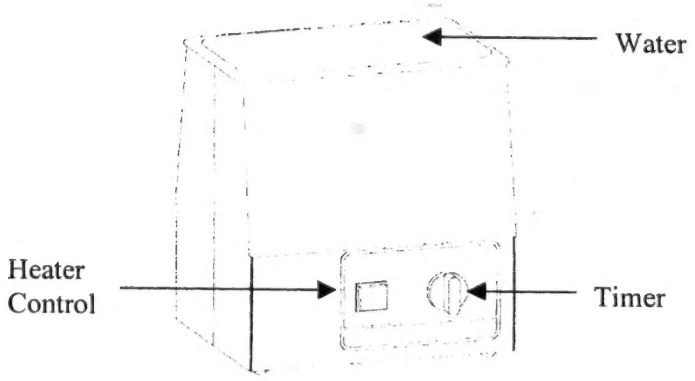

Figure 3.2 Fisher Ultrasonic Bath

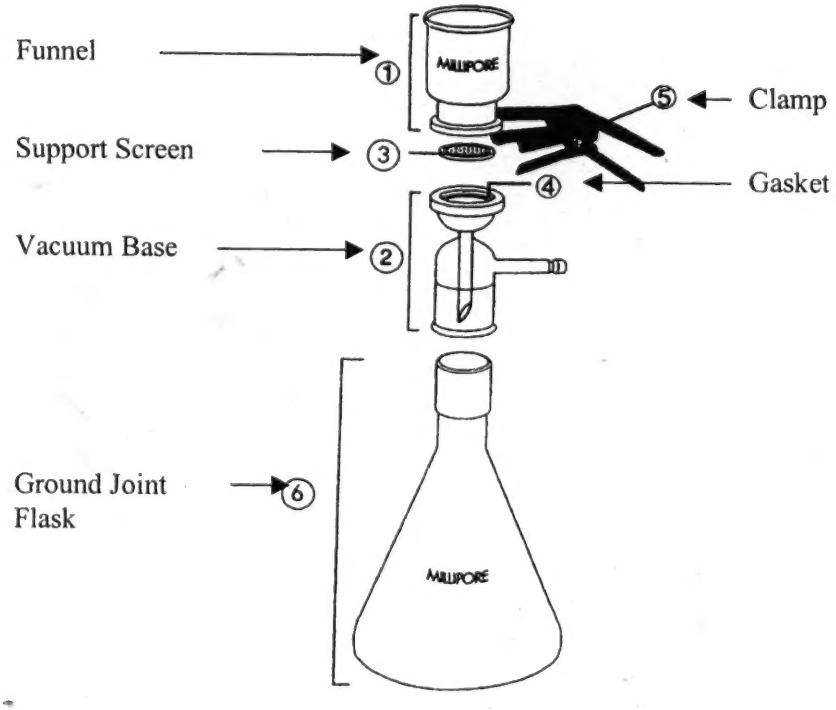

Figure 3.3 Millipore 47 mm all glass vacuum filter holder

Figure obtained from http://www.millipore.com *(Viewed May 02, 2005)*

3.3 X-ray Photoelectron Spectroscopy (XPS)

3.3.1 Introduction

X-ray photoelectron spectroscopy (XPS) is a surface sensitive spectroscopic technique used to characterize surface composition and elemental oxidation state. The surface of a material is probed with photons at a depth of 50 to 100 Å. XPS provides elemental identification and oxidation state information at the surface for all elements with $z \geq 3$ (Nelson and Wanke, 2005). Samples are placed in a high vacuum chamber and bombarded with a beam of photons and as a result, core and valence electrons are ejected. This process is illustrated in Figure 3.4.

In order to obtain information about the chemical environment and bonding nature of a species, it is necessary to determine the binding energies of the core and valence electrons (Thomas and Thomas, 1997). XPS measures the kinetic energy of the emitted electrons with respect to the zero level of the spectrometer (Thomas and Thomas, 1997). Thus, from the kinetic energy and the known value of the incident radiation beam, it is possible to determine the binding energy of an electron (Equation 9).

$$E_k = h\nu - E_B - \phi \qquad (9)$$

where E_k is the measured kinetic energy, $h\nu$ is the energy of the incident radiation, E_B is the binding energy of the electron in the sample and ϕ is the work function. The resulting spectrum from the analysis consists of the peak intensity as a function of binding energy. The chemical composition of a sample is determined from the survey spectrum and Equation 10.

$$C_E(\%) = \frac{I_i / RSF_i}{\sum I_i / RSF_i} 100\% \qquad (10)$$

where C_E *(%)* is the percent elemental composition, I_i is the intensity (in XPS analysis, the intensity is equivalent to the area under the peak) and RSF_i is relative sensitivity factor for the element of interest. The following RSF values were used to calculate the elemental composition; C = 0.318, O = 0.736, Cu = 4.871, N = 0.505, S = 0.723, and Na = 1.378.

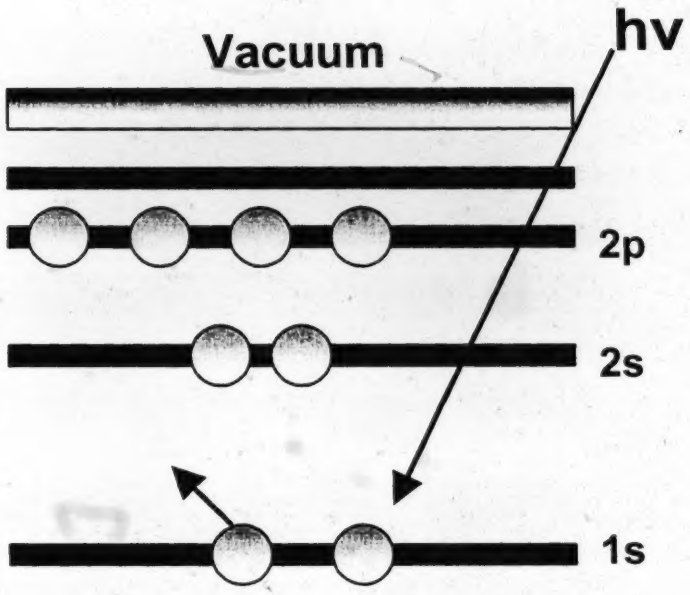

Figure 3.4 The photoemission process

Figure adapted from www.lasurface.com (Viewed April 28, 2005)

3.3.2 Sample Preparation

Care must be taken to prevent contamination of the powdered samples prior to analysis. Until the samples were analyzed, all finely powdered samples were stored in their original glass vials, which were packaged inside plastic lined aluminum bags (Cu and Ni powdered samples for process characterization were obtained from Umicore Canada Ltd). The copper samples coated with a surfactant were kept in aqueous phase during all reactions to minimize oxidation in the atmosphere.

The analysis copper stubs (diameter 12 mm OD) were cleaned with ethanol to remove any residue and then air-dried. Carbon tabs (12 mm OD, PELCO) are inserted into the copper stubs. Immediately prior to XPS analysis, each vial was opened in the normal air of the room where the XPS was kept and a small, 50 to 100 mg, portion of the sample was removed with a clean nichrome spatula and placed onto the carbon tab. The powder is then compressed slightly with a clean metal die (diameter 12 mm). Excessive force is not used to ensure that the particle structures are not changed to avoid unnecessary heat induced oxidation

3.3.3 Experimental Method

The Axis HSi 165 XPS analysis system is equipment with 3 main chambers – the loading chamber, transfer chamber and analysis chamber as shown in Figure 3.5.

Samples are placed on a sample stub and loaded into the loading chamber. In this particular chamber, the samples were degassed until a pressure of $\sim 2.5 \times 10^{-7}$ torr is achieved. Degassing takes approximately 30 minutes. The sample was then transferred through the transfer chamber into the analysis chamber. In the analysis chamber, the sample was irradiated with a beam of x-rays (Briggs, and Seah, 1983). Conventional x-ray beams consist of either Al $k\alpha$ (1486.6 eV), Al mono (monochromatic Al) or Mg $k\alpha$ (1253.6 eV) (Nelson and Wanke, 2005). XPS analysis was used to generate a survey and a narrow scan spectrum (Nelson and Wanke, 2005). The survey scan was used to obtain elemental identification and compositional information (concentration of each of the elements that are present in the sample), whereas, the narrow scan was used to determine the exact binding energy of a given element. In turn, we can obtain oxidation state information (Nelson and Wanke, 2005).

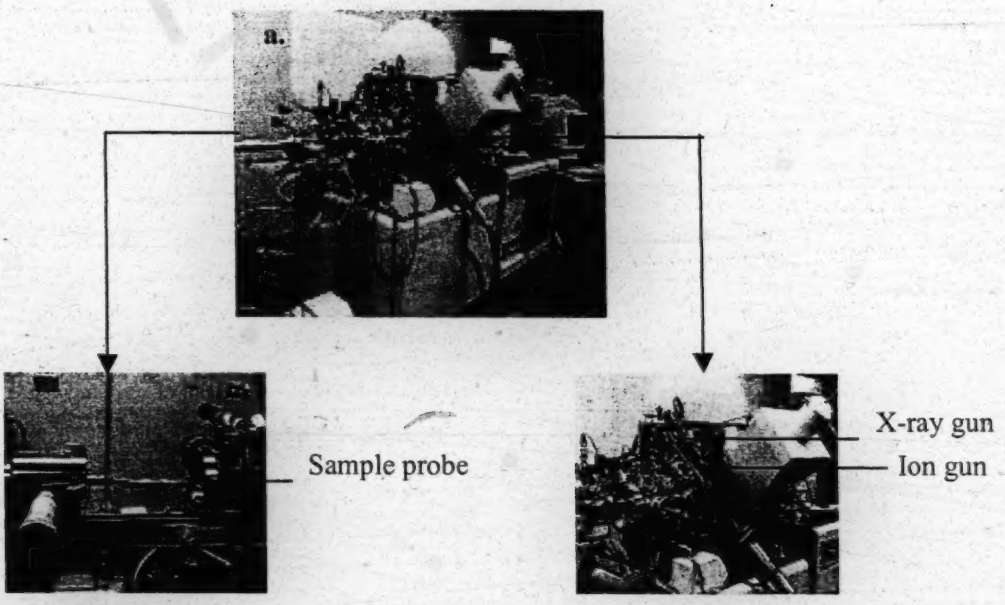

Figure 3.5 Kratos Axis His 165 System. Figure 3.5a indicates the relationship of the major components, including the loading chamber, x-ray source, ion source and analysis chamber in the AXIS His 165 XPS analysis system. As shown in Figure 3.5 b, the copper powders were mounted on the end of the sample introduction probe. The x-ray source is located perpendicular to the analyzer axis and the ion beam is nearly normal to the surface of the sample (Figure 3.5c). In the analysis chamber, an x-ray beam strikes the sample and the detector measures the kinetic energy of the emitted electrons.

The XPS data for the supported nano-particles were collected using a Kratos Axis His 165 spectrometer with either Mg $k\alpha$, or Al mono $k\alpha$ radiation (see Tables 3.3 to 3.6). The data were collected at a tilt angle of 0 ° and analyzed using a hemispherical analyzer. A charge neutralizer was also used to ensure that the surface of the metal powders was not charging. Furthermore, survey scans were performed with pass energy of 120 eV and narrow scans at pass energy of 20 eV.

The software, SDP Version 4.0 (Copyright 2004, XPS International®), was used to peak fit each of peaks obtained from the narrow scan spectra. This software allows the user to control the full width at half maximum (FWHM) value of any peak, binding energy of any peak, peak areas, the energy difference between the maximum of two peaks and the percentage asymmetry of any peak. A reduced chi-squared value was used to indicate the goodness of a peak fit. Additionally, a Shirley-type baseline was used for all peak fits. Using a Gaussian-Lorentian ratio between 80:20 and 90:10, the optimization of the peak shapes for the main XPS signals was possible.

3.3.4 Chemicals used as standards

By comparing the binding energy and the intensity of the samples to known standards, the oxidation state of the sample can be determined. Since the binding energies of the core and valence electrons provide information about the local chemical environment and bonding, small changes in binding energy indicate a different oxidation state. For example, Cu^0 and Cu^{+2} represent different oxidation states, thus XPS will measure different binding energies and the Cu 2p peaks shapes will also be very different. The relative intensity of the XPS peaks will depend on the concentrations of atoms of an element in the surface of the metal, the probability of photoemission occurring for a particle core level and the efficiency of the spectrometer to detect electrons as a function of kinetic energy (Attard and Barnes, 1998). Table 3.2 indicates the standards that were analyzed in the XPS analysis.

Table 3.2. Chemicals used for preparation of standards

Compound	Purity	Other Info	Supplier
Copper foil	99.99+ % (metals basis)	0.127 mm thick	Alfa Aesar
Copper (II) oxide	99.995 % (metals basis)		Alfa Aesar
Nickel foil	99+ % (metal basis)	0.127 mm	Alfa Aesar
Nickel (II) oxide	99.998 % (metals basis)		Alfa Aesar
Nickel (II) black	Ni 76 %	contains Ni_2O_3	Alfa Aesar

3.3.5 Analysis Conditions

Tables 3.3 to 3.5 describe the settings that were used during analysis. Using these parameters in all sample analysis ensures reproducibility of the data. Table 3.6 describes charge neutralizer operating parameters. A charge neutralizer is a special feature of the XPS instrument that grounds the particles in a powdered sample to make certain that they do not build up a static charge. The filament current, filament basis and charge balance values are preset to ensure that the filament does not burn out. The aluminum (mono) source was used to analyze the copper and nickel standards and the copper samples along the production pathway to obtain well-defined peak shapes. The disadvantage of using this source is that the peak intensity is significantly less in comparison to peaks obtained using a magnesium source. As a result, it may be difficult to observe a low intensity peaks. A low step size of 0.1 eV was used to collect more data points. The pass energy indicates the kinetic energy of the particles that can pass through the analyzer to the detector. The magnesium source was used to study the samples coated with a surfactant. The peaks in the survey and narrow scans were resolved using this particular source.

Table 3.3: Analysis conditions for the copper and nickel standards and the samples studied in copper production process

Sample	powder
Lens mode	hybrid
Source	Al mono
Analysis source characteristic energy	1486.71 eV
Dwell time for survey and narrow scans	120.0 ms
Pass energy (survey scans)	120 eV
Pass energy (narrow scans)	20 eV
Step size	0.1 eV
Sweeps (survey scan)	3
Sweeps (narrow scan)	12
Charge neutralizer	Yes
Spot size	700 × 300 μm

Table 3.4 Analysis Conditions for the samples obtained in Nickel Production

Sample	powder
Lens mode	hybrid
Source	Magnesium
Analysis source characteristic energy	1253.6 eV
Dwell time for survey and narrow scans	120.0 ms
Pass energy (survey scans)	120 eV
Pass energy (narrow scans)	20 eV
Step size	0.1 eV
Sweeps (survey scan)	3
Sweeps (narrow scan)	12
Charge neutralizer	Yes
Spot size	700 × 300 μm

Table 3.5 Analysis Conditions for the samples obtained in Copper coated with propylamine, butylamine, benzenethiol and polyacrylic acid

Sample	Powder
Lens mode	Hybrid
Source	Magnesium
Analysis source characteristic energy	1253.6 eV
Dwell time for survey and narrow scans	120.0 ms
Pass energy (survey scans)	120 eV
Pass energy (narrow scans)	20 eV
Step size	0.1 eV
Sweeps (survey scan)	3
Sweeps (narrow scan)	12
Charge neutralizer	Yes
Spot size	700 × 300 μm

Table 3.6 Charge Neutralizer Operating Settings

Filament current	1.7A
Filament basis	1.1 V
Charge balance	1.8 V

3.4 Scanning Electron Microscopy (SEM) and Energy Dispersive Spectroscopy (EDS)

3.4.1 Introduction

Scanning electron microscopy (SEM) is an electron-based visualization technique used to determine the size and shape of particles. During analysis, the area to be examined is bombarded with a finely focused electron beam (Niemantsverdriet, 1993). Both elastic and inelastic scattering produces detectable signals from the emitted secondary electrons (Goldstein et al. 1981). Local topography is determined from the magnitude of these signals. The SEM micrograph is generated when the electron beam is swept across the surface of the sample.

The basic components of the SEM are the lens system, electron gun, condensing and objective lens, the electron beam and the detector and amplifier. These components are shown in Figure 3.6.

Energy dispersive spectroscopy (EDS) is an experimental technique that is used in conjunction with SEM, and thus additional sample preparation is not necessary. EDS is not a surface technique because the x-rays originate from a depth of up to 2 micrometers in the sample (Nelson and Wanke, 2005).

EDS is based on the emission of x-rays from a sample. When an incident beam of electrons impacts a sample surface, empty holes in the electron shells are evident (Figure 3.7). If the holes are present in the inner shell, atoms are not stable. As a result, stabilization is achieved if the electrons from the outer electron shell drop to the inner electron shell. When electrons drop from a high energy to a lower energy, x-rays are emitted. These x-rays are collected and analyzed to provide qualitative and quantitative information.

Energy dispersive x-ray analysis was used to determine the composition of a sample. The analysis quantifies the elements by determining the area under each peak in the spectrum. It accounts for accelerating voltage of the electron beam that is necessary to produce the spectrum. Sensitivity factors are then used to convert the area under each peak into atomic percent.

EDS uses a lithium drifted silicon detector. When x-rays strike the detector, a photoelectron is generated within silicon. Electron-hole pairs are generated as the photon

electron travels through Si. A strong electric field allows electrons and holes to be attracted at opposite ends of the detector (Nelson and Wanke, 2005). The quantity of electron hole pairs that are produced is dependent on the energy of the incident ray.

3.4.2 Sample Preparation

The powder sample was deposited on a carbon tab (12 mm OD, PELCO) that was mounted 0.5 in. sample holder. Carbon adhesive tabs are the most common material for sample mounting as it allows for the conduction of charge, is inexpensive and invisible to x-rays. A conductive surface is necessary because electrons tend to accumulate on the surface of the metal and the images cannot be collected. The conductive surface grounds the sample to prevent sample charging. The powder was not crushed as it may alter the morphology of the sample. All images and data obtained from SEM (scanning electron microscope C-2700) and EDS were obtained from Tina Barker (Department of Chemical and Materials Engineering, University of Alberta).

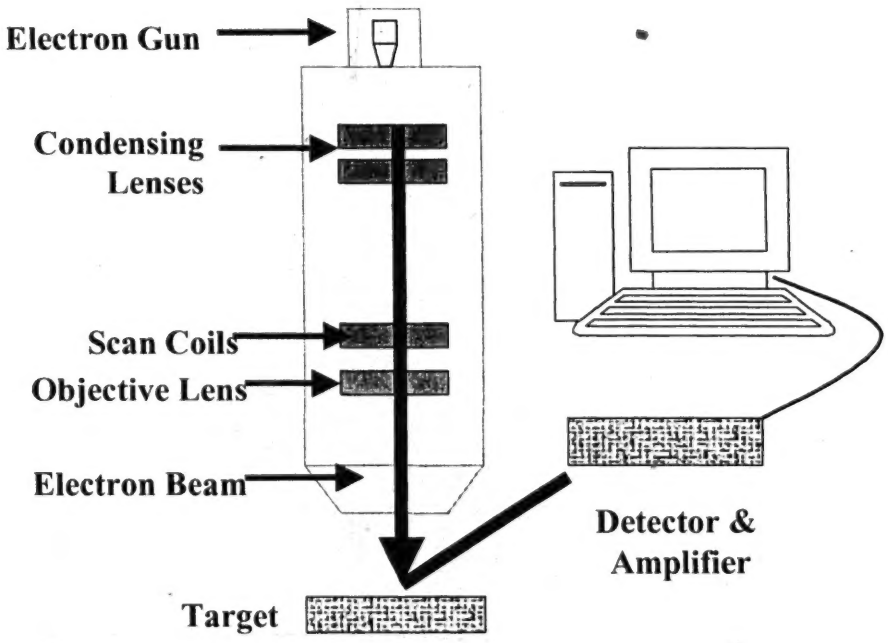

Figure 3.6: The scanning electron microscope.

Figure adapted from http://www.mos.org/sln/SEM/works.html (Viewed April 28, 2005)

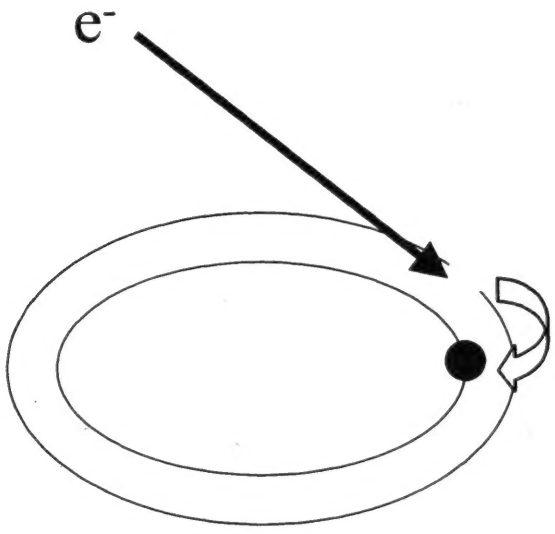

Figure 3.7: Energy Dispersive Spectroscopy

Figure adapted from http://www.seallabs.com/howedx.html *(Viewed May 02,2005)*

3.4.3 Experimental Method

Once the powdered sample was mounted on the sample holder, it was placed into the microscope vacuum column through an airtight door. Up to 5 samples can be analyzed at a given time. Air was pumped out of the column for approximately 5 minutes to achieve high vacuum. An electron gun emits an electron beam and the beam travels down a column of lenses (condensing and objective lenses) that are used to focus the electron beam. The scan coils, above the objective lens, move the focused electron beam back and forth across a sample. As the electron beam is emitted onto each spot on the surface of the powder, secondary electrons are emitted from the surface. A detector counted these electrons and the signal is sent to the amplifier, and an image is produced from the number of electrons that are emitted from a sample.

In EDS analysis, the characteristic x-rays are produced when a material was bombarded with electrons at an accelerating voltage of 20 keV in an electron beam instrument. A silicon detector collected the x-rays and the energy is measured. The specific energies of the characteristic x-ray peaks for each element are tabulated in a data library. Consequently, the benefit of using SEM in conjunction with EDS is that it is possible to obtain both qualitative and quantitative data.

3.4.4 Analysis Conditions

In the EDS analysis of the copper coated particles, some specific parameters were used. To provide adequate over voltage to excite x-ray lines in the range of 1 to 10 keV, a beam energy of 20 keV was used. This acceleration voltage is a good comprise between the need for adequate voltage and need to minimize absorption in the sample. Absorption in the samples tends to increase the beam energy and the penetration depth (Goldstein et al., 1981). The take off angle or the angle at which x-ray are removed from the sample was 30.5 °. The sample was not tilted in the sample holder, and thus, the tilt angle was 0°. For EDS operating at its best energy resolution, the total spectrum count rate was 150 counts per second. EDS systems with a high count rate leads to the introduction of artifacts. Lastly, the data was collected and corrected using the ZAF (Z = atomic number, A = absorption and F = fluorescence) correction factors.

3.5 Infrared Spectroscopy

3.5.1 Introduction

Infrared Spectroscopy (IR) involves the study of interaction of electromagnetic radiation or light with matter, and is used to determine molecular structure (Nelson and Wanke, 2005). IR can also be used analytically to assess the purity of a sample (Niemantsverdriet, 1993).

Infrared refers to the visible and microwave regions of an electromagnetic spectrum. The waves differ from one another in the frequency and length. The frequency (ν) of a wave refers to the number of wave cycles that passes through a point in one second (measured in Hertz) while the wavelength (λ) is the length of one complete wave cycle (measured in centimeters). These parameters are related by the following equation:

$$\nu = \frac{c}{\lambda} \qquad (11)$$

where, c is the speed of light ($3\times10^{10}\,\mathrm{cm/sec}$). Furthermore, the wavenumber is also related to the wavelength by:

$$\bar{\nu} = \frac{1}{\lambda} \qquad (12)$$

The energy of the waves is also related to frequency and wavelength by:

$$E = h\nu = \frac{hc}{\lambda} \qquad (13)$$

where, h is Planck's constant = $6.6\times10^{-34}\,J/\mathrm{sec}$.

The importance of frequency of electromagnetic radiation involves the interaction between the electromagnetic alternating field and the vibration of atoms in a molecule. Thus, the IR instrument measures the vibrational frequency between molecules in a

sample and with the use of Equation 13, the OMNIC software determine the wavelength of the molecule. It is convenient to define wavelength and frequency in terms of wave number (Equation 12) in order to distinguish and correlate the various spectral features that are present when copper is coated with a surfactant. The stretching and bending vibrations form the IR spectrum. Both of these particular vibrations allow for the determination of functional groups and structural characteristics of the copper coated samples.

3.5.2 Sample Preparation

The following procedure was used to prepare the copper powders for analysis using the Nicolet 8700 spectrometer. In DRIFTS mode, it was not necessary to dilute the sample with KBr, and as a result, approximately 0.50 g of copper powder was added to a mortar and ground to a very fine powder. It was necessary to ensure that only fine particulates are evident as they reduce the possibly of reflectance in the spectrometer. The powder was transferred to the sample slide.

A background scan was collected before every sample. The sample slide was then placed into the Smart Collector Apparatus in the Nicolet 8700 spectrometer, and a sample spectrum was collected. Collecting a background scan prior to running a sample more closely pairs the energy of the background and environmental contamination to the sample data collection. It is also important that the background collection represents the experimental conditions used to sample data collection because the single beam of the background is used as a ratio against the single beam of the sample to produce a spectrum. The ratio represents a measurement of the maximum energy available at every wavelength that may be absorbed by the sample (OMNIC operations manual, 2005)

3.5.3 Experimental Method

Molecules in a sample absorb infrared radiation. In essence, an incident beam of IR radiation strikes the sample and interacts with the active dipoles in or on the material. During vibrations, the dipole moment must change. There are two dominant types of molecular vibrations, bending and stretching (Niemantsverdriet, 1993). Stretch vibrations refer to the changing of the bond strength. Bending vibrations refer to changes in bond

angles while the bond lengths remain unchanged. Bending vibrations out of plane is also evident. In this case, one atom oscillates through a plane containing three neighboring atoms (Nelson and Wanke, 2005).

Absorption is evident only when the radiant energy matches the energy of a specific molecular vibration (Niemantsverdriet, 1993). In other words, only certain molecular vibrations can be detected. The selection rules are based on molecular symmetry.

Diffuse reflectance infrared Fourier-transform infrared spectroscopy (DRIFTS) is used for loose powders. DRIFTS is a technique that collects and analyzes scattered energy (OMNIC operations manual, 2005). When energy enters a sample, it can be either reflected off of the surface of the particle or transmitted through the particles. Thus, at the sample surface radiation is reflected, absorbed, scattered and transmitted. The diffusively scattered radiation is then captured by an ellipsoidal mirror and is then focused on a detector (Figure 3.9).

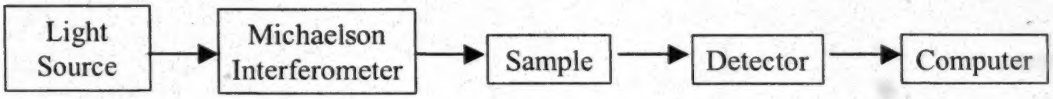

Figure 3.9 Schematic diagram for a typical IR system.

If weak signals are obtained, the sample must be ground and mixed with a non-absorbing matrix such as KBr. Dilution is necessary to ensure a deeper penetration of the incident beam into the sample.

DRIFTS is a low energy technique. As a result, the number of scans is increased to improve the signal to noise ratio (OMNIC operations manual, 2005). A Kubelka-Munk conversion must be applied to a diffuse reflectance spectrum to account for the differences that are evident when a reflectance spectrum is transformed into its transmission equivalent (Niemantsverdriet, 1993). In other words, the units were developed to account for the fact that the band intensities of the diffuse reflectance spectrum are proportional to concentration and molar absorptivity and inversely proportional to the scattering coefficient.

The Kubelka-Munk equation is expressed as;

$$F(R) = \frac{(1-R)^2}{2R} = 2.3\frac{ac}{s} \qquad (14)$$

where R is the absolute reflectance of the layer, a is the absorptivity, c is the concentration, and s is the scattering coefficient.

Equation 14 expresses a linear relation of spectral intensity with the concentration of a sample. The expression assumes infinite sample dilution in a non-absorbing matrix, a constant scattering coefficient, and an infinitely thick sample layer (Niemantsverdriet, 1993). The OMNIC software does an automatic conversion of either transmission or absorption into Kubelka Munk units.

3.5.4 Experimental Parameters

The parameters in Table 3.7 were used in the analysis. The Nicolet 8700 spectrometer used a DTGS-TEC detector and a potassium bromide beam splitter. These are fixed parameters. Resolution refers to the ability of the instrument to detect spectral features. Thus, with a resolution of 4 cm^{-1}, it was possible to distinguish between closely spaced frequencies. In infrared spectroscopy, it is desired to have the highest possible signal to noise ratio. Increasing the number of scans of the sample beyond 132 scans does not bring about a significant increase in the signal to noise ratio.

The velocity parameter refers to the speed with which the moving mirror moves inside the interferometer. This setting is highly dependent on the type of detector. Since the DRIFTS mode was used in sample analysis, the final format of the data uses Kubelka-Munk units.

Table 3.7: IR operating parameters for all copper and nickel analysis

Detector	DTGS – TEC
Beamsplitter	KBr
Max range limit	4000 cm^{-1}
Min range limit	400 cm^{-1}
Velocity	0.6329 cm/s
Number of scans	132
Resolution	4 cm^{-1}
Final format	Kubelka-Munk

3.6 Differential Scanning Calorimetry (DSC) and Thermogravimetric Analysis (TGA)

3.6.1 Introduction

Thermogravimetry is an experimental technique in which the mass changes of a substance are measured as a function of temperature in a thermobalance. A thermobalance is a combination of an electron microbalance, a temperature programmer and a computer. The experimental set-up in Figure 3.7 allows the sample to be simultaneously weighed and heated or cooled in a controlled manner (Haines, 2002). The thermal analysis system consists for four major components; (1) a sample holder, (2) sensors that detect and measure properties of a sample and thermocouples are used to measure temperature, (3) an enclosure in which temperature, pressure and gas atmosphere can be controlled, and (4) a computer that is used to control the experimental parameters. The hardware also collects the data.

Mass losses are detected if a volatile component such as a coating are lost. Thus, TGA results are often presented as the rate of mass loss against time. The derivative of the original experimental curve is taken to give dm/dt or d%/dt.

An important accessory in measuring the changes in mass of a sample is the balance. Approximately 1.5 g of the powdered sample is inserted in an alumina crucible, which is placed on a rigid vertical support above a balance beam. Convection baffles are used to protect the suspension system and they prevent hot gases from rising as this affects the balance mechanism. The furnace surrounds the microbalance and sample holder.

For experiments that require temperatures up to 1100 $^{\circ}$C, resistive alloy wires, such as Nichrome, are wound on a ceramic or silica tube. The alloy wires are coated with furnace cement and the tube is mounted in a metal container packed with insulation material (Haines, 2002). The outer wall is kept at lower temperatures with the use of a cooling water jacket. In the surfactant-metal studies, the powdered samples were placed into aluimina crucibles.

The alumina crucibles are inert with respect to most gases and molten inorganic materials. They are resistant to high temperatures and only melt when exposed to temperatures greater that 1769 $^{\circ}$C. Advantages of using these particular crucibles includes

that the alumina ensures that the heat capacity is low. In turn, the crucible follows the furnace temperature without lags in temperature (Haines, 2002).

3.6.2 Sample Preparation

The surfactant – metal studies were carried out using the Netzsch DSC-TGA. An alumina crucible was soaked in 50 % nitric acid for 30 minutes, rinsed with distilled water and dried. This acid treatment removes any copper film that is baked onto the surface of the alumina crucible. Once the crucible was clean and dry, ~ 1.5 g of the copper coated sample was alumnia crucible. The crucible was then tapped gently on a hard surface to even out the powder.

3.6.3 Experimental Method

The sample was placed onto a sample holder in the Netzsch DSC-TGA in a temperature-controlled environment with a thermocouple. The furnace was moved to ensure that the sample holder was located in the center of the oven and is completely sealed from the environment. The atmosphere around the sample is also controlled by purging the oven with nitrogen gas from a cylinder. The microbalance connected to the sample was used to measure the mass of the sample. CS-32 controllers were used to control the power supply, signal amplification, and temperature measurements.

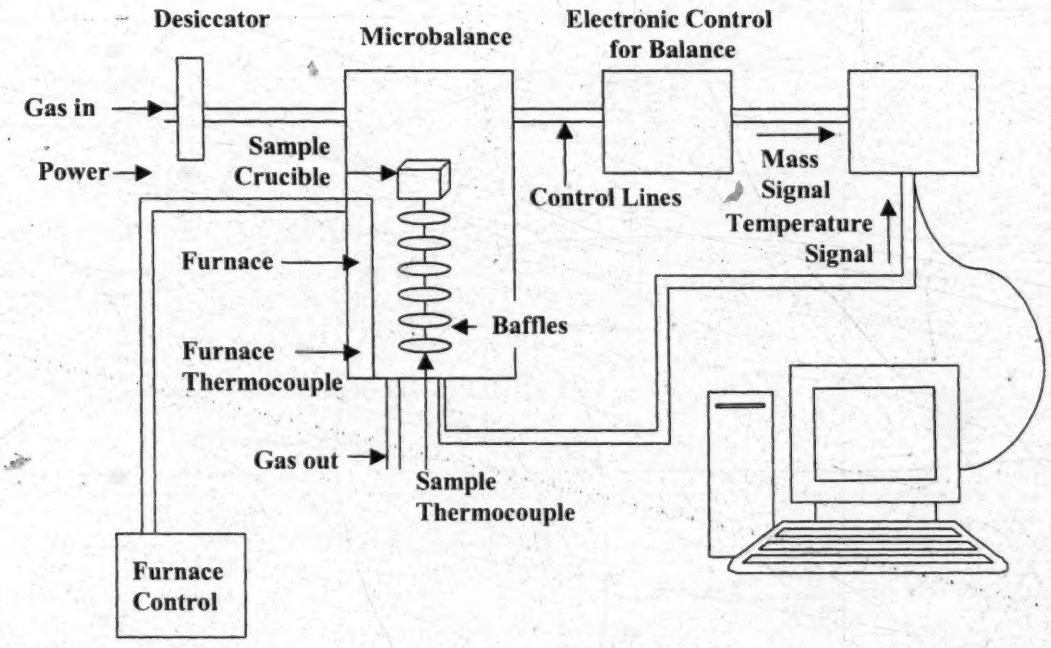

Figure 3.10 Schematic diagram of the thermo-gravimetric system.

Adapted from Haines, P.J .2002. Principles of Thermal Analysis and Calorimetry, RSC Paperbacks, Survey, UK. Page 14.

3.6.4 Analysis Conditions

Following sample preparation, experimental parameters were generated in the STA 409C program. The nitrogen flow rate was set at 10 ml/min. The inert flowed over the copper powder to prevent the sample from reacting with air. Any excess moisture in the gas was removed by passing it through a zeolite desiccator prior to contact with the sample. Next, the powdered sample was heated using the following temperature program. The sample was initially held at 25 °C for 15 minutes, and then the temperature was increased from 25 °C to 550 °C at a ramp rate of 10 °C/min. A heating rate of 10 °C/min is the recommended value to ensure good temperature equilibrium across the sample. The sample was then held isothermal at 550 °C for 15 minutes and cooled to ambient temperature. After 2 hours, the crucible was removed from the sample holder and the microbalance. The powdered residue was collected into a glass vial and kept for further IR and XPS analysis.

A blank run (the crucible is empty) was carried out on the balance before samples were used. This run determines whether random fluctuations are present and whether stability within the baseline is evident.

3.7 Particle Size Distribution Analysis

Particle size distribution analysis was performed in the analytical laboratory at Umicore Canada Ltd (Jody Pratch). The analysis was performed using the wet feeder in the Malvern Mastersizer 2000 instrument. Isopropyl alcohol, a dispersant was used to circulate the powder past the laser. Triton X-100 was also used as a detergent to aid in dismantling the agglomerated particles during sonication. Preparing the sample for analysis requires mixing a small amount of powder with one or two drops of surfactant and 50 to 100 ml of isopropyl alcohol. The mixture is then sonicated for 6 minutes. Following sonication, the dispersed powder is transferred to the Malvern 2000 instrument.

CHAPTER 4: RESULTS

4.1 Introduction

Nanometer sized metal particles are of large interest in current research as the materials exhibit unique physical and chemical properties. These materials will greatly advance diverse fields such as optics and electronics. Before studying the effect of surfactant addition on copper powder agglomeration, it is important to understand the properties of the powders throughout the production process.

Following the study of the production process, the raw copper powder was then coated with 1 vol%, 2 vol%, 5 vol%, and 10 vol% propylamine, butylamine, benzenethiol and polyacrylic acid (each surfactant was studied separately). The composition and oxidation state of the copper samples coated with a surfactant were investigated using XPS. XPS analysis on the coated copper powders provides insight into the changes in oxidation state and composition with changes in surfactant concentration. The survey scan of each sample was used to obtain the relative composition of each element. The narrow scan spectra were peak fitted to determine the binding energy. Furthermore, the binding energies were corrected for adventitious carbon assuming that the C 1s binding energy is 285.0 eV.

DRIFTS, or diffuse reflectance infrared fourier transform infrared spectroscopy, was used to collect and analyze scattered energy. A background single beam spectra, with nothing in the sample compartment, was collected before every sample. Spectra were collected for the duplicate samples of copper coated with propylamine, butylamine, benzenethiol and polyacrylic acid.

Thermogravimetric analysis (TGA) was used to determine whether the applied coating could be removed with exposure to elevated temperatures. The samples were then re-analyzed by IR and XPS to confirm that the coating was removed from the surface of the particles.

Electron microscopy is a straightforward technique used to determine the size and shape of the coated particles. SEM analysis on the particles after addition of the surfactant provides insight to whether the degree of agglomeration is lessened. Four categories were used to describe the images of the copper coated samples: Category A describes a state in which less than 25% of the particles are agglomerated; Category B

describes a state in which 25% the particles are agglomerated; Category C describes an environment in which 50% of the particles are agglomerated; In Category D, greater than 50% of the particles are agglomerated.

A laser diffraction particle size analyzer was used to determine the size of the copper particles. These results obtained from Umicore Canada are used as a quantitative measure to confirm the results gathered from SEM analysis.

The results from the above techniques are demonstrated in the following sections.

4.2 Overview of the Commercial Process

Industry produces high quality copper powders, as illustrated in Figure 4.1. A copper solution, water, organic additives, ammonium hydroxide and a reducing agent are added to a batch reactor held at 40 °C. Copper particles are suspended in an aqueous phase. The raw copper powder at this stage is obtained and used as the basis for coating the surface with a surfactant. As previously stated in chapter 2, in a commercial process, the precipitated copper particles are washed with water and spray dried at 100 °C. In our experimental procedure (Chapter 3), a surfactant is added to the raw copper powder at 40 °C in an ultrasonic water bath, filtered to remove the aqueous phase and then dried at 100 °C for 30 minutes in a drying oven.

Figure 4.1 Simplified flow sheet for the production of copper powders.

4.3 XPS Analysis of the Copper Powders

4.3.1 Analysis of Copper Standards by XPS

Initially, a series copper standards (obtained from Alfa Aesar) were analyzed with XPS. These standards were used as a basis of comparison for the subsequent determination of oxidation state. The binding energies of the copper samples are compared to the binding energies of the copper standards. Copper samples with a higher oxidation state consist of the valence levels of Cu 2p at a higher binding energy. In other words, a shift in chemical state is evident between metallic copper and Cu^{+2}. In order to produce metallic copper, copper foil was Ar^{+} sputtered to remove any deposited particles and/or oxide surface layer.

Figures A.1 and A.2 in Appendix A show representative survey and narrow spectra of copper metal and copper (II) oxide respectively. In these samples, the position and shape of the Cu $2p_{3/2}$ and Cu $2p_{1/2}$ peaks were analyzed to allow for discernment of metallic and oxidized copper.

Copper metal is identified by having two distinct and symmetric peaks, and copper (II) oxide is recognized by having broad, unsymmetric peaks. In addition, copper (II) atoms have a higher formal oxidation state, and in turn yield XPS peaks at a higher binding energy relative to the transitions for metallic copper.

Table 4.1 provides a summary of the observed binding energies and atomic concentration of the copper standards.

In respect to Cu^{0}, a binding energy shift of 0.6 eV is evident when corrected for adventitious carbon. The binding energies of the dominant Cu $2p_{3/2}$ and Cu $2p_{1/2}$ peaks are 932.9 eV and 951.7 eV, respectively. With an oxygen-to-copper ratio of 0.01, it can be concluded that the sample consists of copper metal and surface oxide layers are not present.

A binding energy shift of 0.7 eV is evident between the Cu^{0} and Cu^{+2} samples. The corrected binding energy of the dominant Cu $2p_{3/2}$ and Cu $2p_{1/2}$ are 933.6 eV and 953.4 eV, respectively, which are higher binding energies than metallic copper. Atomic concentrations indicate that the ratio of oxygen to copper in the sample is 1.25. Thus, it can be concluded the copper in this sample is +2 with the additional oxygen attributed to adsorbed carbon oxides (CO, CO_2).

Table 4.1 Summary of spectral features for copper standards

	Element / Transition	Binding Energy (eV)	FWHM (ev)	Conc. (at. %)	Oxygen to Cu Ratio
Cu Foil	C 1s	285.6 (285.0)	2.04	4.4	
	O 1s	532.0 (531.4)	1.64	0.7	0.01
	Cu 2p3/2	932.5 (932.9)	0.81	94.9	
	Cu 2p1/2	952.3 (951.7)	1.31		
Cu +2 Standard	C 1s'	284.7 (285.0)	1.09	23.3	
	C 1s"	285.5 (285.7)	1.11		
	C 1s '''	286.4 (286.6)	1.09		
	O 1s'	529.8 (530.1)	1.20	42.6	1.25
	O 1s"	531.3 (531.6)	1.19		
	O 1s'''	532.4 (532.7)	1.15		
	O 1s''''	533.6 (533.8)	1.09		
	Cu 2p3/2'	933.3 (933.6)	1.87	34.1	
	Cu 2p3/2"	934.9 (935.1)	1.88		
	Cu 2p3/2'''	941.5 (941.8)	1.90		
	Cu 2p3/2''''	943.8 (944.0)	1.90		
	Cu 2p1/2'	953.1 (953.4)	2.26		
	Cu 2p1/2"	954.8 (955.1)	2.22		
	Cu 2p1/2'''	960.9 (961.2)	2.14		
	Cu 2p1/2''''	962.5 (962.8)	2.02		

NOTE:
The values in parentheses are corrected binding energies assuming the C 1s photoemission band corresponds to carbon at 285.0 eV.
Atomic concentrations were quantified from the survey spectra.

4.3.2 Characterization of Commercial Copper Powders

The copper production process was studied to determine where particle agglomeration is the greatest, and to identify the optimum stage at which a surfactant can be added to suppress agglomeration. Figure 4.2 depicts the production flow diagram, and includes XPS and SEM data. During the production of copper powders, a copper solution, a reducing agent, water, ammonium hydroxide and organic additives are added to a reaction vessel. The copper powder is precipitated from solution, and the resultant powder is washed, filtered, dried, and screened to produce different grades of copper powder. Samples were obtained from various stages the production process for analysis. Additionally, two sample aliquots from two different batches were taken out of the reactor, with the first being a copper sample with an unknown coating and another sample that remained uncoated. Figure 4.2 also presents a summary of powder morphology and oxidation state information for the copper samples obtained throughout the production process. A detailed discussion of the XPS and SEM analysis follows in the subsequent sections.

Table 4.2 presents the XPS results for the various copper samples. These powders were exposed to magnesium radiation, with a characteristic energy of 1253.6 eV, under high vacuum conditions.

For the copper sample obtained following the reaction vessel (uncoated), the data indicates that Cu $2p_{3/2}$ is located at a binding energy of 933.3 eV and Cu $2p_{1/2}$ is located at 953.1 eV. When these binding energies are compared to the copper standard spectra, the binding energies are more closely associated with the +2 oxidation state. Furthermore, the O/Cu ratio of ~1 shows that the stoichiometry of oxygen to copper is 1:1 (Table 4.2). The binding energy and the O/Cu ratio correspond to the Cu^{+2} state.

Following washing and filtration, Cu $2p_{3/2}$ and Cu $2p_{1/2}$ are located at binding energies of 932.9 eV and 952.7 eV, respectively (Table 4.2). The Cu $2p_{3/2}$ and Cu $2p_{1/2}$ peaks are symmetric. The sample consists of 18.3 at.% oxygen (relative atomic concentration) and 15.2 at.% copper (relative atomic concentration). Thus, the O/Cu ratio of ~1.2 suggests that the stoichiometry of oxygen to copper is 1:1. The additional oxygen in this sample is attributed to adsorbed carbon oxides (CO and CO_2). The binding energy and the O/Cu ratio correspond to the Cu^{+2} state.

Spray drying does not change the copper oxidation state. The primary copper peaks are located at a corrected binding energy of 933.0 eV and 952.7 eV (Table 4.2). The survey spectrum is used to obtain the relative atomic concentrations of the elements in the powder. 16.0 at.% of the sample consists of oxygen while 12.4 at.% of the sample is composed of copper. This results in an O/Cu ratio of ~1.3.

The final step in the flow diagram (Figure 4.2) involves the classification of the powder. In this stage, the copper powder is classified according to the size of the particles. Cu $2p_{3/2}$ is evident at a corrected binding energy of 932.8 eV and Cu $2p_{1/2}$ is evident at 952.7 eV. The core energy level peaks are fairly symmetric. Relative atomic concentrations show that 15.9 at.% of the sample consists of oxygen while 14.1 at.% of the sample is copper. This results to O/Cu of ~1.1. Thus, the oxidation state is that of Cu^{+2}.

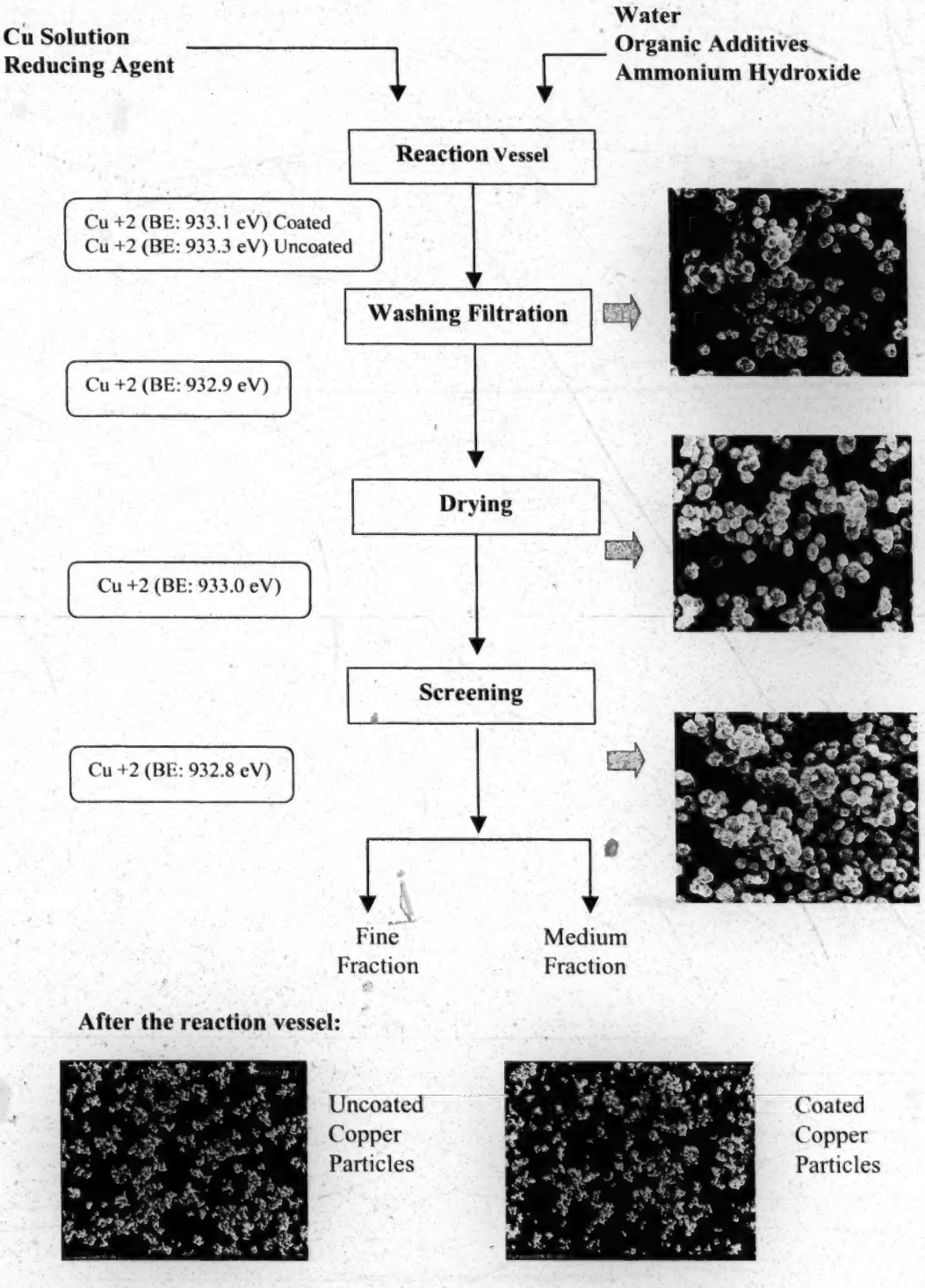

Figure 4.2 Copper flow diagram – changes in oxidation state and morphology

Table 4.2 Summary of spectral features from XPS for the copper process samples

	Element / Transition	Binding Energy (eV)	FWHM	Conc. (at. %)	Oxygen to Cu Ratio
Cu 2005-01-20A	C 1s'	283.1 (285.0)	0.79	71.5	
After Drying	C 1s"	283.7 (285.6)	0.89		
	C 1s '"	284.6 (286.6)	0.87		
	O 1s'	529.0 (530.9)	1.26	16.0	1.29
	O 1s"	530.3 (532.2)	1.28		
	O 1s'"	531.5 (533.4)	1.24		
	Cu 2p3/2'	931.1 (933.0)	1.22	12.4	
	Cu 2p3/2"	932.4 (934.4)	1.15		
	Cu 2p1/2'	950.8 (952.7)	1.24		
	Cu2p1/2"	952.0 (953.9)	1.30		
Cu 2005-01-20B	C 1s'	283.3 (285.0)	0.85	70.0	
After Screening	C 1s"	283.8 (285.6)	0.75		
	C 1s '"	284.5 (286.2)	0.78		
	O 1s'	529.1 (530.8)	1.11	15.9	1.13
	O 1s"	530.0 (531.8)	1.04		
	O 1s'"	530.8 (532.5)	1.00		
	Cu 2p3/2	931.1 (932.8)	1.59	14.1	
	Cu 2p1/2	951.0 (952.7)	1.67		
Cu 2005-01-20C	C 1s'	283.2 (285.0)	0.80	66.5	
After Filitration	C 1s"	283.8 (285.6)	0.84		
	C 1s '"	284.7 (286.6)	0.87		
	O 1s'	529.1 (530.9)	1.19	18.3	1.20
	O 1s"	530.3 (532.1)	1.22		
	Cu 2p3/2	931.1 (932.9)	1.40	15.2	
	Cu 2p1/2	950.9 (952.7)	1.46		
Cu 2005-01-20D	C 1s'	283.2 (285.0)	0.84	47.4	
After Reaction	C 1s"	283.8 (285.6)	0.88		
Vessel (coated)	C 1s '"	284.7 (286.5)	0.77		
	O 1s'	529.1 (530.9)	1.17	25.1	1.02
	O 1s"	530.2 (531.9)	1.17		
	O 1s'"	531.1 (532.9)	1.13		
	Cu 2p3/2	931.4 (933.1)	1.70	24.6	
	Cu 2p1/2	951.2 (952.9)	1.65		
	Si 2p	Small amount		3.0	
Cu 2005-01-20E	C 1s'	284.3 (285.0)	0.73	23.9	
After Reaction	C 1s"	284.8 (285.6)	0.81		
Vessel (uncoated)	C 1s '"	285.5 (286.2)	0.76		
	O 1s'	530.6 (531.3)	1.15	39.5	1.08
	O 1s"	531.8 (532.5)	1.10		
	Cu 2p3/2	932.5 (933.3)	1.36	36.6	
	Cu 2p1/2	952.3 (953.1)	1.39		

NOTE:
The values in parentheses are corrected binding energies assuming the C 1s photoemission band corresponds to carbon at 285.0 eV.
Atomic concentrations were quantified from the survey spectra.

4.3.3 Characterization of Propylamine ($CH_3CH_2CH_2NH_2$) Addition

The composition and oxidation state of the copper samples coated with *n*-propylamine was investigated using XPS. Figure A.4 a) and b) show representative survey and narrow spectra respectively of the effect of adding a surfactant.

In principle, a separate XPS peak and binding energy should be observed for every chemically distinct atom. In the copper control sample, binding energies of 933.1 eV and 952.9 eV (Table 4.3) are attributed to the core energy levels of Cu $2p_{3/2}$ and Cu $2p_{1/2}$ respectively. Figure A.3b exemplifies two symmetrical peaks with relatively no shoulders. When this figure is compared to Figure A.1b (Cu^0 standard), it is evident that the samples have a similar chemical state. Once again, the Cu 2p peaks in metallic copper are located at binding energies of 932.9 eV and 951.7 eV. The chemical shifts in the copper control samples are consistent with the copper metal standard.

When the copper powder is coated with 10 vol% propylamine, the core energy levels are shifted to a higher binding energy. There is a chemical shift of ~0.8 eV with respect to the binding energy of Cu 2p in Cu^0. From Table 4.3, the core energy levels of Cu $2p_{3/2}$ and Cu $2p_{1/2}$ are located at binding energies of 933.7 eV and 953.6 eV respectively. Figure A.4a illustrates the survey spectra of copper coated with 10 vol% propylamine, whereas, figure A.4b shows the narrow scan of the representative Cu 2p peaks. The narrow spectrum is consistent with the results of the copper (II) standard. The Cu $2p_{3/2}$ and Cu $2p_{1/2}$ peaks are not symmetric and have leading tails and large shoulder peaks. Copper has a +2 oxidation state.

A similar trend occurs when the copper particles are coated with 1 vol%, 2 vol% and 5 vol% propylamine. The binding energies of the core energy levels are shifted to a higher binding energy (Figure 4.3). The Cu 2p peaks are also significantly broader and non-symmetrical in comparison to the Cu 2p peaks in the control sample. Consequently, from peak fit results, copper adopts a +2 oxidation state.

The quantitative analysis of the XPS signals is based on the area of the peaks in the survey spectrum. The chemical composition (based on an average of the sample sets) of each of the samples is shown in Table 4.4. The surface of the particles is composed of approximately 30 at.% oxygen, ~20 at.% copper and ~10 at.% nitrogen and ~35 at.% carbon. The sample that serves as a control contains more carbon (48.4 at.%) in

comparison to the coated samples. The relative atomic ratio of O/Cu for the control sample is 0.7 and the relative atomic ratio of O/Cu for the Cu–10 vol% propylamine sample is also 0.7. The XPS results support the conclusion that the coated samples are composed of CuO and an amine constituent. Using the procedure in section 3.2, it is possible to coat the copper particles with propylamine.

4.3.4 Characterization of Butylamine ($CH_3CH_2CH_2CH_2NH_2$) Addition

XPS analysis on the copper powders provides an insight to the changes that occur in oxidation state and composition after addition of various amounts of butylamine (1 to 10 vol%). Table 4.5 illustrates a summary of the key spectral features.

In the copper control sample, binding energies of 933.3 eV and 953.1 eV (Table 4.5) are attributed to the core energy levels of Cu $2p_{3/2}$ and Cu $2p_{1/2}$ respectively. The data reveals that there is roughly a 0.4 eV shift of the Cu $2p_{3/2}$ peak toward higher binding energy in comparison to the binding energy of Cu $2p_{3/2}$ in the metallic copper standard. From Figure 4.4, the Cu $2p_{3/2}$ and Cu $2p_{1/2}$ peaks are very symmetrical without any tails or shoulders. When these peaks are compared to Figure A.1, it is evident that the samples have a similar chemical state. The chemical shifts in the copper control samples are consistent with the copper metal standard.

When the copper particles are coated with 1 vol%, 2 vol% and 5 vol% butylamine, the binding energies of the core energy levels are shifted to a higher binding energy (Figure 4.4 and Table 4.5). The Cu 2p peaks are also significantly broader and non-symmetrical in comparison to the Cu 2p peaks in the control sample. Consequently, from peak fit results, copper adopts a +2 oxidation state.

However, when the copper particles are coated with 10 vol% butylamine, the binding energy of the Cu $2p_{3/2}$ and Cu $2p_{1/2}$ peaks are very similar to the binding energy of the metallic copper standard. These copper peaks are symmetrical without any shoulder features. Unlike, the other coated copper samples, Cu-10 vol% butylamine has a metallic oxidation state.

The quantitative analysis of the XPS signals is based on the area of the peaks in the survey spectrum. The chemical composition (based on an average of the sample sets) of each of the samples is shown in Table 4.6. The surface of the copper particles is

composed of carbon, oxygen, nitrogen and copper. From Table 4.6, it is evident that the concentration of nitrogen increases with an increase in the amine concentration. The relative atomic ratio of O/Cu for the 1 vol% sample is 1.5, 2 vol% sample is 1.2 and for the 5 vol% sample the ratio of O to Cu is 1.4. This further concludes that the surface of the powder consists of a copper oxide layer. Thus, the XPS results support the conclusion that the coated samples are composed of CuO and an amine constituent. The ratio of O/Cu for the copper sample coated with 10 vol% butylamine is ~1.0. In this case, only a thin oxide layer is present on the surface. Using the procedure in section 3.2, it is possible to coat the copper particles with butylamine.

Table 4.3 Summary of spectral features for the copper-propylamine samples

	Element / Transition	Binding Energy (eV)	FWHM (ev)	Conclusions
Cu Control	Cu 2p3/2	932.4 (933.1)	1.41	
No Surfactant	Cu 2p1/2	952.2 (952.9)	1.40	Cu^0
Cu Powder &	Cu 2p3/2'	931.7 (933.7)	2.12	Cu^{+2}
1 vol% Propylamine	Cu 2p3/2"	933.6 (935.6)	2.15	
	Cu 2p3/2"'	940.5 (942.4)	2.10	
	Cu 2p3/2""	942.9 (944.8)	2.15	
	Cu 2p1/2'	951.7 (953.7)	1.67	
	Cu 2p1/2"	953.5 (955.5)	1.70	
	Cu 2p1/2"'	959.8 (961.8)	2.15	
	Cu 2p1/2""	961.6 (963.6)	2.10	
Cu Powder &	Cu 2p3/2'	931.7 (933.7)	2.15	Cu^{+2}
2 vol% Propylamine	Cu 2p3/2"	933.6 (935.6)	2.20	
	Cu 2p3/2"'	941.0 (943.0)	2.50	
	Cu 2p3/2""	943.0 (945.0)	2.48	
	Cu 2p1/2'	951.1 (953.1)	1.83	
	Cu 2p1/2"	952.6 (954.6)	1.90	
	Cu 2p1/2"'	961.0 (963.0)	1.89	
	Cu 2p1/2""	962.5 (964.5)	1.90	
Cu Powder &	Cu 2p3/2'	931.9 (933.6)	1.87	Cu^{+2}
5 vol% Propylamine	Cu 2p3/2"	933.7 (935.3)	1.92	
	Cu 2p3/2"'	941.9 (943.5)	1.70	
	Cu 2p3/2""	943.7 (945.3)	1.69	
	Cu 2p1/2'	952.0 (953.7)	1.76	
	Cu 2p1/2"	953.9 (955.5)	1.83	
	Cu 2p1/2"'	961.6 (963.2)	1.01	
	Cu 2p1/2""	963.1 (964.8)	0.90	
Cu Powder &	Cu 2p3/2'	931.9 (933.7)	1.87	Cu^{+2}
10 vol% Propylamine	Cu 2p3/2"	933.5 (935.4)	1.90	
	Cu 2p3/2"'	941.0 (942.9)	2.25	
	Cu 2p3/2""	942.9 (944.8)	2.20	
	Cu 2p1/2'	951.7 (953.6)	1.98	
	Cu 2p1/2"	953.7 (955.6)	1.95	
	Cu 2p1/2"'	961.3 (963.2)	1.47	
	Cu 2p1/2""	962.4 (964.3)	1.50	

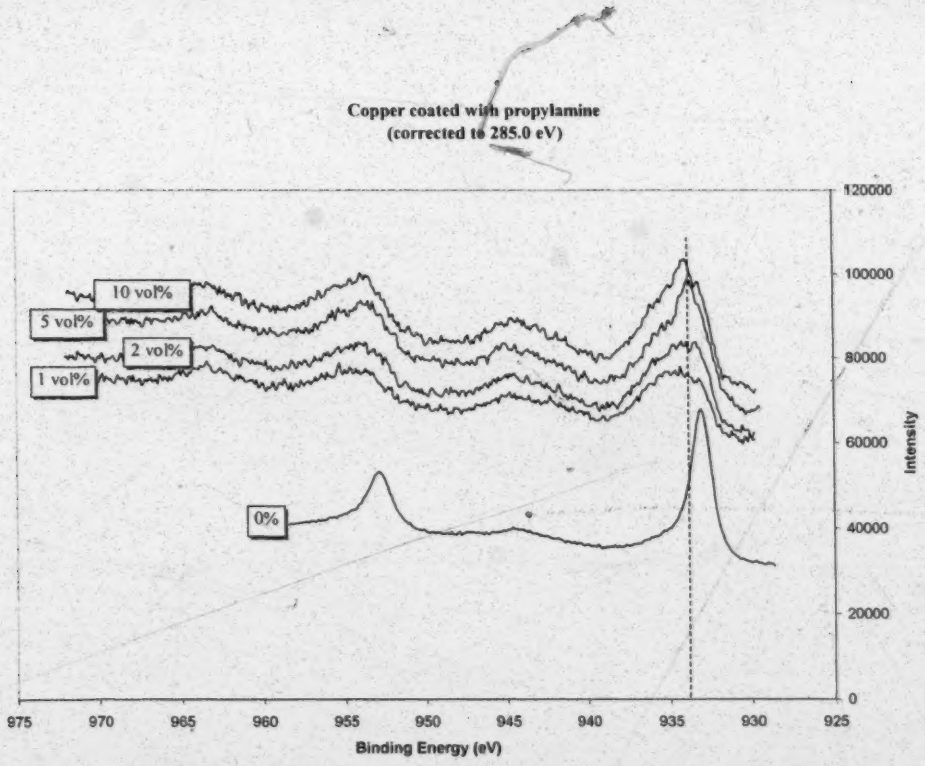

Figure 4.3 Comparing the binding energy of Cu 2p in the various copper propylamine samples

Table 4.4 Chemical composition of the copper - propylamine samples

Composition of the Copper / Propylamine Sample

	Control	**1 vol%**	**2 vol%**	**5 vol%**	**10 vol%**
C 1s	48.4	29.6	37.5	35.0	34.9
O 1s	30.0	37.1	35.4	32.4	29.8
N 1s		6.6	10.2	13.0	14.0
Cu 2p	21.6	26.7	16.9	19.7	21.3

Table 4.5 Summary of spectral features for the copper-butylamine samples

	Element / Transition	Binding Energy (eV)	FWHM (ev)	Conclusions
Cu Control	Cu 2p3/2	932.3 (933.3)	1.46	Cu^0
No Surfactant	Cu 2p1/2	952.1 (953.1)	1.46	
Cu Powder &	Cu 2p3/2'	932.2 (933.6)	1.98	Cu^{+2}
1 vol% Butylamine	Cu 2p3/2"	933.9 (935.3)	1.92	
	Cu 2p1/2'	951.9 (953.3)	2.07	
	Cu 2p1/2"	953.6 (954.9)	2.13	
Cu Powder &	Cu 2p3/2'	931.7 (932.7)	2.24	Cu^{+2}
2 vol% Butylamine	Cu 2p3/2"	933.4 (934.4)	2.28	
	Cu 2p3/2"'	940.6 (941.7)	2.25	
	Cu 2p3/2""	942.7 (943.8)	2.23	
	Cu 2p1/2'	951.3 (952.3)	2.14	
	Cu 2p1/2"	952.9 (954.0)	2.15	
	Cu 2p1/2"'	960.5 (961.6)	1.94	
	Cu 2p1/2""	961.8 (962.9)	1.95	
Cu Powder &	Cu 2p3/2'	931.5 (933.3)	2.25	Cu^{+2}
5 vol% Butylamine	Cu 2p3/2"	933.2 (934.9)	2.24	
	Cu 2p3/2"'	940.4 (942.2)	2.28	
	Cu 2p3/2""	942.5 (944.3)	2.24	
	Cu 2p1/2'	951.1 (952.9)	2.18	
	Cu 2p1/2"	952.7 (954.5)	2.20	
	Cu 2p1/2"'	960.9 (962.7)	1.15	
	Cu 2p1/2""	961.9 (963.7)	1.13	
Cu Powder &	Cu 2p3/2	932.3 (933.2)	1.22	Cu^{+2}
10 vol% Butylamine	Cu 2p1/2	952.1 (952.9)	1.43	

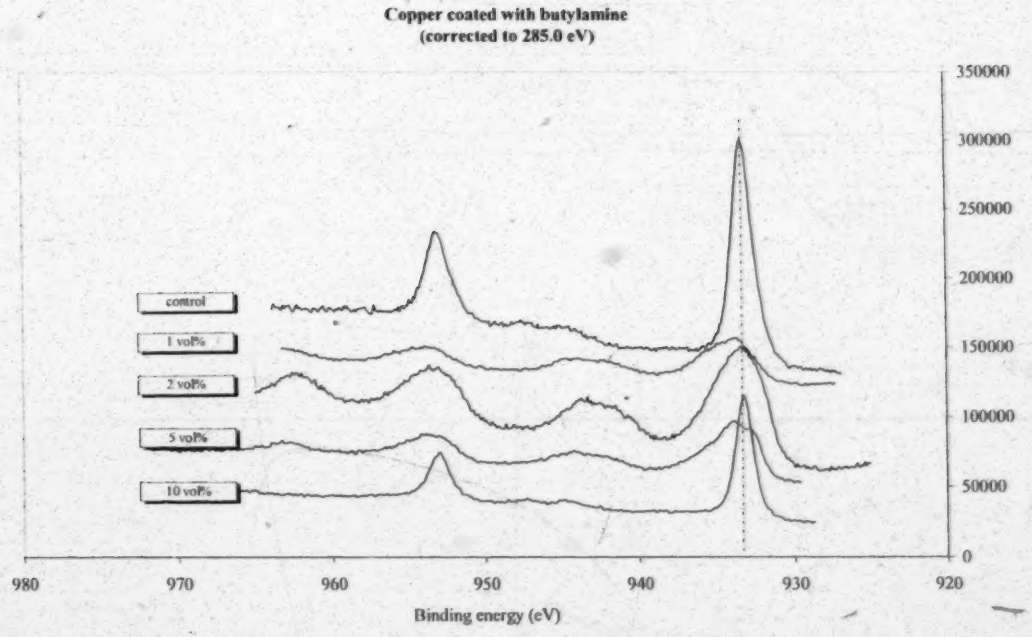

Figure 4.4 Comparing the binding energy of Cu 2p in the various copper butylamine samples

Table 4.6 Chemical compositions of the copper - butylamine samples

Composition of the Copper / Butylamine Sample

	Control	**1%**	**2%**	**5%**	**10%**
C 1s	41.5	45.6	45.0	38.2	45.9
O 1s	36.7	29.2	26.7	31.3	23.0
N 1s		5.9	7.5	8.3	8.5
Cu 2p	21.9	19.3	20.8	22.3	22.7

4.3.5 Characterization of Benzenethiol (C_6H_6S) Addition

Table 4.7 illustrates a summary of the key spectral features. A control sample is used as a source of comparison. It is apparent that by increasing the concentration of benzenethiol on the surface of the copper particles, the chemical shift towards higher binding energy also increases. In other words, there is an increased coulombic attraction between core electrons and the nucleus. When copper is coated with 10 vol% benzenethiol, there is a chemical shift of 0.53 eV (in comparison to Cu^0). The core energy levels, Cu $2p_{3/2}$ and Cu $2p_{1/2}$, are located at 933.5 eV and 953.2 eV, respectively. The peaks are non-symmetrical and they have a trailing edge (Figure 4.5). This sample has a +2 oxidation state.

The data in Table 4.7 and the Cu 2p peaks in Figure 4.5 shows that the oxidation state in the copper samples coated with benzenethiol (1 vol%, 2 vol%, 5 vol% and 10 vol%) is +2. A shift can be seen when the Cu 2p peaks are compared to the control sample. Thus, atoms in a high formal oxidation state yield peaks at higher binding energies relative to the same atom in a low oxidation state.

The chemical composition (based on an average of the sample sets) of each of the samples is shown in Table 4.8. The area of the peaks (Cu 2p, C 1s, O 1s, and S 2p) in the survey spectrum was used to calculate the relative composition. By increasing the benzenethiol content in the copper powder, the concentration of sulfur on the surface also increases. The copper control sample is composed of 53.3 at.% carbon, 28.2 at.% oxygen and 18.5 at.% copper. The 10 vol% benzenethiol-copper sample consists of 66.4 at.% carbon, 12.6 at.% oxygen, 8.1 at.% sulfur and 12.9 at.% copper. The carbon content in these samples is relatively higher compared to the copper samples that were coated with propylamine and butylamine. The ratio of oxygen to copper is 0.9. This further supports the fact that the oxidation state of copper in this sample is +2.

Table 4.7 Summary of spectral features for the copper – benzenethiol samples

	Element / Transition	Binding Energy (eV)	FWHM (ev)	Conclusions
Cu Control	Cu 2p3/2	932.4 (932.9)	1.27	Cu^0
No Surfactant	Cu 2p1/2	952.6 (953.1)	2.30	
Cu Powder &	Cu 2p3/2	932.6 (933.3)	1.23	Cu^{+2}
1 vol% Benzenethiol	Cu 2p1/2	952.5 (953.3)	1.30	
Cu Powder &	Cu 2p3/2	932.7 (933.5)	1.19	Cu^{+2}
2 vol% Benzenethiol	Cu 2p1/2	952.4 (953.3)	1.30	
Cu Powder &	Cu 2p3/2	932.4 (933.2)	1.65	Cu^{+2}
5 vol% Benzenethiol	Cu 2p1/2	951.9 (952.7)	2.12	
Cu Powder &	Cu 2p3/2	932.3 (933.5)	2.01	Cu^{+2}
10 vol% Benzenethiol	Cu 2p1/2	952.1 (953.2)	2.10	

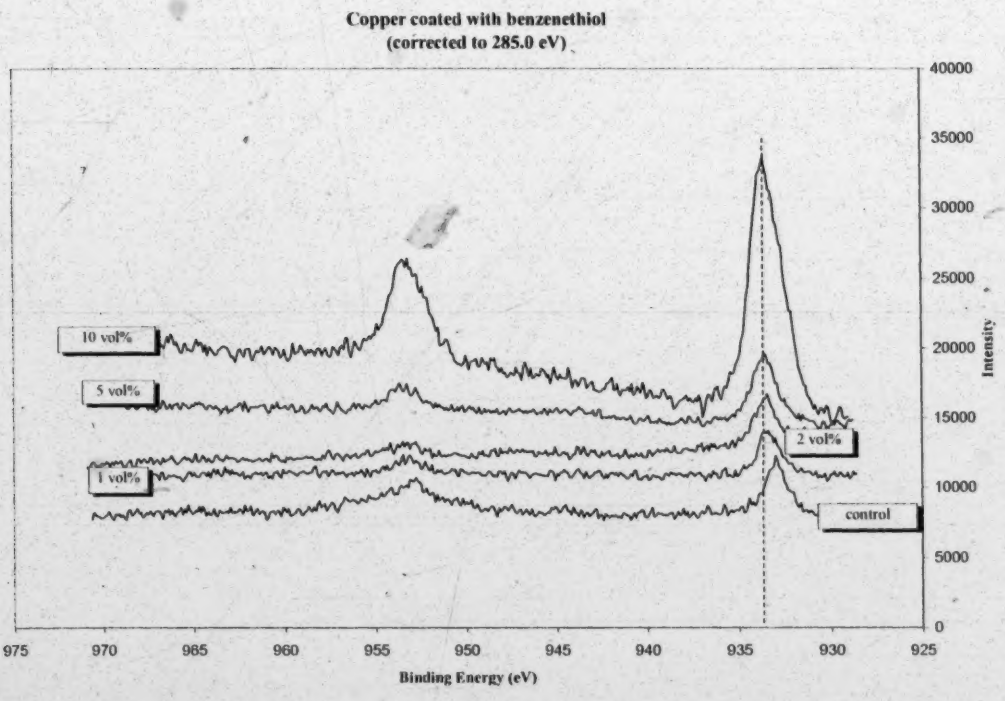

Figure 4.5 Comparing the binding energy of Cu 2p in the various copper benzenethiol samples

Table 4.8 Chemical composition of the copper – benzenethiol samples

Composition of the Copper / Benzenethiol Sample					
	Control	**1 vol%**	**2 vol%**	**5 vol%**	**10 vol%**
C 1s	53.3	61.3	63.3	65.9	66.4
O 1s	28.2	20.0	19.7	15.8	12.6
S 2p		4.7	4.8	6.9	8.1
Cu 2p	18.5	14.1	12.3	11.4	12.9

4.3.6 Characterization of Polyacrylic Acid ($C_3H_4O_2$) Addition

The composition and oxidation state of the copper samples coated with 0.5 M or 1.0 M polyacrylic acid was investigated using x-ray photoelectron spectroscopy. In order to prepare the surfactant solution, sodium polyacrylate was dissolved in nanopure water. Ethanol could not be used, as sodium polyacrylate is insoluble in the solvent. Also, a 1.0 M solution was the highest possible concentration of the surfactant; the surfactant was saturated at this level.

When the copper particles are coated with 0.5 M polyacrylic acid, the core energy levels are shifted to a higher binding energy with respect to the control sample. The copper control is metallic in nature. There is a chemical shift of 0.3 eV. From Table 4.9, the core energy levels of Cu $2p_{3/2}$ and Cu $2p_{1/2}$ are located at binding energies of 933.2 eV and 953.2 eV, respectively. In Figure 4.6, the Cu 2p peaks are comparatively broader with distinct shoulders. Each of the peaks also has a leading edge. The spectral features of this sample are consistent with Cu^{+2}.

By coating the copper particles with 1.0 M polyacrylic acid, a chemical shift of 0.4 eV is evident. To determine the oxidation state of the metal in the sample, we are interested in the binding energy of the Cu 2p peaks. The core energy levels of Cu $2p_{3/2}$ and Cu $2p_{1/2}$ are located at binding energies of 933.3 eV and 953.0 eV respectively. From the narrow spectra, the peaks are also vastly broad with long tails. Thus, after addition of 1.0 M polyacrylic acid to copper powder, it is seen that the results are consistent with Cu^{+2}. The copper standards and copper control are the basis of comparison.

In the surfactant preparation, sodium polyacrylate was added to nanopure water to produce polyacrylic acid. Compositional analysis showed that traces of sodium were still evident on the surface of the copper particles. The control sample consists of 36.9 at.% carbon, 33.8 at.% oxygen and 29.4 at.% copper. Following addition of polyacrylic acid, there is an increase in the concentration of carbon and sodium. With 0.5 M-polyacrylic acid on the surface of copper, the composition consists of 49.9 at.% carbon, 24.3 at.% oxygen, 21.2 at.% copper and 4.6 at.% sodium. The oxygen to copper content ratio is 1.1. This further supports that the oxidation state of copper is +2. Compositional analysis results are shown in Table 4.10.

Table 4.9 Summary of spectral features for the copper-polyacrylic acid samples

	Element / Transition	Binding Energy (eV)	FWHM (ev)	Conclusions
Cu Control	Cu 2p3/2'	932.4 (933.2)	1.13	Cu^0
No Surfactant	Cu 2p1/2'	952.2 (952.9)	1.26	
Cu Powder &	Cu 2p3/2'	932.4 (933.2)	1.86	Cu^{+2}
0.5M Polyacrylic Acid	Cu 2p3/2"	934.1 (934.9)	1.90	
	Cu 2p3/2"'	941.3 (942.2)	2.10	
	Cu 2p3/2""	943.5 (944.4)	2.08	
	Cu 2p1/2'	952.4 (953.2)	1.65	
	Cu 2p1/2"	954.1 (954.9)	1.62	
	Cu 2p1/2"'	961.2 (962.0)	1.70	
	Cu 2p1/2""	962.2 (963.0)	1.68	
Cu Powder &	Cu 2p3/2'	932.3 (933.3)	1.50	
1.0M Polyacrylic Acid	Cu 2p3/2"	933.1 (934.2)	1.06	
	Cu 2p3/2"'	942.8 (943.9)	2.31	Cu^{+2}
	Cu 2p3/2""	944.8 (945.8)	2.30	
	Cu 2p1/2'	951.9 (953.0)	1.14	
	Cu 2p1/2"	952.7 (953.7)	1.15	
	Cu 2p1/2"'	962.3 (963.3)	2.81	
	Cu 2p1/2""	966.2 (967.2)	2.80	

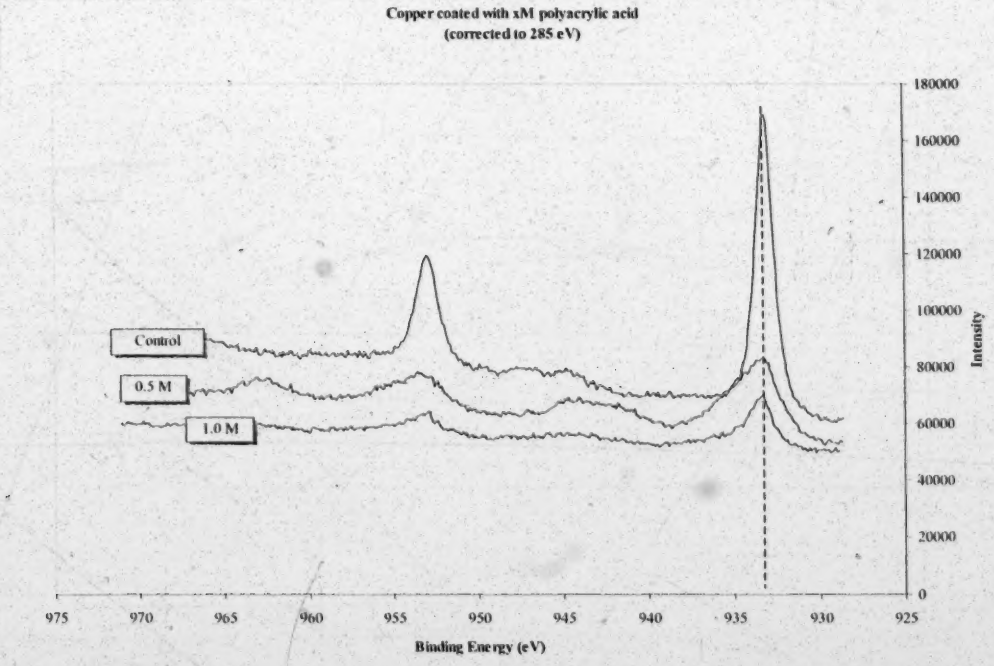

Figure 4.6 Comparing the binding energy of Cu 2p in the various copper-polyacrylic acid samples

Table 4.10 Chemical compositions of the copper-polyacrylic acid samples

Composition of the Copper / Polyacrylic Acid Sample

	Control	0.5 M Polyacrylic Acid	1.0 M Polyacrylic Acid
C 1s	36.9	49.9	50.3
O 1s	33.8	24.3	24.8
Na 1s		4.6	6.1
Cu 2p	29.4	21.2	18.8

4.4 Infrared Spectroscopy and Thermogravimetric Analysis of the Copper Powders

4.4.1 Characterization of Propylamine ($CH_3CH_2CH_2NH_2$) Addition

Figures A.5, A.6 and A.7 in the appendix depict the spectra of copper control, copper coated with 10 vol% propylamine and copper coated with 10 vol% propylamine following TGA analysis. In all of the spectra, copper oxide is identifiable by the strong Cu-O band at ~650 cm^{-1}.

In resonance systems, the NH_2-group is considered one of the strongest resonance electron donor groups. In the 10 vol% propylamine copper sample, the primary amine band is found at 3400 cm^{-1}. The intense stretching band is also accompanied by a second band, the $\delta(NH_2)$ vibration at a wavenumber of ~1563 cm^{-1}. Other dominant bands include the C-H (ν) at 2950 cm^{-1} and C-C (ν) at 1050 cm^{-1}. Broad bands at ~3500 cm^{-1} are associated with the bonding of hydroxyl groups onto the surface of the copper particles (Figure A.6).

The copper samples coated with 1 vol%, 2 vol%, and 5 vol% propylamine all show N-H primary amine (ν) vibrations at ~3550 cm^{-1} and $\delta(NH_2)$ vibrations at ~1550 cm^{-1} (Table 4.11). C-H (alkane) (ν) vibrations are present at ~2950 cm^{-1} and the bands at ~1050 cm^{-1} correspond to C-C (ν). C-O bands in the 1 vol% and 5 vol% propylamine-copper samples are evident at 1350 cm^{-1}. C-O originates from the ethanol that was used to dissolve propylamine in solution. Following heating, the coating is removed and only copper oxide is present in the sample. Cu-O vibrations are present at a frequency of 640 cm^{-1}.

In thermogravimetric analysis (TGA), the samples are heated from room temperature to 550 °C. Figure 4.7 exemplifies the rate of mass change with modifications in temperature for the various copper coated samples. Negative rate of change corresponds to a mass lost. At 50 °C, the changes in mass are initiated. At a temperature of 150 °C, the coating is completely removed. The TGA data implies that the applied coating onto the copper particles decomposes in a single stage. The peak is fairly broad. It is possible that both the ethanol and propylamine are removed from the surface at similar temperatures. The boiling temperature of ethanol is 78.3 °C and the boiling temperature of propylamine is 48 °C. By analyzing the boiling temperatures, propylamine is removed

from the surface initially. Removal of ethanol follows. Since the boiling temperatures are so close, the analytical instrument has a difficult time to resolve the peaks.

The TGA detected a 2.2% mass change in the copper-1 vol% propylamine sample, a 3.9% mass change in the copper-2 vol% propylamine sample, a 4.0% mass change in the copper-5 vol% propylamine sample and a 3.9% change in mass when the copper particles are coated with 10 vol% propylamine.

IR analysis of the sample confirms that at a temperature of 150 °C the propylamine coating was removed. An intense band at 642 cm^{-1} corresponds to the Cu-O (ν) vibration. There are no bands representing the primary amine or alkane groups. XPS analysis on the heated samples also confirms that at 150 °C, nitrogen is no longer present on the sample. The surface is composed of 37.2 at.% carbon, 39.5 at.% oxygen and 23.3 at.% copper. These compositions are similar to the composition of the control sample in Table 4.4. The core energy levels of Cu $2p_{3/2}$ and Cu $2p_{1/2}$ are located at 933.6 eV and 953.2 eV, respectively. Thus, the surface is composed of CuO.

Since a single peak is present in the rate of change vs temperature plot, bonding occurs primarily through the η^1(N). In other words, nitrogen is bonded directly to the surface of the copper oxide.

Table 4.11 Results from infrared spectroscopy: copper coated with propylamine

Sample	Frequency (cm^{-1})	After TGA Analysis Frequency (cm^{-1})	Band
Cu 1 vol% Propylamine	3550		Bonded OH (v)
	3450		N-H primary amine (v)
	2969		C-H alkane (v)
	2887		C-H alkane (v)
	1563		C-N (v)
	1390		C-O (v)
	1040		C-C (v)
	645	644	Cu-oxide (v)
Cu 2 vol% Propylamine	3550		Bonded OH (v)
	2430		N-H primary amine (v)
	2950		C-H alkane (v)
	2885		C-H alkane (v)
	1579		C-N (v)
	1314		C-O (v)
	1050		C-C (v)
	659	643	Cu-oxide (v)
Cu 5 vol% Propylamine	3590		Bonded OH (v)
	3450		N-H primary amine (v)
	2950		C-H alkane (v)
	2885		C-H alkane (v)
	2820		C-H alkane (v)
	1560		C-N (v)
	1350		C-O (v)
	1050		C-C (v)
	645	642	Cu-oxide (v)
Cu 10 vol% Propylamine	3579		Bonded OH (v)
	3400		N-H primary amine (v)
	2950		C-H alkane (v)
	1563		C-N (v)
	1403		C-N (v)
	1348		C-O (v)
	1050		C-C (v)
	650	638	Cu-oxide (v)

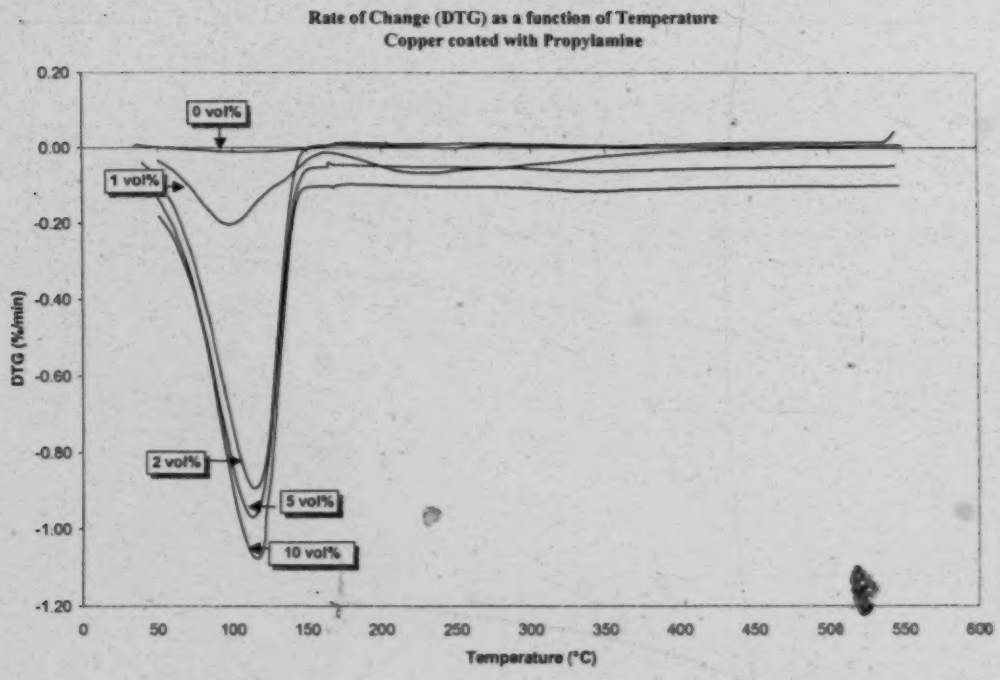

Figure 4.7 Rate of mass change as a function of temperature: copper-propylamine

4.4.2 Characterization of Butylamine ($CH_3CH_2CH_2CH_2NH_2$) Addition

As with the other coated samples, diffuse reflectance spectra were collected for the duplicate samples of copper coated with butylamine. A background spectrum was run before each sample run. In addition, following TGA analysis, the samples were re-analyzed by IR and XPS to confirm whether the coating was removed with exposure to elevated temperatures.

Figures A.13 and A.14 depict the spectra of copper coated with 10 vol% butylamine and copper coated with 10 vol% butylamine following TGA analysis. In all of the spectra, copper oxide is identifiable by the strong Cu-O band at ~640 cm^{-1}.

An intense band at a wavenumber of 641 cm^{-1} identifies the copper control sample. In the copper sample coated with 10 vol% butylamine, a broad peak for the NH_2 (ν) band is found at 3433 cm^{-1}. The corresponding C-N bending vibration is found at 1558 cm^{-1}. Other dominant bands include C-H (alkane) (ν) at 2900 cm^{-1} and C-C (ν) at 1020 cm^{-1} (Table 4.12). Following TGA analysis, the sample was re-analyzed and it was found that the amine coating was removed from the surface. The oxide layer was not removed due to the temperature constraints. As a result, an intense stretching vibration at 641 cm^{-1} corresponds to Cu-O (ν).

The copper samples coated with 1 vol%, 2 vol%, and 5 vol% butylamine all show N-H primary amine (ν) vibrations at ~3400 cm^{-1} and $\delta(NH_2)$ vibrations at ~1450 cm^{-1} (Table 4.12). C-H alkane (ν) vibrations are present at ~2900 cm^{-1} and the bands at ~1050 cm^{-1} correspond to C-C (ν). Bonded OH groups are also present in the sample. A less intense band is evident at a wavenumber of 3450 cm^{-1}.

Figure 4.8 exemplifies the rate of mass change with modifications in temperature for the copper samples that are coated with butylamine. The TGA curves indicate that multi-stage decomposition is taking place. At 70 °C, a loss of mass from the sample is evident. At this temperature, ethanol is being removed from the copper sample. The first unstable component is completely removed from the surface of the copper particles at a temperature of ~160 °C. At 180 °C to 250 °C another volatile component is removed. For the low concentration surfactants, butylamine is removed from the copper particles in a single step. However, when copper is coated with 10 vol% butylamine, it becomes

apparent that fragmentation is evident. Two distinct peaks are presents in the temperature range of 180 °C to 350 °C.

In order to determine which components are being removed at the various temperatures, the samples were heated from room temperature to 150 °C and then to 350 °C. At 150 °C, the IR results indicate that nitrogen is present on the surface of the copper particles. A broad peak for the NH_2 (ν) band is found at 3401 cm^{-1}. The corresponding C-N bending vibration is found at 1360 cm^{-1}. An intense band for Cu-O (ν) is found at 645 cm^{-1}. However, when the powdered sample is heated to 350 °C, there is no evidence of any amine groups in the powder containing copper oxide (Cu-O (ν) has a vibrational frequency of 645 cm^{-1}).

XPS was also used to determine the composition of the heated samples. By heating copper coated with butylamine to 150 °C, the composition on the surface consisted of 30.8 at.% carbon, 6.5 at.% nitrogen, 43.4 at.% oxygen and 19.3 at.% copper. This is consistent with the IR results because at this temperature amine is still on the surface. However, by increasing the temperature to 350 °C, the carbon content increases to 38.8 at.%, oxygen content decreases to 32.4 at.% and the concentration of copper increases to 28.8 at.%. These compositions are consistent with the copper control sample in Table 4.6.

Therefore, the TGA results imply that alkanes are removed at lower temperatures and nitrogen is removed from the surface at relatively higher temperatures. By moderating the temperatures, it is possible to remove butylamine from the surface of the copper particles.

Table 4.12 Results from infrared spectroscopy – copper coated with butylamine

Sample	Frequency (cm^{-1})	After TGA Analysis Frequency (cm^{-1})	Band
Cu Control (0% Butylamine)	3392		C=H alkene (ν)
	1558		C-H alkane (γ)
	641	630	Cu - oxide (ν)
Cu 1 vol% Butylamine	3450		bonded OH (ν)
	3412		N-H primary amine (ν)
	2969		C-H alkane (ν)
	1558		C-N (ν)
	1507		C-N (ν)
	1457		C-N (ν)
	1362		C-O (ν)
	1020		C-C (ν)
	601	629	Cu - oxide (ν)
Cu 2 vol% Butylamine	3442		bonded OH (ν)
	3410		N-H primary amine (ν)
	2950		C-H alkane (ν)
	2885		C-H alkane (ν)
	1560		C-N (ν)
	1458		C-N (ν)
	1356		C-O (ν)
	1030		C-C (ν)
	602	634	Cu - oxide (ν)
Cu 5 vol% Butylamine	3428		bonded OH (ν)
	3405		N-H primary amine (ν)
	3428		C=H alkene (ν)
	2950		C-H alkane (ν)
	1505		C-N (ν)
	1455		C-O (ν)
	1030		C-C (ν)
	609	628	Cu - oxide (ν)
Cu 10 vol% Butylamine	3530		bonded OH (ν)
	3433		N-H primary amine (ν)
	3294		C=H alkene (ν)
	2889		C-H alkane (ν)
	2823		C-H alkane (ν)
	1558		C-N (ν)
	1506		C-N (ν)
	1417		C-O (ν)
	1020		C-C (ν)
	642	641	Cu - oxide (ν)

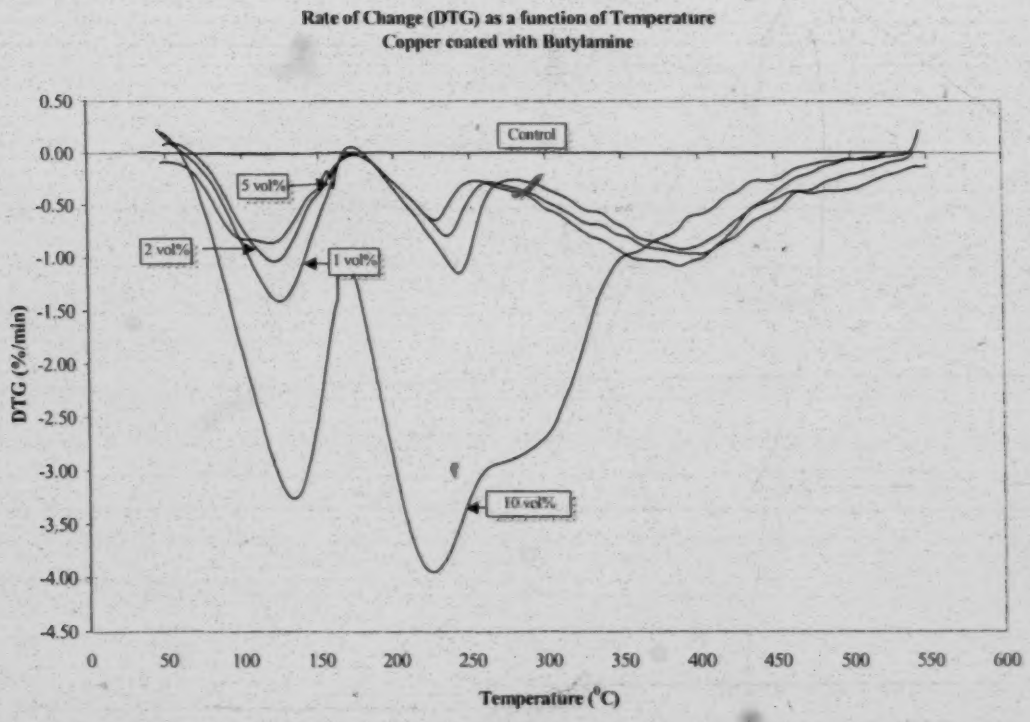

Figure 4.8 Rate of mass change as a function of temperature: copper-butylamine

4.4.3 Characterization of Benzenethiol (C_6H_6S) Addition

Benzenethiol is an aromatic compound and the carbon atoms adopt a sp^2 molecular configuration (Niemantsverdriet, 1993). Upon binding to the copper surface, from the IR spectra, we should expect to see C-H (alkene), C=C, Cu-S, Cu-O vibrations. A background was run prior to each sample run and the powders were not diluted with KBr. An intense band at a wavenumber of 640.0 cm^{-1} identifies the copper control sample. An IR spectrum of benzenethiol (from the www.webbook.nist.gov) was used to identify the principle vibrational bands.

Figures A.19 and A.20 in the appendix depict the spectra of copper coated with 10 vol% benzenethiol and copper coated with 10 vol% benzenethiol following TGA analysis. In all of the spectra, copper oxide is identifiable by the strong Cu-O band at ~640 cm^{-1}.

Copper coated with 10 vol% benzenethiol is associated with C-H alkene (ν) at a frequency of 3065 cm^{-1}, C=C (ν) at 1578 cm^{-1} and the CH_2 (γ) vibration band is at 1475 cm^{-1} (Table 4.13). Sulfur is also bonded to the surface of copper. Evidence that supports this observation includes that two intense vibrational bands are located at 735 cm^{-1} and 687 cm^{-1}. Table 4.13 shows all of the vibrational frequencies in detail.

Coating the copper particles with 1 vol%, 2 vol% and 5 vol% benzenethiol also generates very similar results. All of the characteristic bands are located at similar wave numbers. The principle IR bands do not shift with alterations in surfactant concentrations.

The results from thermal gravimetric analysis demonstrate that with exposure to elevated temperatures, benzenethiol is easily removed from the copper particles. At a temperature of approximately 50 °C changes in mass are evident. Ethanol is removed at 50 to 110°C as it is a low boiling solvent with a boiling point of 78 °C. By further increasing the temperature to 225 °C, another peak is seen in the DTG vs temperature plot (Figure 4.9).

IR and XPS were used to identity which volatile components are removed at a given temperature. The powders were heated to 150 °C. From XPS compositional analysis, there is approximately 7 at.% sulfur, 62 at.% carbon, 18.2 at.% oxygen and 12.8 at.% copper remaining in the sample. The IR results show that the OH group is removed from the copper. Thus, at lower temperatures ethanol is removed. The first peak in the DTG vs

temperature corresponds to the removal of ethanol. At 150 °C, the aromatic ring and sulfur remain bonded to copper.

By further heating the sample to 350 °C, the surface composition consists of 48.8 at% carbon, 0.1 at.% sulfur, 35.9 at.% oxygen and 15.2 at.% copper. These compositions are consistent with the content of the copper sample in Table 4.8. The TGA and XPS results are consistent with the IR data because at 350 °C all of the sulfur vibrational bands are non-existent (Table 4.13). A single intense vibrational band is present at 645 cm^{-1}. Heating the samples removed 3.7 wt% of the initial mass. Thus, the second peak in Figure 4.9 signifies the removal of sulfur and the benzene ring.

Table 4.13 Results from infrared spectroscopy – copper coated with benzenethiol

Sample	Frequency (cm^{-1})	After TGA Analysis Frequency (cm^{-1})	Band
Cu Control (0% Benzenethiol)	640	646.3	Cu - oxide (ν)
Cu 1 vol% Benzenethiol	3402		Bonded -OH (ν)
	3064		C-H alkene (ν)
	1578		C=C (ν)
	1475		CH_2 (γ)
	1440		CH_2 (γ)
	1080		CH_2 - OH (ν)
	1024		CH_2 - CH (ν)
	730		Cu - S (ν)
	685		Cu - S (ν)
	636	645	Cu - oxide (ν)
Cu 2 vol% Benzenethiol	3402		Bonded -OH (ν)
	3050		C-H alkene (ν)
	2987		C-H alkane (ν)
	1578		C=C (ν)
	1475		CH_2 (γ)
	1438		CH_2 (γ)
	1080		CH_2 - OH (ν)
	1066		CH_2 - CH (ν)
	1050		CH_2 - CH (ν)
	1025		CH_2 - CH (ν)
	730		Cu - S (ν)
	691		Cu - S (ν)
	641	635	Cu - oxide (ν)
Cu 5 vol% Benzenethiol	3392		Bonded -OH (ν)
	3065		C-H alkene (ν)
	2990		C-H alkane (ν)
	1578		C=C (ν)
	1475		CH_2 (γ)
	1438		CH_2 (γ)
	1080		CH_2 - OH (ν)
	1066		CH_2 - CH (ν)
	1025		CH_2 - CH (ν)
	1000		CH_2 - CH (ν)
	730		Cu - S (ν)
	685		Cu - S (ν)
	635	643	Cu - oxide (ν)

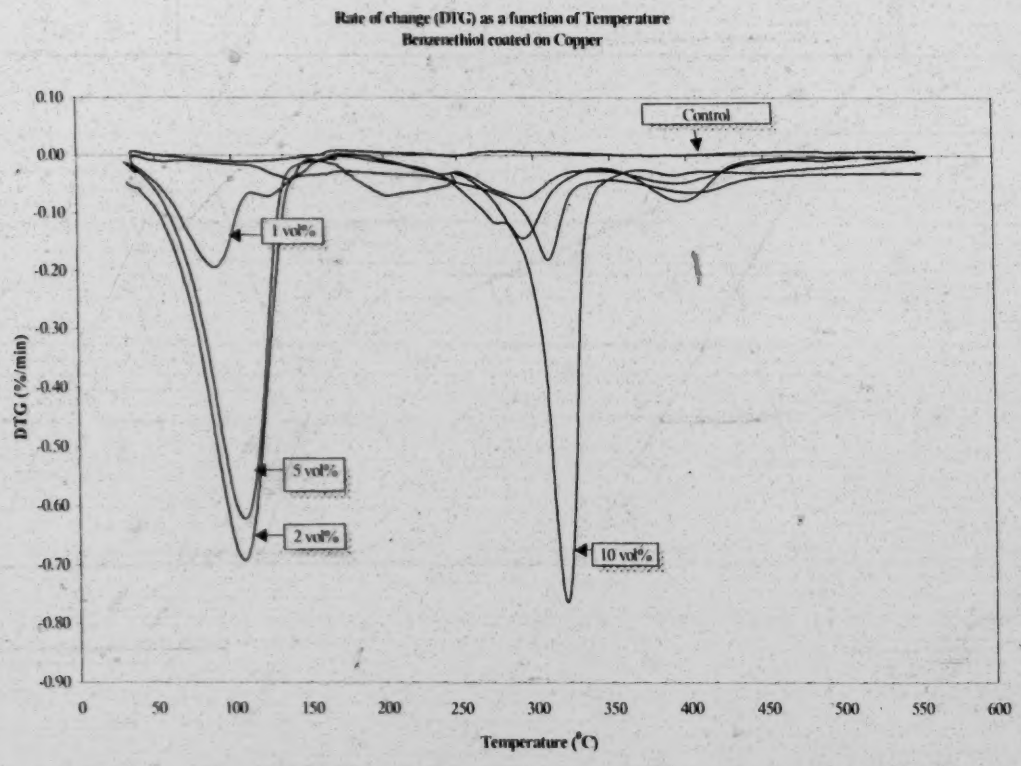

Figure 4.9 Rate of mass change as a function of temperature: copper-benzenethiol

4.4.4 Characterization of Polyacrylic Acid ($C_3H_4O_2$) Addition

Figures A.25 and A.26 in the appendix depict the spectra of copper coated with 1.0 M polyacrylic acid and copper coated with 1.0 M polyacrylic acid following TGA analysis. In all of the spectra, including the copper control, copper oxide is identified by a strong band at ~645 cm^{-1}.

When copper is coated with 0.5 M polyacrylic acid, a broad band at 3410 cm^{-1} identifies the bonded -OH group. C=O stretching is represented at 1457 cm^{-1} and 1411 cm^{-1} (Table 4.14). Other dominant bands include COO^- (ν) at 1577 cm^{-1}, CH_2 groups (ν) at 3020 cm^{-1} and C-H alkane (ν) at 2930 cm^{-1}.

In thermal gravimetric analysis ~1.5 g of samples were exposed to a constant flow of nitrogen. At a temperature of approximately 50 °C changes in mass are evident. By further increasing the temperature to 300 °C and 400 °C, broad peaks are seen in the DTG vs temperature plot (Figure 4.10).

The results from TGA analysis demonstrate that with exposure to elevated temperatures, polyacrylic acid is removed from the copper particles. However, the mass of the sample changes only by 1.0 wt%. It becomes apparent that by increasing the temperature of the environment, some of the copper powder decomposes but at the same time it rebinds to the surface. In other words, it re-decomposes onto the surface. This conclusion is supported by the IR results. Bonded hydroxide groups, and C=O groups are still present in the samples. The peaks in the IR spectra are slightly broader but are less intense. As a result, heating the sample did not entirely remove surfactant coating.

Table 4.14 Results from infrared spectroscopy – copper coated with polyacrylic acid

Sample	Frequency (cm^{-1})	After TGA Analysis Frequency (cm^{-1})	Band
Cu Control	640	646	C-O (v)
Cu 0.5M Polyacrylic Acid	3410	3338	Bonded -OH
	3020		CH_2 (alkene) (v)
	2930		C-H alkane (v)
	1578		COO^-
	1457	1438	C=O (v)
	1411		C=O (v)
	644	643	Cu-O (v)
Cu 1M Polyacrylic Acid	3390	3400	Bonded -OH
	3100		CH_2 (alkene) (v)
	2930		C-H alkane (v)
	1574	1525	COO^-
	1455	1439	C=O (v)
	1412		C=O (v)
	644	644	Cu-O (v)

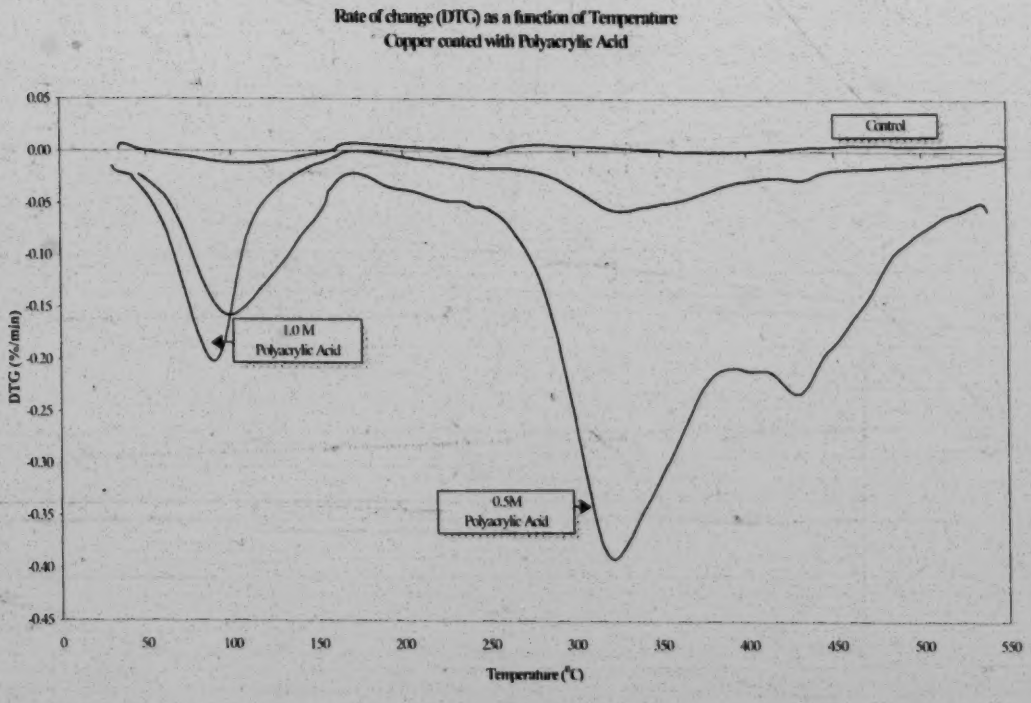

Figure 4.10 Rate of mass change as a function of temperature: copper-polyacrylic acid

4.5 SEM/EDS Analysis and Particle Size Distribution of the Copper Powders

4.5.1 Characterization of Commercial Copper Powders

Figure 4.2 also shows the SEM images collected from the copper process. Images were collected at two different resolutions 1000× and 10×. Only the low-resolution images are presented in the figure.

SEM images collected from the sample aliquots obtained from the reactor show the differences in morphology between the coated and uncoated particles. The uncoated copper particles are almost spherical and crystalline. Clusters of copper particles are evident, indicating agglomeration is a problem. The particles also exhibit a narrow size distribution of approximately 2 μm to 2.5 μm. These individual particle sizes are determined qualitatively from the SEM micrographs. The micrographs representing the coated copper particles show less cluster formation. Thus, coating the particles lessens the degree of agglomeration.

Following washing / filtration and drying, the particles remain almost spherical in shape. Clusters of copper particles are not significant due to the sparse population. The particles are approximately 2 μm in diameter.

Agglomeration is evident following the screening of the copper powder. Figure 4.2 shows the evidence of cluster formation. The copper particles are almost spherical in shape and are approximately 2 μm to 3 μm in diameter. The smaller particles have a tendency to bind to the larger granules.

These results show that agglomeration becomes a problem following precipitation of copper in the reactor. The most reasonable place to add a surfactant to suppress agglomeration would consist of surfactant addition in the reactor.

Results from the energy dispersive analysis show that each of the samples from the copper process is relatively pure. If thin layers of oxide are present on the surface, the concentrations are undetectable by the instrument. In essence, the copper signal is stronger than the signal of an oxide.

4.5.2 Characterization of Propylamine ($CH_3CH_2CH_2NH_2$) Addition

Four categories were used to describe the images (Figure 4.11). Category A describes a state in which < 25% of the particles are agglomerated. By adding a 5 vol% propylamine solution to the copper particles, some particle clusters are present. A coating is evident on the surface and the crystalline copper particles are approximately 2 μm in size. Coating copper with 10 vol% propylamine also inhibits the agglomeration effect. Less than 25% of the particles are agglomerated. Qualitatively, the individual particles are almost spherical and are 2 to 2.5 μm in size. The cluster formation is sparse. There is no additional benefit of increasing the surfactant concentration to 10 vol% propylamine as the particle distribution does not improve significantly.

Copper coated with 2 vol% propylamine can be described by category B (Figure 4.11). In this state, ~25% of the particles are agglomerated. A coating is evident on the surface of the copper, and the particles are crystalline. Cluster formation is more pronounced.

Category C describes an environment in which 50% of the particles are agglomerated. When a 1 vol% propylamine solution is added to the copper, the morphology of the particles is different in comparison to the other samples. A uniform distribution of particles is not apparent, and the copper particles tend to aggregate into smaller clusters. Adhesion forces bind smaller particles to the surface of the larger particles.

The uncoated copper control falls within category D (Figure 4.11). Greater than 50% of the particles are agglomerated. The copper particles are almost spherical and vary in size from 3 to 5 μm. A uniform distribution of segregated particles is not evident.

Results from EDX analysis are inconclusive, as the oxide layer is not detected.

The laser diffraction particle size analyzer results obtained from Umicore Canada are used as a quantitative measure to confirm the results gathered from SEM analysis. The uncoated particles are 4.1 ± 2.6 µm in size (Table 4.15). With the addition of propylamine, it becomes apparent that the size of the copper particles also decreases. The particles have a 3.8 ± 3.3 µm diameter when coated with 1 vol % propylamine. Figures A.8 to A.12 in the appendix, exemplify the particle size distribution. The distribution is skewed to the right. A small quantity of surfactant has an impact of the size of the particles.

Table 4.15 Particle size distribution results

Sample	Particle Size
Cu control	4.1 ± 2.6 μm
Cu coated with 1 vol % propylamine	3.8 ± 3.3 μm
Cu coated with 2 vol % propylamine	4.0 ± 3.1 μm
Cu coated with 5 vol % propylamine	3.8 ± 2.9 μm
Cu coated with 10 vol % propylamine	4.1 ± 3.0 μm

Category A
< 25 % of the particles are agglomerated

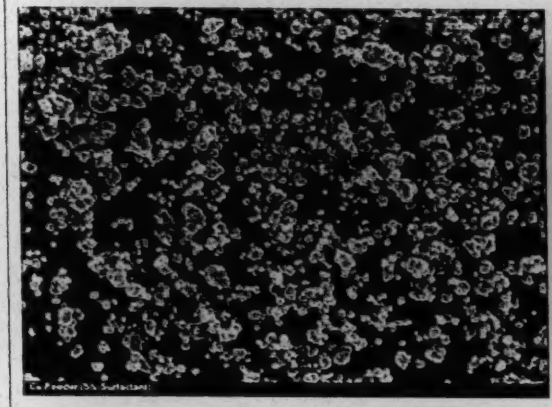

Category B
25 % of the particles are agglomerated

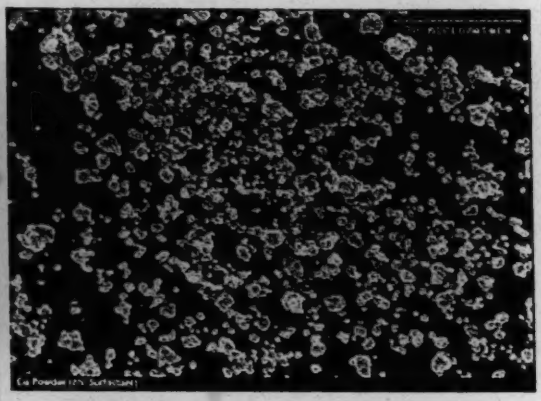

Category C
50 % of the particles are agglomerated

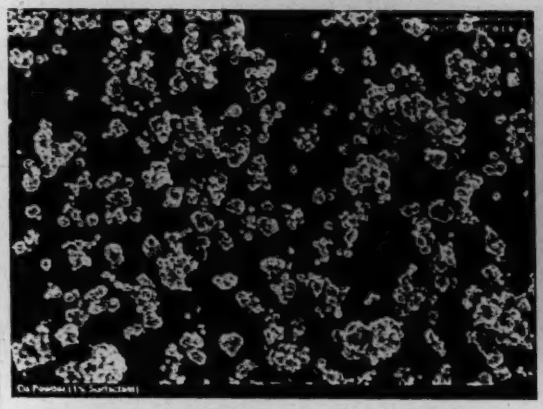

Category D
> 50 % of the particles are agglomerated

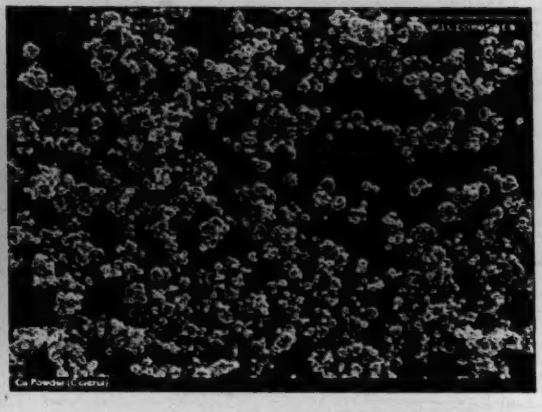

Figure 4.11 Categories of agglomeration and representative images from SEM: copper-propylamine

4.5.3 Characterization of Butylamine ($CH_3CH_2CH_2CH_2NH_2$) Addition

The same categories of agglomeration that were used in section 4.5.2 are used to describe the images. Two areas on each sample were analyzed to ensure consistency in the results. The copper control sample consists of ~2 μm irregularly shaped particles. No coating is visible on the surface and there is no significant quantity of crystal structures. The SEM micrograph in Figure 4.12 shows that there are several large clusters of particles. The uncoated copper control falls within category C (50% of the particles are agglomerated).

When the copper is coated with 1 vol% butylamine, the particles are ~2 μm in size. Some crystals are present and a coating is evident on the surface. The particles appear more distributed and only a few agglomerated clusters are present. When compared to the copper control micrograph, there is a larger quantity of single particulates. Approximately 25% of the copper coated particles are agglomerated (category B).

Coating copper particles with 10 vol% butylamine generates a state in which there is a vast quantity of individual particles (category A). The particles are hexagonal, crystalline and ~2 μm in size. A thicker coating is visible on the surface of the dried powder. There is a small quantity of agglomerated clusters in which small particles are bound to larger particles.

Therefore, with SEM analysis, it was possible to determine whether agglomeration is significant in each sample. It is also important to keep in mind that before it is possible to achieve the development of nano-sized particles, it is critical to understand the agglomeration mechanisms of larger particles.

The particle size distribution results shown in Table 4.16 and Figures A.15 to A.18 give a further quantitative insight into the effect of butylamine addition to copper powder. The particle size of the uncoated copper particles is 4.1 ± 2.6 μm. A decrease in particle size is also evident when butylamine is added to the copper powder. Copper coated with 1 vol% butylamine contains particles with a diameter of 3.5 ± 3.1 μm, whereas, coating copper with 2 vol% butylamine results in 3.8 ± 2.6 μm sized particles. Adding 10 vol% butylamine to the copper powder leads to 3.7 ± 2.9 μm sized particles. Thus, it is beneficial to add butylamine to the copper powder as the particles decrease in size. Agglomeration is hindered with surfactant addition.

Table 4.16 Particle size distribution results

Sample	Particle Size
Cu control	4.1 ± 2.6 μm
Cu coated with 1 vol% butylamine	3.5 ± 3.1 μm
Cu coated with 2 vol% butylamine	3.8 ± 2.6 μm
Cu coated with 5 vol% butylamine	3.9 ± 2.8 μm
Cu coated with 10 vol% butylamine	3.7 ± 2.9 μm

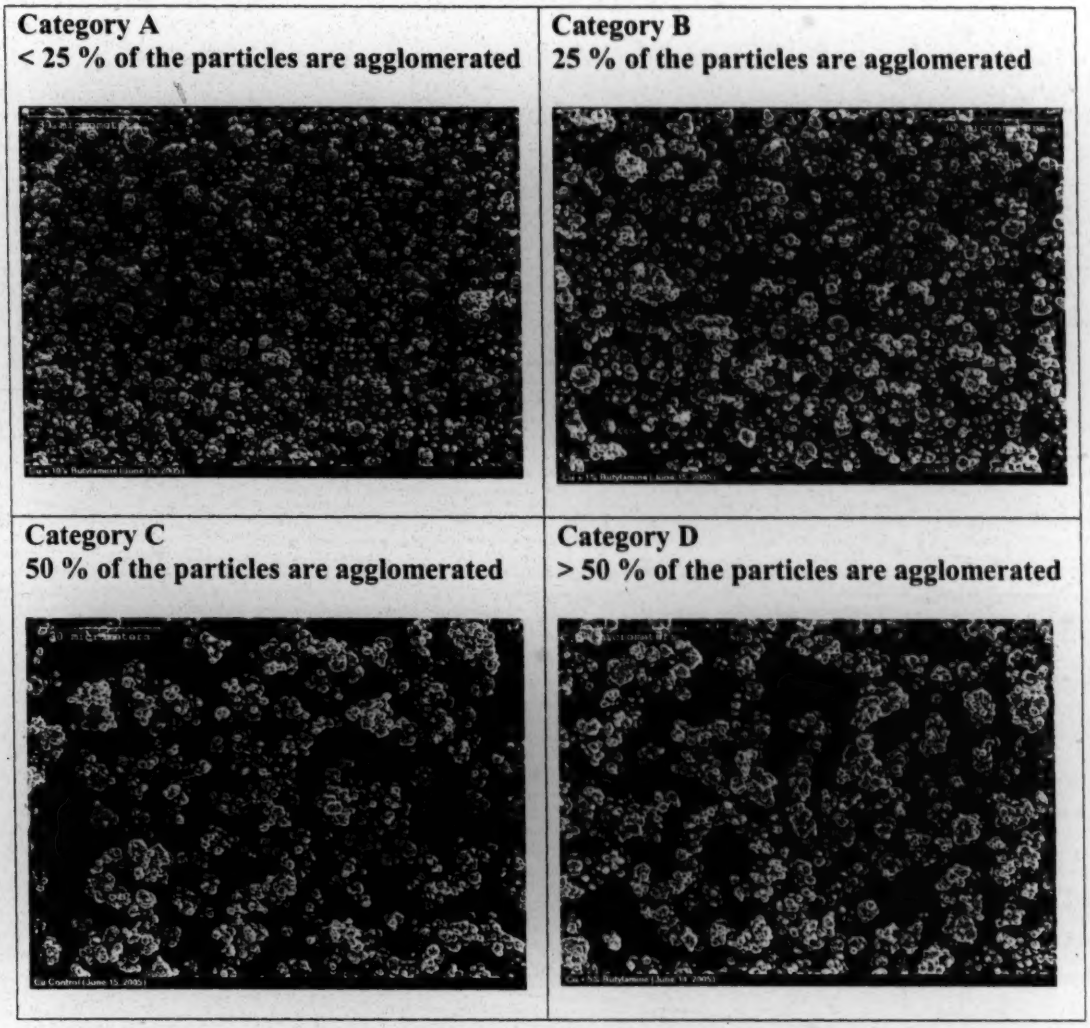

Figure 4.12 Categories of agglomeration and representative images: copper-butylamine

4.5.4 Characterization of Benzenethiol (C_6H_6S) Addition

From the Figure 4.13, it is apparent that the benzenethiol does not significantly improve the particle distribution.

Category B is used to describe the state in which approximately 25% of the particles are agglomerated. When copper is coated with 10 vol% benzenethiol, the particles are approximately 2 to 3 μm in size. They are irregularly shaped and are clearly not spherical. A coating is evident on the surface and the smaller particles have an affinity to bind to the larger particles.

Category C is used to describe the condition in which 50% of the particles are agglomerated. The control, 2 vol% benzenethiol-copper and 5 vol% benzenethiol-copper fall into this class. The control copper particles are non-spherical and the surface is not smooth. With the addition of 2 vol% and 5 vol% benzenethiol, the particles remain heavily agglomerated. A thin coating is evident on the particles. Smaller particles bind readily to the smaller particles until large clusters are evident. The individual particles are approximately 4 μm in diameter.

Category D describes a circumstance in which greater than 50% of the particles are agglomerated. Coating copper with 1 vol% benzenethiol seem to promote agglomeration. The particles are ~3 μm in size and are fairly irregularly shaped.

Particle size distribution measurements are used as a quantitative measure to determine the size of the copper particles coated with a surfactant. The uncoated copper powder has an average particle size of 4.1 ± 2.6 μm (Table 4.17). By adding 5 vol% benzenethiol to the copper powder, the particles increase in size to 5.5 ± 3.1 μm. It becomes apparent that an increase in surfactant concentration results in an increase in particle size. Copper coated with 10 vol% benzenethiol has a particle size of 4.0 ± 2.9 μm. Size distribution plots are given in figures A.21 to A.24. The distributions are skewed to the right with a trailing tail. There is a larger quantity of particles with a larger diameter. SEM measurements are useful to determine whether the particles are sticking to one another and to describe the shape of the particles. Size distribution is very useful to describe the actual size of each of the granules.

Table 4.17 Particle size distribution results

Sample	Particle Size
Cu control	4.1 ± 2.6 μm
Cu coated with 1 vol% benzenethiol	4.8 ± 2.6 μm
Cu coated with 2 vol% benzenethiol	4.5 ± 2.9 μm
Cu coated with 5 vol% benzenethiol	5.5 ± 3.1 μm
Cu coated with 10 vol% benzenethiol	4.0 ± 2.9 μm

Category B
25% of the particles are agglomerated

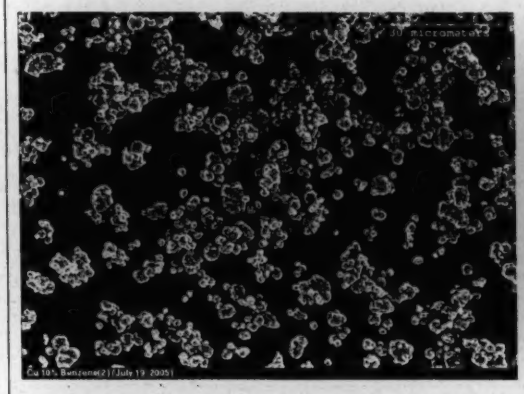

Category C
50% of the particles are agglomerated

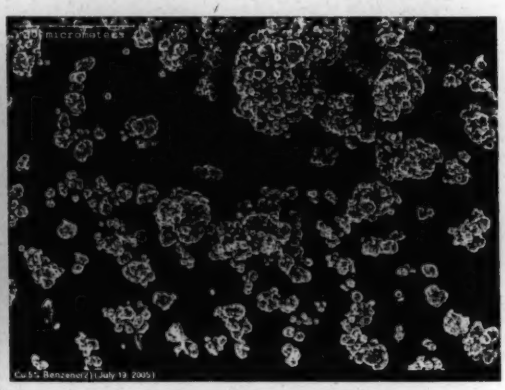

Category D
>50 % of the particles are agglomerated

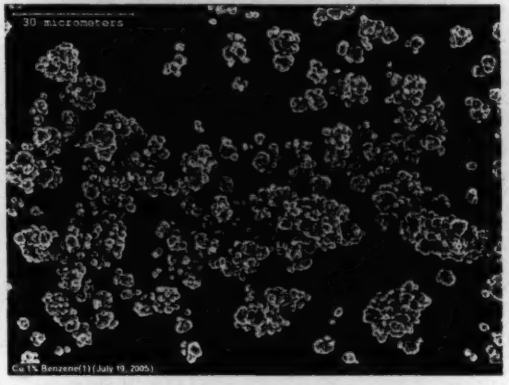

Figure 4.13 Categories of agglomeration and representative images: copper-benzenethiol

4.5.5 Characterization of Polyacrylic Acid ($C_3H_4O_2$) Addition

When polyacrylic acid was added in varying concentrations to the copper powder, it was found that there were significantly more agglomerated particle clusters. Using the same categories of agglomeration as in previous studies, the morphology could be only classified into two groups, C and D.

The copper powder containing no polyacrylic acid can be described by category C. The particles are approximately 4 μm in size and they adopt a non-crystalline shape (Figure 4.14). No coating is visible on the surface and larger clusters of particles are present. It seems as though the smaller particles have an affinity to bind to the surface of the larger particles. The copper particles are heavily agglomerated.

With the addition of 0.5 M and 1.0 M polyacrylic acid to the copper powder, the particles formed larger agglomerated clusters. The samples were sonicated and prepared in the same manner as the other copper coated samples. The particles are greater than 4 μm in size and they have a non-spherical shape (Figure 4.14). Even with the addition of a surfactant, the coated particles continue to reside in clusters. Higher magnification micrographs show that a coating is evident on the surfactant.

Particle size distribution data further clarifies that addition of this particular surfactant did not hinder agglomeration. The size of the copper particles coated with 0.5 M polyacrylic acid is 6.2 ± 2.2 μm. There is a 2 μm increase in diameter with respect to the uncoated particles. Increasing the concentration of polyacrylic acid to 1.0 M, results in even larger particles. Table 4.18 shows the data gathered from the laser diffraction particle size analyzer. The distribution plots are shown in Figures A.27 and A.28 in the appendix. The data has a significantly wider distribution that is skewed to the right. There is an increased quantity of particles that have a larger diameter.

Table 4.18 Particle size distribution results

Sample	Particle Size
Cu control	4.1 ± 2.6 μm
Cu coated with 0.5 M polyacrylic acid	6.2 ± 2.2 μm
Cu coated with 1.0 M polyacrylic acid	7.4 ± 2.6 μm

Category C **50% of the particles are agglomerated**	**Category D** **>50% of the particles are agglomerated**
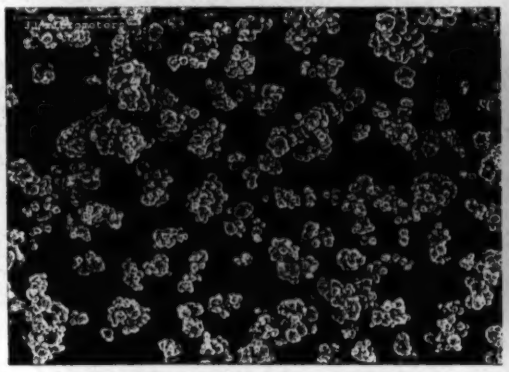	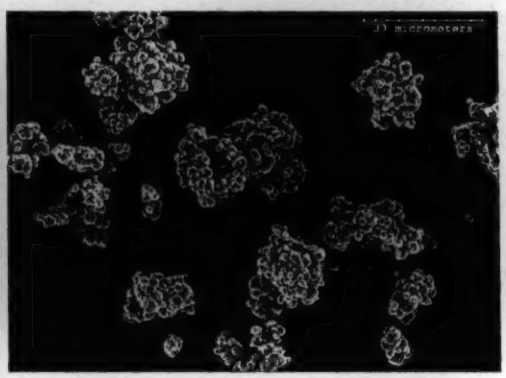

Figure 4.14 Categories of agglomeration and representative images: copper-polyacrylic acid

4.6 Summary

Initially, the industrial process was studied to identity the optimum location to add the surfactant. Agglomeration was predominant in the stages that followed the reactor. Four surfactants were used to determine whether dispersion of copper particles could be achieved: propylamine, butylamine, benzenethiol and polyacrylic acid. Using the model experimental conditions, it was not possible to achieve nano-sized particles. The key is to determine which surfactant is the most effective in hindering agglomeration. Thus, we could push particle size to become smaller in future studies.

It was found that the uncoated copper sample has a metallic oxidation state. However, upon addition of a surfactant in any given concentration, the oxidation state of copper is +2. XPS data was consistently compared to a set of standards and to the control group. IR was used to confirm the composition of each of the coated samples. The data was useful to determine how each of the substituents bonded to the surface of the copper particles. It was found that the amines bind through the lone pair on the nitrogen and benzenethiol binds to copper through the sulfur atom. Propylamine, butylamine and benzenethiol bind fairly strongly to the surface of the copper particles, however, with increased temperatures, these surfactants are easily removed. IR and XPS analysis were completed on the heated samples. At 150 °C, propylamine is completely removed from the surface of copper. At 350 °C both butylamine and benzenethiol are removed from the surface. It was also determined that polyacrylic acid is very difficult to remove from the copper particles.

SEM analysis on the particles after addition of the surfactant provides insight to whether the degree of agglomeration is lessened. Copper coated with propylamine and butylamine generated well-distributed particles. Agglomeration was minimized. Particle size distribution data was used as a quantitative measure to support the qualitative SEM data. This data shows that the average size of the particles decreased in comparison to the control when propylamine and butylamine was added to the raw copper powder. SEM and particle size distribution results also showed that benzenethiol and polyacrylic acid were poor surfactants. The copper particles were not dispersed. The coated particles were larger than the control group. The next chapter discusses which surfactant loading is better.

CHAPTER 5: DISCUSSION

5.1 Introduction

Studying the nano-scale system presents several challenges because there are large differences between the properties found in bulk particles and the properties of nano-sized particles. Gravity and friction have different effects on various sized particles, and on the nano-scale level, atomic forces, chemical bonds and quantum mechanics are important factors that affect the size of a given particle. There is a demand to generate small copper particles, as there is a growing trend to miniaturize electronics.

Copper powder produced at Umicore Canada Ltd. is primarily used in the electronic industry. These copper particles have to be as small as possible to prevent resistive heating of the small and compact electrical components. At the present time, copper produced for semiconductor applications is approximately 5 μm in diameter, and SEM analysis indicates particle agglomeration is an issue at this size requirement.

Attraction forces between solids often cause undesired agglomeration. The most important binding mechanisms include van der Waals, electrostatic and magnetic forces (Pietsch, 1991). These forces become very important in small particles because the distance between the adhesion partners is relatively small. As a result, we need a surfactant that will bind readily to the surface of the copper particles to reduce the forces of attraction between the particles.

In this work, suggestions for possible causes of agglomeration are made. However, a significant amount of time was used to suggest organic media that could be used to coat the surface of dispersed particles prior to drying. Coating the copper particles with a small chain amine, a thiol or a polymer was expected to hinder aggregate formation. It was found that some surfactants worked better than others. The results will be discussed in detail in this chapter. The copper-coated particles were primarily micro-sized instead of the desired nano-sized particles. It is very important to stress that this is the current size limitation due to production factors and agglomeration. By understanding which organic surfactant works best, it is possible to push the particle size smaller and smaller into the nanoscale level.

Furthermore, once the copper particles are coated it is essential to also determine whether it is possible to remove the coating. The coating is used to prevent agglomeration during the drying stage and during transportation. When the raw powder is sold to the electronic market, the manufacturers have to remove the coating prior to constructing the semi-conductors. Thermogravimetric analysis, infrared spectroscopy and x-ray photoelectron spectroscopy were used to monitor the removal of the surfactant coating. In summary, the ideal organic coating is one that can be easily added to the surface of the copper particles and easily removed at elevated temperatures.

5.2 Characterization of the copper process by x-ray photoelectron spectroscopy (XPS) and secondary electron microscopy (SEM)

Initially, the copper production process was studied to determine where agglomeration becomes a concern. In this study, XPS was used to determine the composition of the copper powder at each step along the process. The ratio of the atomic concentration of oxygen to the atomic concentration of copper allows for the determination of the oxygen to metal ratio. Furthermore, the shifts in the binding energy of the Cu 2p orbitals in copper provide a significant amount of information to determine the oxidation state of the metal. These binding energies are then compared to the binding energy of Cu^0 and Cu^{+2} standards. In conjunction with secondary electron microscopy, it was possible to determine the optimum stage in which a surfactant can be added to hinder agglomerate growth.

The XPS results show that the copper samples obtained from industry do not exhibit a change in oxidation state during production. Samples obtained after the reaction vessel, washing, drying and particle screening stages maintain a +2 oxidation state. The shifts of the Cu $2p_{3/2}$ and Cu $2p_{1/2}$ valence levels are compared to the binding energies of the copper standards.

Many theories have been developed to understand the formation of an oxide film. A reduction model proposed by Voogt (1999) suggests that inside an oxide particle, a metallic core is present. The metallic core grows until there is no oxide on the surface. In his study of palladium catalysts, he predicted that a particle containing both Pd and PdO will consist of a metallic core and an oxidic layer. Our copper particles exhibit a thin

copper oxide film. In XPS analysis, the penetration depth of the x-ray beam is 50 to 100 Å (Nelson and Wanke, 2005). Thus, the analysis depth can be used to approximate the thickness of the oxide layer as 50 Å.

If the powders are exposed to air, this could lead to the development of an oxide layer. Copper oxidizes at a rapid rate when exposed to air (Greenwood, 1998). The copper powder was prepared onto the stub in the normal air of the XPS room, and although exposure was less than 5 minutes prior to degassing in a vacuum atmosphere, it is possible for molecular oxygen, CO or CO_2 to bind to the surface.

SEM images were collected from the copper process. Size measurements are based on the diameter of an individual particle and not the size of the entire particle cluster. To ensure that the qualitative results are not biased, Tina Barker (Department of Chemical and Materials Engineering, University of Alberta) examined two positions on each sample. The results from each analysis were in agreement.

It is apparent that copper agglomerates are present in all aliquots that were collected from the process. SEM micrographs from the uncoated copper sample collected from the reactor shows particle cluster formation (~10 μm). The copper particles are almost spherical. A sample batch containing copper coated with an unknown coating was also obtained from Umicore. The individual particles are slightly smaller (~2 μm). Even though some agglomerates are evident in the SEM micrographs, the clusters are smaller (~5 μm). Despite not knowing the identity of the coating, it is apparent that coating the surface of the copper particles lessens the degree of agglomeration.

Agglomeration of the copper particles becomes a problem in the first stage of production. If a surfactant can be added to the reactants in the batch reactor, then the particles will be stabilized and will not form agglomerates upon washing or drying.

5.3 Copper Coated with Propylamine

Propylamine was chosen as a surfactant to reduce agglomeration of copper particles. Amines are called cationic surfactants as they have a positively charged head group and a hydrophobic tail (Sharma, 1995). It is expected that the hydrophobic tails will repel the other copper particles to prevent the formation of agglomerates.

The copper particles were coated (in excess) with 1 vol%, 2 vol%, 5 vol% and 10 vol% propylamine in ethanol. It was found, by XPS, that the control sample has an oxidation state of zero. The binding energy of Cu $2p_{3/2}$ and Cu $2p_{1/2}$ are 933.1 eV and 952.9 eV, respectively. Metallic copper is located at a binding energy of 932.9 eV and 951.7. The binding energies of the Cu 2p peaks are closer to the binding energies of the Cu^{+2} standard. Thus, samples containing propylamine on the surface have a +2 oxidation state.

Using Voogt's (1999) analogy of the reduction model, particles containing Cu and CuO have a metallic core and a thin oxide layer on the surface. Bowe et al. (2003) state that amines bond strongly to the surface of metals. By increasing the concentration of the surfactant, there was also an increase in the atomic concentration of nitrogen on the surface of copper. In comparison to the control sample, there was a slightly lower atomic concentration of carbon and a slightly higher concentration of copper and oxygen. Even though the samples were exposed to atmosphere for a short period of time, some of the CO_2 and CO from the air bound to the surface of the powder. These molecules may further contribute to the development of a thin oxide layer on the surface of copper. During sample preparation, it was seen that the surface of the aqueous phase had a blue tint. This particular color change is further evidence of oxide formation (CuO) of the copper particles.

Unfortunately, the literature on propylamine adsorption and decomposition on metal surfaces is very limited. Sexton (1985) studied pyrrole adsorption on the Cu(100) surface. Using HREELS and TDS, he found that adsorption of pyrrole on the surface of copper is initiated at 85 K. The adsorption appeared to be molecularly reversible and weakly bonded to the surface in a parallel mode. Studies have also suggested that the adsorption geometry is dependent on surface coverage and temperature.

Abdallah et al. (2004) studied the vibrational frequencies of pyridine adsorption on Mo(110). Although in our studies we studied the adsorption of propylamine or butylamine on the surface of copper, some similarities can be drawn from Abdallah's work since a nitrogen-containing group is bonding to the surface of a metal. It was found that C-C are found at frequencies of 1304 cm^{-1} and 1478 cm^{-1}, and C-N stretching

vibrations are found at 1478 cm^{-1} and 1614 cm^{-1}. C-H stretching was found at 3082 cm^{-1}, 3084 cm^{-1}, 3111 cm^{-1}, and 3114 cm^{-1}.

Since propylamine is dissolved in ethanol, from IR results there is evidence that hydroxide groups are present. The broad adsorption band at 3550 cm^{-1} is a clear indicator of hydrogen bonding. IR data is also very useful to conclude that the amine was chemisorbed onto copper. The NH_2 group is considered to be one of the strongest electron donor groups. The corresponding amine stretching bands are found at 3450 cm^{-1}, C-H (ν) is found at a wavenumber of ~2950 cm^{-1}. An intense band at a wavenumber of 1500 cm^{-1} provides evidence that carbon is bound to nitrogen and the lone pair of electrons bind to the surface of the copper. C-C stretches are also seen at a wavenumber of 1050 cm^{-1}. In our studies, the C-O stretch frequency is an excellent indicator for the manner that CO is bound to the surface. A C-O (ν) of 1400 cm^{-1} indicates that CO is chemisorbed onto the surface of copper through four-fold bonding (Gunzler and Gremlich, 2002). With varying surfactant concentrations, there is no evidence of shifts in the adsorption frequencies. When these vibrations are compared to Abdallah et al. (2004) studies, the stretching vibrations for C-C and C-N are in agreement. Further studies are necessary to determine the binding orientation of nitrogen to copper.

Electron microscopy is a rather straightforward qualitative technique to determine the size and shape of the copper particles. The copper control is used as a basis of comparison to determine whether propylamine addition to the powder reduced the size of the particles. The uncoated particles were severely agglomerated and greater than 50% of the total particles were agglomerated. However, with the addition of propylamine, the degree of agglomeration is lessened. With the addition of 5 vol% and 10 vol% propylamine, a uniform distribution of single particles was evident. At higher magnifications, it was possible to see a coating on the surface of the copper. On a qualitative basis, it is difficult to see a significant difference in the morphology of the particles. Both concentrations are suitable to disperse the particles, however, qualitatively there is no additional benefit of adding 10 vol% propylamine to the powder.

Particle size distribution data is very beneficial because it provides quantitative information in regards to the particle size. The copper control has an average particle size of 4.1 ± 2.6 μm. With surfactant addition, a noticeable decrease in the size of the copper

particles is evident. Copper coated with 5 vol% propylamine has an average particle size of 3.8 ± 2.9 μm while copper coated with 10 vol% propylamine has an average particle size of 4.1 ± 2.6 μm. Adding 10 vol% propylamine to the copper slurry does not provide any further additional benefit to lessen aggregate formation. Consequently, adding 5 vol% propylamine as a surfactant hinders the formation of agglomeration. The hydrophobic tail of the amine repels the surrounding copper particles. With an increase in the distance between atoms, the strength of the electrostatic force decreases.

Propylamine is also a suitable surfactant for this study because it is a low boiling solvent (bp 48 °C). Propylamine was dissolved in ethanol to dilute each of the surfactants and ethanol also a low boiling solvent (bp 78 °C). Once the copper particles are coated, we have to ensure that the coating can be easily removed prior to use in the various applications. Thermogravimetric analysis was used to measure mass changes of the sample as a function of temperature. The temperature program was designed to heat the samples in the presence of nitrogen gas from room temperature to 550 °C at a rate of 10 K/min. At temperatures above 900 °C, the copper oxide layer on the particles begins to decompose (this result was found experimentally upon heating the sample to 1000 °C).

It was found that all of the copper samples coated with propylamine encountered a mass change of 1 to 4 wt.%. At 50 °C the removal of the coating was initiated and at 150 °C the coating was fully removed. XPS analysis on the heated samples also confirms that at 150 °C nitrogen groups are no longer present on the sample and the surface is composed of 37 at.% carbon, 40 at.% oxygen and 23 at.% copper. These compositions are comparable to the composition of the copper control sample (Table 4.4). Furthermore, infrared spectroscopy indicated that there are no bands representing the primary amine or alkane groups. A single intense band at a wavenumber of 642 cm^{-1} represents the Cu-O (ν) vibration. Consequently the results in this study demonstrate that nitrogen binds to copper on the surface, however, with an increase in temperature, the surfactant can be removed. Essentially, both ethanol and propylamine are removed at the similar temperatures, as there is a single peak in the TGA spectrum. Propylamine does not decompose on the surface of copper.

Consequently, 5 vol% propylamine is a suitable surfactant loading to disperse the copper particles. SEM and particle size distribution analysis shows that there is a

noticeable decrease in the size of the copper particles with surfactant addition. Both XPS and IR results conclude that the amine group is bound to the metallic surface. Also, the coating is easily removed in a single step when the sample is heated to 150 °C. Fragmentation of the amine chain is not evident.

5.4 Copper Coated with Butylamine

The adsorption of butylamine onto metallic surfaces has not been studied greatly in literature, however, for any type of surfactant, other hydrophobic groups can substitute the hydrocarbon component. In this study, butylamine will act as a substitute for propylamine to determine if larger hydrocarbon chains are better surfactants to hinder agglomerate growth.

The copper particles were coated with 1 vol%, 2 vol%, 5 vol% and 10 vol% butylamine. A copper control sample was also prepared as a source of validity for the data. The Cu $2p_{3/2}$ and Cu $2p_{1/2}$ peaks for the copper control sample were very symmetrical and the binding energies were consistent with the copper metal standard. When the particles are coated with 1 vol%, 2 vol%, 5 vol% and 10 vol% butylamine, the binding energies of the core energy levels are shifted to higher energy levels. For example, for the copper-1 vol% butylamine sample, Cu $2p_{3/2}$ and $Cu2p_{1/2}$ are located at 933.6 eV and 953.3 eV, respectively. When these binding energies are compared to the copper standards (Table 4.1), the results are comparable to the binding energies of Cu^{+2}. The composition results from XPS show that with an increase in the surfactant concentration, there is also an increase in the concentration of atomic nitrogen on the surface. For the 1 vol%, 2 vol% and 5 vol% copper-butylamine samples, the ratio of the relative concentration of oxygen to copper is ~0.7.

Difference reflectance spectra were collected for the duplicate samples of copper coated with butylamine. All of the IR spectra contained an intense band at a wave number of ~640 cm^{-1} representing the copper oxide stretch vibration. It is possible to differentiate the bands that are associated with stretching of amines and bands due to stretching of the hydroxide group. The bands of the N-H (ν) are found at somewhat lower frequencies than the corresponding -OH band. In each of the coated copper samples, a hydroxide group from the ethanol binds to the surface. In the IR spectra, bands representing C-H are found

at ~2950 cm^{-1}, C-C at 1050 cm^{-1} and C-N (ν) at ~1400 cm^{-1}. The corresponding amine stretching bands are found at ~3400 cm^{-1} and the bending vibrational bands are found at ~1400 cm^{-1}. When these vibrational frequencies are compared to Abdallah et al. (2004) study of pyridine adsorption on Mo(110), it is evident that the results are comparable. Both the C-N and C-C (ν) bands are located at very similar wavenumbers.

Consequently, nitrogen binds to copper through the lone pair on the nitrogen and this bonding can be described as η^1(N). Further experiments are necessary to determine the bonding orientation and geometry.

In SEM analysis, two regions on each sample were analyzed to ensure consistency in the results. The uncoated copper sample contained approximately 50 % agglomerated particles. However, with the addition of butylamine in low concentrations (1 or 2 vol%), the particles became relatively well distributed. There was a small quantity of agglomerated clusters in which small particles were bound to the larger particles. The coated particles are crystalline and a thick coating is visible on the surface of the dry powder.

Particle size distribution results are used to verify the qualitative conclusions obtained from SEM analysis. The control sample contained particles with an average size of 4.1 ± 2.6 μm and with the addition of butylamine, the average size of the particles decreases. It is difficult to state which concentration is suitable to hinder agglomeration. Either 1 vol% butylamine or 10 vol% butylamine are suitable concentrations to ensure dispersion of copper powder. Copper coated with 1 vol% butylamine has an average particle diameter of 3.5 ± 3.1 μm while 10 vol% butylamine addition results in particle with an average diameter of 3.7 ± 2.9 μm.

It was found with thermogravimetric analysis that at 70 °C, changes in mass were evident. Ethanol and the hydrocarbon chain in butylamine are being removed at a temperature range of 70 °C to 150 °C. XPS results at this temperature indicate that nitrogen is not removed in this temperature range. IR results also confirm that nitrogen is present on the surface of the copper as a broad peak for the NH_2 (ν) was found at 3401 cm^{-1}. However, the atomic concentration of carbon at the surface decreases with an increase in temperature and the stretching bands for the C-H are no longer present. It is

possible that with an increase in temperature, the bond between nitrogen and carbon weakened leading to fragmentation.

In the temperature range of 180 °C to 250 °C, nitrogen is removed from the sample. XPS analysis indicates that the atomic concentration of nitrogen is 0 at.% and there are no amine bands in the IR spectrum. At 250 °C, the sample consists of 42 at.% carbon, 35 at.% oxygen and 23 at.% copper. This relative composition is very similar to the composition of the uncoated sample.

Consequently, the results in this study show that the core of each particle is metallic in nature and a thin oxide layer is present on the surface. Coated samples have a +2 oxidation state while uncoated copper has an oxidation state of 0. There are no impurities, such as chlorides, in the samples that may affect the interruption of agglomerate formation. Either a 1 vol% or 10 vol% butylamine loading is suitable to disperse the copper particles. Economically, it is beneficial to use a low surfactant loading to the sample because it is less expensive and addition of large quantities of amines results in diminishing returns. The probability of developing agglomerated particle clusters decreases with butylamine because the cationic head of the surfactant binds to the copper surface while the hydrophobic tail increases repels the surrounding particles. As the distance between the copper particles increases, the electrostatic forces decrease. The particles no longer have a strong force of attraction. Lastly, it is possible to remove butylamine from the surface of the copper particles. Nitrogen is more strongly bound to copper in comparison to propylamine. The TGA analysis indicates that the surfactant is removed from copper by means of fragmentation.

5.5 Copper Coated with Benzenethiol

The third study involved coating the copper particles with benzenethiol. Previous studies completed by Husein et al. (2003) claimed that benzenethiol was effective in microemulsion systems. Thiol compounds have a long hydrophobic tail (Woo Han et al. 2001) that form micelles.

The copper particles were coated with 1 vol%, 2 vol%, 5 vol% and 10 vol% benzenethiol. From XPS analysis, Cu $2p_{3/2}$ and Cu $2p_{1/2}$ have a binding energy of 933.3 eV and 953.3 eV, respectively. With an increase in surfactant concentration, there is no

shift in the Cu 2p peaks. When these binding energies are compared to the binding energy of the Cu^{+2} standard (Cu $2p_{3/2}$: 933.6 eV, and Cu $2p_{1/2}$: 953.4 eV), it is apparent that the copper-benzenethiol samples have a +2 oxidation state.

The composition results from XPS show that with an increase in the surfactant concentration, there is also an increase in the concentration of atomic sulfur on the surface. The ratio of the concentration of oxygen to copper is approximately 1.5 for all of the samples. The coated samples contain approximately 65 at.% carbon while the control sample contains 53 at.% carbon.

Woo Han et al. (2001) studied the chemisorption of benezenethiol on silver powder by diffuse reflectance infrared spectroscopy (DRIFTS). From IR, it was determined that the contribution from the benzene ring and in-plane phenyl ring geometry modes include the bands at 3052, 1575, 1473, 1022 and 1000 cm^{-1}. All of these bands have dipole moments parallel to the molecular axis.

In our studies, it was found that when the surfactant is bound to copper, C-H (ν) (3050 cm^{-1}), C=C (ν) (1578 cm^{-1}), CH_2 (γ) (1438 cm^{-1}), Cu-S (ν) (730 cm^{-1}) and Cu-O (ν) (641 cm^{-1}) vibrational bands are evident. These vibrational bands are very similar to the data collected by Woo Han et al. (2001). The results indicated that η^1(S) bonding is present, but further studies are necessary to determine whether benzenethiol has a perpendicular or parallel orientation with respect to the surface of copper. Sulfur is bound to the surface of copper and the benzene ring remains bonded to sulfur. The saturated benzene ring behaves like a hydrophobic tail of a micelle repelling the other copper particles. For all of the coated samples, all of the characteristic bands were located at similar wave number. The principle IR bands do not shift with alterations in surfactant concentrations.

From Figure 4.13, it is apparent that the surfactant does not significantly improve particle distribution. Coating the copper particles with 10 vol% benzenethiol resulted in less particle aggregates. The particles were irregularly shaped and had a diameter of 4.0 ± 2.9 μm. The copper control particles had an average diameter of 4.1 ± 2.6 μm.

It was also found that particle aggregation and flocculation took place when the concentration of the surfactant was decreased. This was attributed to a decrease in the interaction between the surfactant protective layer and the nanoparticles (Husein, et al.

2004). The copper particles were heavily agglomerated and non-spherical when 1 vol%, 2 vol% and 5 vol% benzenethiol was added to the powder. Quantitatively, the particle size distribution results supported the qualitative results because the average size of the particle increased with a increase in surfactant loading. Table 4.17 showed that with the addition of benzenethiol, the particles were larger in comparison to the control group.

The TGA results demonstate that with elevated temperatures it is possible to remove benzenethiol from the surface of the metal. When the powders were heated to 150 °C, XPS analysis shows that the sample consists of 7 at.% sulfur, 62 at.% carbon, 18 at.% oxygen and 13 at.% copper. However, the IR results show that the -OH group is removed from the surface of the particles. The first peak in Figure 4.9 represents the removal of ethanol. By further increasing the sample to 350 °C, the bonds between copper and sulfur are removed. The TGA results are consistent with the IR data because at 350 °C all of the sulfur and alkane vibrational bands are non-existent. The copper sulfur bond is the weak and the benzene ring does not fragment due to resonance stabilization. It is very difficult to break a double bond. Thus, the second peak in Figure 4.9 represents the removal of benzenethiol from the copper particles.

Consequently, emulsions containing micelles provide a convenient medium for the preparation of a wide variety of nanoparticles because the efficient mixing at the molecular level leads to the development of a highly homogenous product. In this study, benzenethiol was not an effective surfactant to minimize aggregate formation. The effect of surfactant concentration at fixed experimental parameters on agglomeration was studied. Husein et al. (2004) also studied the effect of surfactant and co-surfactant concentrations, water to surfactant mole ratio, pH, mixing time and temperature of reaction on nucleation, growth and particle agglomeration. His group determined that adding a low concentration of a surfactant resulted in the production of smaller particles. Thus, altering some of the experimental variables can lead to well distributed particles. This was well beyond the objective of this study.

5.6 Copper coated with polyacrylic acid

XPS analysis showed that Cu $2p_{3/2}$ is located at a binding energy of 933.2 eV and Cu $2p_{1/2}$ is present at 953.2 eV. These binding energies are consistent with the +2 oxidation state. The Cu 2p peaks indicated in Figure 4.6 are fairly broad with distinct shoulders in comparison to the Cu 2p peaks associated with the copper control. The features of the Cu $2p_{3/2}$ and Cu $2p_{1/2}$ peaks are very similar to the characteristics of the Cu^{+2} standard.

The data shows that increasing the concentration of surfactant results in an increase in the concentration of carbon and sodium. The copper control consists of 36.9 at.% carbon, 33.8 at.% oxygen and 29.4 at.% copper. With the addition of 0.5 M polyacrylic acid to the copper powder, the sample consists of 49.9 at.% carbon, 24.3 at.% oxygen, 4.6 at.% sodium and 21.2 at.% copper. Residual sodium is present in the samples as sodium polyacrylate was dissolved in nanopure water to develop the polyacrylic acid surfactant.

DRIFTS was used to collect the IR spectra of the copper control and copper coated samples. The vibrational bands in the coated samples represent –OH (3410 cm^{-1}), CH_2 (3020 cm^{-1}), C-H (2930 cm^{-1}), COO^- (1578 cm^{-1}), C=O (1457 cm^{-1}) and Cu-O (644 cm^{-1}) stretching. The copper control has only Cu-O (ν) vibrations. Both the 0.5 M and 1.0 M polyacrylic acid copper samples had similar vibrational frequencies. With increasing surfactant concentration, a shift in the stretching or bending frequencies was not seen. Shifts in vibrational frequencies due to changes in surfactant concentration were also no seen in the propylamine, butylamine and benzenethiol studies.

As determined by SEM, adding 0.5 M and 1.0 M polyacrylic acid to the copper powder resulted in a vast quantity of agglomerated clusters. The particles were non-spherical and a coating was evident on the surface. Particle size distribution data further advocates that addition of this particular surfactant does not hinder agglomeration. Copper particles coated with 0.5 M polyacrylic acid have an average diameter of 6.2 ± 2.2 μm. The uncoated particles have a diameter that is approximately 2 μm smaller than the coated particles. Addition of 1.0 M polyacrylic acid further increases the particle size to 7.4 ± 2.6 μm. It is possible that these large clusters are formed because the long surfactant tails interfere with one another. The surfactant molecule is too large in comparison to the micro-scale copper particles. Instead of repulsion, the tails of the surfactant intertwine to generate large particle clusters.

TGA analysis showed that at approximately 50 °C, changes in mass were evident. Several peaks are evident in Figure 4.10. In essence, the polymer is fragmenting off of the copper particles. XPS and IR analysis of samples taken at 550 °C indicated that the polymer is still on the metallic surface.

As a result, it was determined that polyacrylic acid is not a suitable surfactant to hinder copper agglomeration. With minimal surfactant addition, there was a larger quantity of particle clusters. Particle size distribution results clearly supported the qualitative findings from SEM analysis. In essence, it was relatively easy to coat the particles with the polymer surfactant but the molecules were too large for a small particle.

5.7 Comparison of Organic Surfactants

In this study, four different surfactants were used to determine whether agglomeration of copper particles could be suppressed. From this study, it was determined that 5 vol% propylamine was the best surfactant to hinder copper agglomerate growth. With this surfactant loading, the particles were well distributed with an average particle size of 3.8 ± 2.9 μm. The control sample was heavily agglomerated with an average particle size of 4.1 ± 2.6 μm. The use of propylamine is advantageous because it is a relatively small molecule compared to larger hydrocarbon chains and benzene rings. Bowe et al. (2003) state that amines bond strongly to the surface of metals. It was determined that nitrogen bonds readily to copper as indicated by XPS and IR analysis. Under mild reaction conditions, the surfactant bound to the surface of the copper particles. Lastly, the use of propylamine as a surfactant is favored because the coating is removed at low temperatures. Propylamine in ethanol has a low boiling point. In the TGA analysis, a small sample of the copper coated powder was heated to 550 °C. At 150 °C, the coating was removed. XPS and IR indicated that there was no residual nitrogen or hydrocarbon chain on the surface. Propylamine did not undergo decomposition or fragmentation on the metallic surface. In essence, the copper–nitrogen bond broke with an increase in temperature and the surfactant was removed.

When copper was coated with butylamine, it was determined that 1 vol% butylamine is the best surfactant loading to hinder agglomerated group. Coating the copper particles with this particular surfactant produces very similar results as propylamine, however,

there are some slight differences that entail that propylamine is a better surfactant to hinder formation of agglomerates.

Butylamine, like propylamine, has a positively charged head group (Sharma, 1995) and a hydrophilic tail. Butylamine was also chosen as a surfactant because amines bind strongly to surfaces of metals and the compound has a low boiling point of 70 °C. An optimistic claim for these experiments involves that butylamine will behave better as a surfactant to hinder agglomerate growth due to its longer hydrocarbon chain and upon heating the coating will be removed. SEM results show that coating the particles with butylamine results in smaller particles in comparison to the control group. Copper coated with 1 vol% butylamine has an average particle size of 3.5 ± 3.1 μm. Thus, the coated butylamine samples are slightly smaller in size in comparison to the propylamine-coated copper particles. However, one disadvantage of using butylamine as a surfactant includes that fragmentation of the amine - hydrocarbon chain is evident upon heating. From the TGA, IR and XPS analysis, it was evident that at low temperatures, the hydrocarbon chain and ethanol are removed from the surface of copper. Nitrogen is still bound to copper at 150 C. Nitrogen is removed from the surface upon further heating. Due to the fragmentation of the amine, it is not suggested to use butylamine to suppress agglomeration. Adding a larger chain amine does not provide any additional benefit to obtain a well-distributed sample.

The results indicate that benzenethiol was not effective in suppressing agglomerate formation. The strength of the electrostatic forces between particles was not reduced as the particles have an affinity to bind to one another. The SEM micrographs showed that the copper coated particles were heavily agglomerated. Particle size distribution results showed that the coated particles were slightly larger than the copper control. It was also determined that benzenethiol does not undergo any structural changes during heating. In other words, the benzene ring does not undergo fragmentation during heating.

The benzene ring was supposed to act as a micelle to hinder formation of aggregates. It can be suggested to replace the S atom with another atom in the benzene ring. Woo Han et al. (2001) also studied the chemisorption of benzeneselenol on the surface of silver. Their results suggested that selenolates cannot be used as alternatives to thiolates when adsorbate – surface interactions are desired.

Therefore, the use of benzenethiol does not provide any additional benefit to suppress agglomerate formation. Using compounds containing sulfur groups is very difficult because upon heating H_2S (g) may form.

The fourth study involved using sodium polyacrylate as a coating on the surface of copper particles. Sodium polyacrylate is a flexible long chain surfactant that has lateral chain-chain interactions (Sharma, 2005). If the hydrophobic tails of the surfactant will interact with one another, it is anticipated that the electrostatic interactions between the copper particles will decrease. It was found that polyacrylic acid was not a suitable surfactant. SEM and particle size distribution results showed that the average particle size was relatively larger than the copper particles. The copper control particles had an average particle size of 4.1 ± 2.6 μm. However, coating copper with 0.5 M polyacrylic acid results in a particle size of 6.2 ± 2.1 μm. Increasing the loading of polyacrylic acid resulted in an average particle size of 7.4 ± 2.6 μm. Polyacrylic acid was not an effective surfactant because the polymer may be too large in comparison to the individual particles.

TGA, IR and XPS analysis showed that upon heating it was very difficult to remove the coating for the copper surface. With an increase in temperature, the polymer decomposed and was re-adsorbed onto the metallic surface.

Therefore, the premium surfactant to suppress agglomeration was 5 vol% propylamine. It binds readily to copper, is easily removed upon heating, and small particles are generated. Nano-sized particles were not generated, however, by changing the mixing techniques, smaller particles can be developed.

CHAPTER 6: CONCLUSIONS AND FUTURE WORK

6.1 Conclusions

The study of identifying a method to prevent the development of copper agglomerates consists of a two-fold experiment. The study involves determining which specific surfactant is better able to prevent agglomeration and whether an increase in temperature could remove the applied coating. Initially, the industrial process was studied to detect the optimum location in which the surfactant should be added. It was determined that a major area of concern for agglomeration was in the stages that followed the reactor. Thus, if a surfactant were added before the copper powder precipitated in the reactor, then the end product would contain dispersed copper particles.

Four surfactants were used to see whether the dispersion of copper particles was possible; propylamine, butylamine, benzenethiol and polyacrylic acid. Smaller amine chains, such as propylamine, are very stable and the surfactant binds to the surface of copper through nitrogen atom. Nitrogen behaves as the coordination donor. Butylamine was used to establish whether a compound containing a longer amine chain was a better dispersant. The hydrophobic tail is expected to repel the surrounding copper particles to prevent agglomeration. Benzenethiol contains a more complicated structure. Most of the thiol compounds that were previously investigated as particle aggregates contain a long hydrophobic tail that form micelles. The coating acts to repel each of the particles away from one another. As a result, there is a reduction in the force of attraction between the copper particles. Lastly, polyacrylic acid is traditionally used as a dispersant in the paper and paint industry.

The copper powders were prepared in duplicates to ensure validity of the data. The production process was modeled after the process currently implemented at Umicore Canada Ltd. A surfactant was added to the raw copper powder, dispersed at 40 °C in an ultrasonic bath, vacuum filtered and dried in a drying oven. The samples were then characterized by XPS, SEM, EDS, SEM, TGA and particle size distribution analysis.

The results demonstrate that copper coated with 5 vol% propylamine was a suitable surfactant capable of dispersing the copper particles. A review of the SEM micrographs illustrated that not only was there a coating evident on the surface of the copper particles,

but the particles were non-agglomerated. Particle size distribution data showed that with propylamine addition, the average size of the particles decreased in comparison to the control data. XPS data showed that the oxidation state of the coated samples was +2. The copper particles consisted of a metallic core and a thin oxide layer on the surface. Compositional data was used to verify that a coating was present on the surface. With an increase in the surfactant loading, there was a corresponding rise in the concentration of atomic nitrogen. IR data showed that copper was bound to the surfactant through the lone pair on the nitrogen. Additionally, TGA analysis verified that the coating could be removed at low temperatures. Fragmentation of the additive was not evident.

Coating copper with butylamine also generated dispersed particles, however, it was evident that removing the coating was a two-step process. At low temperatures, ethanol and the hydrocarbon chain are removed. However, nitrogen is removed at slightly higher temperatures. No further benefit is derived from the addition of a longer chain molecule, as there is not a sufficiently higher magnitude of dispersion.

Ultimately, benzenethiol and polyacrylic acid were poor surfactants, as no dispersion of the cooper particles was observed. It appeared as though the particles combined with each other. Even though these particular surfactants absorbed readily onto the copper particles, there was no reduction in the forces of attraction.

Even though nano-sized particles were not developed in this study, a method was used to suppress agglomeration of copper particles. Alternative levels of particle size could be achieved with slight adjustments in the experimental conditions and mixing techniques.

6.2 Future Work

6.2.1 Copper

Further studies are projected for copper powders. Atomic force microscopy (AFM) will be used to quantify the attractive or repulsive forces between the coated copper particles. This data will be useful to support the qualitative conclusions obtained from the SEM micrographs.

Furthermore, the copper system will be also studied on a fundamental level to determine the interaction of surfactant molecules with the copper surface. The plan is to

deposit different (small) surfactant molecules, such as amines, acids and thiols, onto single crystal copper surfaces with an (111) orientation. These interactions will be studied using High-Resolution Electron Energy Loss spectroscopy (HREELS), Low-Energy Diffraction (LEED) and Auger Electron Spectroscopy (AES) analysis techniques.

In parallel with the experimental work, density functional theory (DFT) calculations will be carried out to determine how amines, thiols and acids bind to the metal surface. Thus, adsorption energies and geometries will be analyzed.

Lastly, the development of nanoparticles will be studied by designing a mixing assembly which micro mixes the reactants to facilitate nanoparticles precipitation. It is also expected that adding a surfactant to the reactants in a confined impinging jet reactor will be of great benefit as the particles are stabilized as soon as they form. It was determined from our studies that adding a propylamine or butylamine to the reactants in a batch reactor generated non-agglomerated particles, but it is necessary to examine if this is valid for a flow reactor.

6.2.2 Preliminary Work on Nickel

6.2.2.1 Introduction

Further studies are also anticipated to determine the effect of surfactants on the agglomeration of nickel powders. Nickel is another important metal as it is a versatile element and will alloy with most metals. In addition nickel and nickel alloys are used in a variety of applications and the majority of uses involve corrosion and heat resistance. It is important to hinder agglomeration effects as thinner films can be used as coatings in the electronic and petrochemical industries. Some initial characterization of nickel powder has been completed with the foresight that similar surfactant studies to that of copper will be carried out.

6.2.2.2 Nickel Standards

Figures A.29 to A.31 represent survey and narrow spectra of nickel foil, nickel +2 and nickel black, which contains Ni^{+3} respectively. In these samples, we are primarily concerned about the position of the Ni $2p_{3/2}$ and Ni $2p_{1/2}$ peaks because from the shift in

the binding energy, it is possible to determine the oxidation state of the metal. Table 6.1 provides the binding energy, and atomic concentration of the nickel standards.

In nickel foil (Ni^0), the primary Ni $2p_{3/2}$ and $Ni2p_{1/2}$ peaks are located at a binding energy of 852.8 eV and 870.1 eV, respectively.

The characteristic nickel peaks are located at binding energies of 854.4 eV and 872.6 eV in the $Ni+^2$ standard. This data revels that there is a shift in the core energy level of Ni toward a higher binding energy. Thus, increasing the binding energy is associated with an increase in oxidation state. There is roughly 0.77 times more atomic oxygen in the sample compared to nickel.

In addition, nickel black was also studied as a sample as it contains Ni^{+3}. The binding energies of the core energy levels are 854.5 eV and 872.5 eV. From this sample, it can be concluded that the binding energy of Ni^{+3} is slightly higher than that of Ni^{+2}. Only relative quantities can be addressed, as this particular sample is that of a mixed oxide.

6.2.2.3 Characterization of the Nickel Process (XPS and SEM Analysis)

The nickel process was studied to determine if the oxidation state and composition of nickel changes through the various stages of production. The morphology of the particles was also be considered to determine the optimal stage of adding a surfactant.

Initially a nickel solution, water, organic additives, ammonium hydroxide and hydrogen at added to a reaction vessel at 40°C. The slurry is then washed with water, dried and classified according to particle shape and size. Figures 6.1 and 6.2 relates the nickel process to changes in oxidation sate and morphology.

The data reveals that there is a change in the oxidation state along the process. Following washing and filtration and classification, a mixed oxidation state is evident. The particles exhibit both properties of Ni^0 and Ni^{+2}. Aliquots collected after the reaction vessel, drying, fine and course classification are associated with Ni^{+2}.

Following the reaction vessel, the core valence levels of Ni $2p_{3/2}$ and Ni $2p_{1/2}$ are located at a binding energy of 855.5 eV and 873.2 eV, respectively. The Ni $2p_{3/2}$ and Ni $2p_{i/2}$ peaks are not symmetric (long trailing tails are present). A summary of the spectral features of Ni 2p is shown in Table A.1. The sample is composed of 29.9 at.% carbon, 35.7 at.% oxygen and 34.3 at.% nickel (Table A.2). A O/Cu ratio of 1.4 shows that the

ratio of oxygen to copper is 1:1. The binding energy and surface composition are related to the +2 oxidation state

In contrast, after the nickel slurry is washed with water, the core valence levels of Ni $2p_{3/2}$ and Ni $2p_{1/2}$ are located at binding energies of 853.6 eV and 872.4 eV, respectively. There is a chemical shift of 0.86 eV in reference to the binding energy of the Ni^0 standard. The peaks are also non-symmetric and they are also relatively broader in comparison to the other spectra. The relative composition is 36.73 at% carbon, 34.45 at% oxygen and 28.22 at% nickel (Table A.2).

Figure 6.2 shows the SEM images collected from samples in the production process. Only low-resolution images are depicted in the figure. Along the process, vast changes are apparent in the morphology of the particles. Nickel is heavily agglomerated following reaction in the reaction vessel and after the washing-filtration stage. The particles are almost spherical but they are located in large clusters. Small particles are bound to the surface of the larger particles. The cluster is approximately 15 μm in diameter. Agglomeration becomes a problem in the initial stages of particle formation.

Following drying, the nickel particles clusters are slightly smaller (8 μm in diameter). They are irregularly shaped. Agglomeration is also a problem in this part of the process. Results from EDX analysis are inconclusive. Elemental analysis shows that the surface of the nickel is relatively pure. The oxide layer is so thin that it is essentially undetectable with our experimental setup.

Consequently, but completing initial characterization on the nickel production process, it is evident that agglomeration is a problem.

Table 6.1 Summary of spectral features for the nickel standards

	Element / Transition	Binding Energy (eV)	FWHM (ev)	Conc. (at. %)
Ni Foil	C 1s'	284.8 (285.0)	1.01	
	Ni 2p3/2'	852.6 (852.8)	1.02	
	Ni 2p1/2'	869.8 (870.1)	1.36	
Ni +2 Standard	C 1s'	284.3 (285.0)	0.90	10.7
	C 1s"	284.9 (285.7)	0.92	
	C 1s '''	285.8 (286.5)	0.91	
	O 1s'	529.1 (529.8)	0.76	38.8
	O 1s"	529.6 (530.3)	0.75	
	O 1s'''	530.7 (531.2)	0.80	
	O is''''	531.6 (531.9)	0.76	
	Ni 2p3/2'	853.8 (854.5)	1.47	50.5
	Ni 2p3/2"	855.7 (856.3)	2.65	
	Ni 2p3/2'''	860.5 (861.2)	2.20	
	Ni 2p3/2''''	862.4 (863.1)	2.21	
	Ni 2p1/2'	871.9 (872.6)	2.60	
	Ni 2p1/2"	874.2 (874.9)	2.70	
	Ni 2p1/2'''	878.1 (878.7)	2.65	
	Ni 2p1/2''''	880.6 (881.3)	2.68	
Ni Black	C 1s'	284.5 (285.0)	0.73	3.8
	C 1s"	285.1 (285.6)	0.74	
	C 1s '''	285.8 (286.3)	0.75	
	O 1s'	529.1 (529.7)	0.76	38.8
	O 1s"	529.6 (530.2)	0.72	
	O 1s'''	530.5 (531.0)	0.70	
	O 1s''''	531.3 (531.8)	0.70	
	Ni 2p3/2'	853.9 (854.5)	1.52	57.4
	Ni 2p3/2"	855.7 (856.2)	1.60	
	Ni 2p3/2'''	860.7 (861.2)	1.80	
	Ni 2p3/2''''	862.1 (862.7)	1.75	
	Ni 2p1/2'	871.9 (872.5)	2.59	
	Ni 2p1/2"	874.1 (874.6)	2.80	
	Ni 2p1/2'''	878.0 (878.6)	2.70	
	Ni 2p1/2''''	888.6 (889.1)	2.99	

NOTE:

The values in parentheses are corrected binding energies assuming the C 1s photoemission band corresponds to carbon at 285.0 eV.

Atomic concentrations were quantifies from the survey spectra.

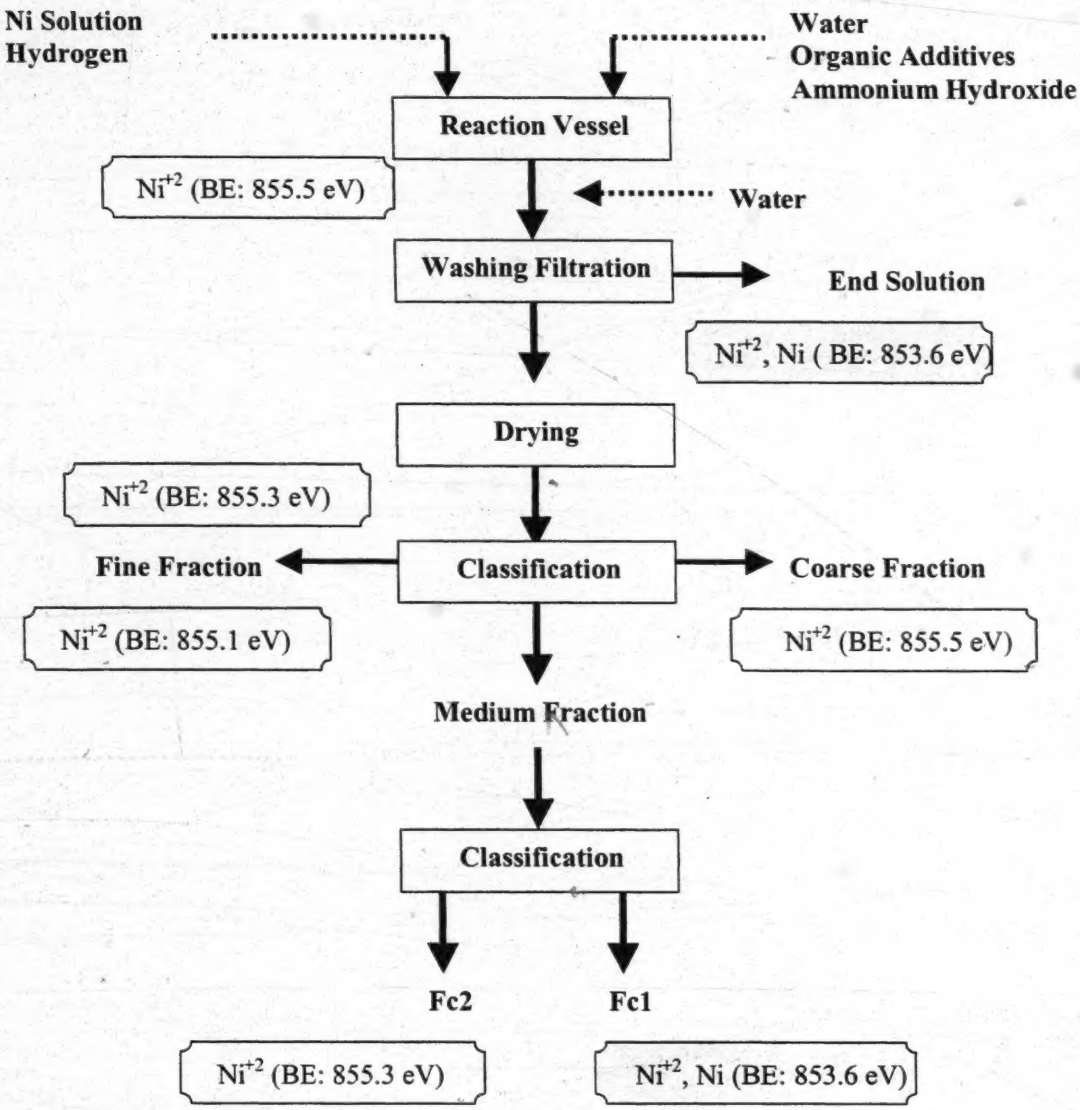

Figure 6.1 Nickel flow diagram – changes in oxidation state

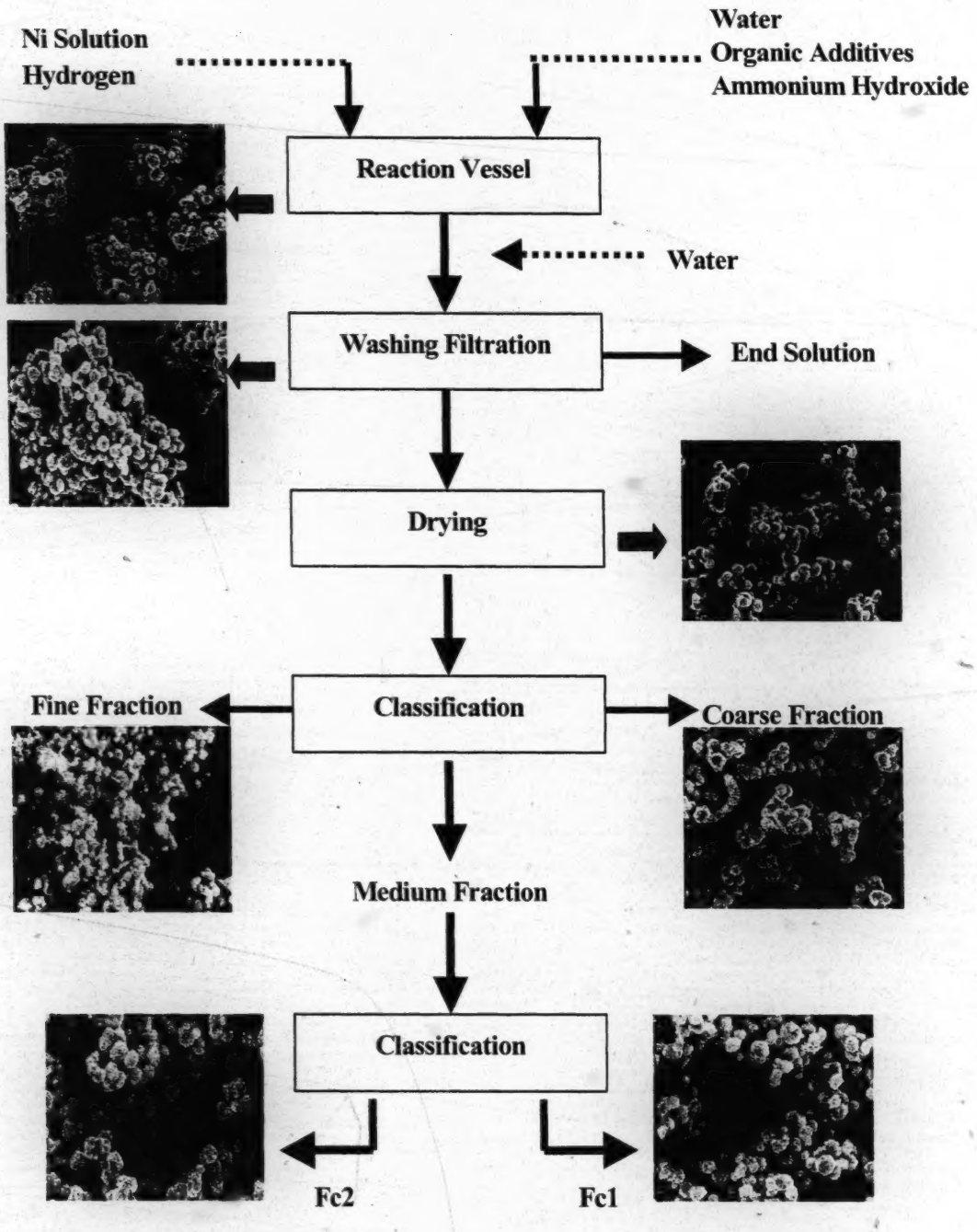

Figure 6.2 Changes in particle morphology along nickel production

REFERENCES:

Abdallah, W., Nelson, A.E. and Gray, M. (2004), "Pyridine adsorption and reaction on Mo(110) and C/N-Mo(110): experiment and modelling," *Surf. Sci.*, **569**, 193-206.

Attard, G. and Barnes, C. (1998), *Surfaces.* Oxford University Press. New York, USA. p. 38-42.

Bowe, C.A., Poore, D.D., Benson, R.F and Martin, D.F (2003). "Extraction of heavy metals by amines adsorbed onto silica gel," *Journal of Environmental Science and Health*, **A38**, 2653 – 2660.

Briggs, D. and Seah M.P. (1990), *Practical Surface Analysis: Volume 1 – Auger and X-ray Photoelectron Spectroscopy*. John Wiley & Sons Ltd. England. p. 36-69.

Carmony, R.C. (1990). *The New Book of Knowledge.* Grolier Incorporated. USA.

Chow, G.M. and Gonsalves, K.E. (1996), *Nanotechnology: molecularly desired materials.* Amercian Chemical Society. Washington, D.C. USA.

Espinos, J.P., Morales, J., Barranco, A., Caballero, A., Holgado, J.P and Gonzalez-Elipe, A.R. (2002), "Interface effects for Cu, CuO, and Cu_2O deposited on SiO_2 and ZrO_2, XPS determination of the valence state of copper in Cu/SiO_2 and Cu/ZrO_2 catalysts." *J.Phys. Chem. B*. 2002, 106, 6921-6929.

Esumi, K. (1995), *Surfactant Adsorption and Surface Solubilization.* American Chemical Society. Washington, D.C. USA. Chapter 8.

Goldstein, J.I., Newbury, D.E., Echlin, P., Joy, D.C., Fiori, C. and Lifshin, E. (1981), *Scanning Electron Microscopy and X-Ray Microanalysis.* Plenum Press. New York, USA.

Greenwood, N.N. (1998). *Chemistry of Elements.* 2nd edition. Butterworth-Heineman. Boston, USA. Chapter 28.

Gunzler, H. and Gremlich, H. (2002), *IR Spectroscopy – An Introduction.* Wiley-VCH. Weinheim, Germany. Chapter 6.

Guy, A.G. (1960), *Elements of Physical Metallurgy.* 2nd edition. Addison-Wesley Publishing Company, INC. London, England. Pages 73, 381, 387.

Haines, P.J. (2002), *Principles of Thermal Analysis and Calorimetry.* RSC Paperbacks. Survey, UK. Chapter Two.

Hills, C.W., Mack, N.H. and Nuzzo, R. (2003), "The size dependent structural phase behaviours of supported bimetallic (Pt-Ru) nanoparticles," *J. Phys. Chem,* **107**, 2626-2636.

Hosford, W.F. (2005), *Physical Metallurgy.* CRC Press. Boca Raton, Florida, USA. Chapters 1 & 12.

Husein, M., Rodil, E. and Vera J.H. (2004), "Formation of silver bromide precipitate of nanoparticles in a single microemulsion utilizing the surfactant counterion," *Journal of Colloid and Interface Science.* **73**, 426-434.

Khare, N. (2003), *Handbook of High-Temperature Superconductor Electronics.* Marcel Dekker Inc. New York, USA. Chapters 1-3.

Messing, G.L., Markhoff, C.J. and McCoy, L.G. (1982), "Characterization of ceramic powder compaction," *American Ceramic Society Bulletin*, **61**, 857-860.

Nelson, A.E. and Wanke, S. (Winter 2005), *Course Notes: CH E 694 Heterogeneous Catalysis and Reactor Analysis.* University of Alberta.

Niemantsverdriet, J.W. (1993), *Spectroscopy in Catalysis.* Wiley, New York, NJ.

OMNIC Operations Manual. Developed by Thermo Electron Corporation. USA. 2005.

Phillips, J.S and Skuse D.R (2003). *"Role of dispersants in the production of fine particle size calcium carbonate," CIM Bulletin.* ***96****, 55-60.*

Pietsch. W. (1991), *Size Enlargement by Agglomeration.* Wiley, New York, NJ.

Pinner, R. (1962), *Copper and Copper-Alloy Plating.* Copper Development Association. London, England. Chapters 2, 17.

Plunkett, J.W. (2004), *Nanotechnology & MEM industry trends & statistics.* Plunkett Research Ltd. Houston, Texas.

Sexton, B.A. and Avery, N.R. (1985), "A vibrational and TDS study of the adsorption of pyroole, Furan and thiophene on Cu(100): evidence for π-bonded and included species", *Surf. Sci.*, **163**, 99-113.

Sharma, R. (1995), *Surfactant Adsorption and Surface Solubilization.* American Chemical Society. Washington, D.C. USA. Chapter 1.

Shi, J. and Verweij, H. (2005), "Synthesis and purification of oxide nanoparticles dispersion by modified emulsion precipitation," *Langmuir*, **21**, 5570-5575.

Suslick, K.S. and Price, G.P. (1999), "Applications of ultrasound to material science," Ann Rev Mater Sci., **29**, 295-326.

Thomas, J.M and Thomas, W.J. (1997), *Principles and Practice of Heterogeneous Catalysis.* VCH, Weinheim, Germany. p. 171-175.

Voogt, E.H., Mens, A.J.M. and Geus, J.W (1996), "XPS analysis of palladium oxide layers and particles," *Surf. Sci.*, **350**, 251-267.

Voogt, E.H., Mens, A.J.M., Gijzeman, I.L.J. and Geus, J.W. (1999), "XPS analysis of the oxidation of palladium model catalysts," *Catalysis Today*, **47**, 321-323.

Woo Hang, S., Lee, S.J. and Kim, K. (2001), "Self-assembled monolayers of aromatic thiol and selenol on silver: comparative study of adsorptivity and stability," *Langmuir*, **17**, 6981-6987.

Websites:

http://www.seallabs.com/howedx.html (Viewed May 02,2005)

http://www.mos.org/sln/SEM/works.html (Viewed April 28, 2005)

http://www.millipore.com (Viewed May 02, 2005)

www.lasurface.com (Viewed April 28, 2005)

APPENDIX A

A.1 Copper Standards

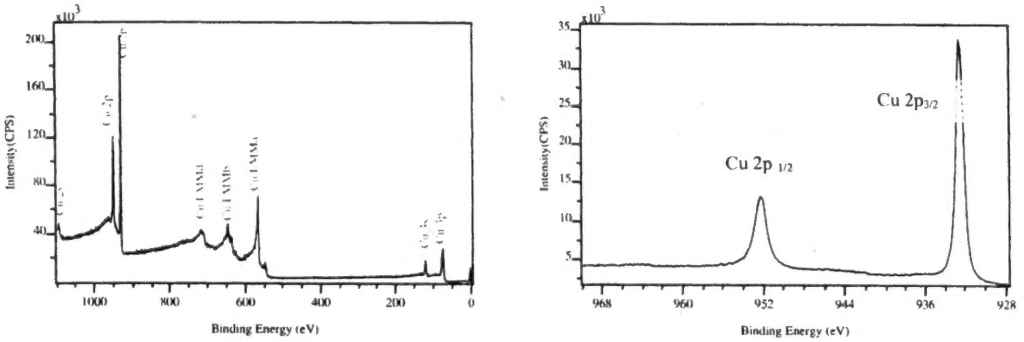

Figure A.1.a Survey Scan for Cu^0 and b Narrow Scan for Cu^0

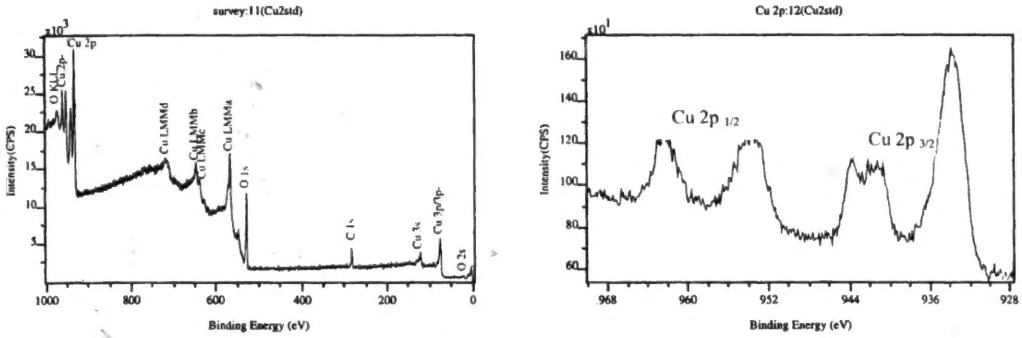

Figure A.2.a Survey Scan for Cu^{+2} and b Narrow scan of Cu^{+2}

A.2 Copper coated with Propylamine

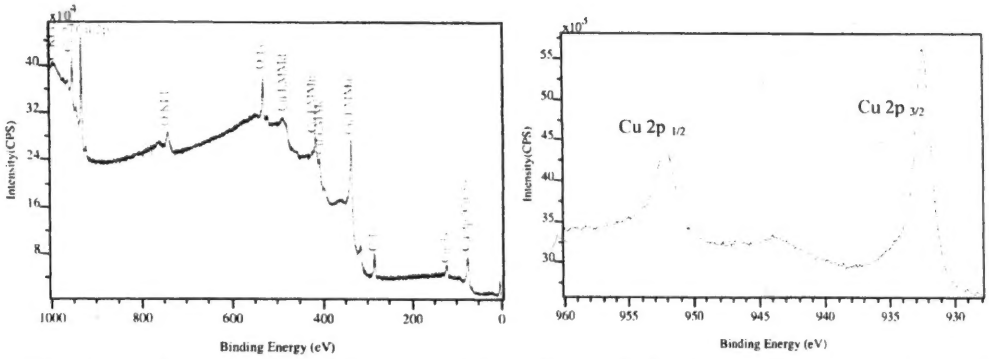

Figure A.3.a Survey scan of Cu control (0 vol% propylamine) and b Narrow scan of Cu 2p.

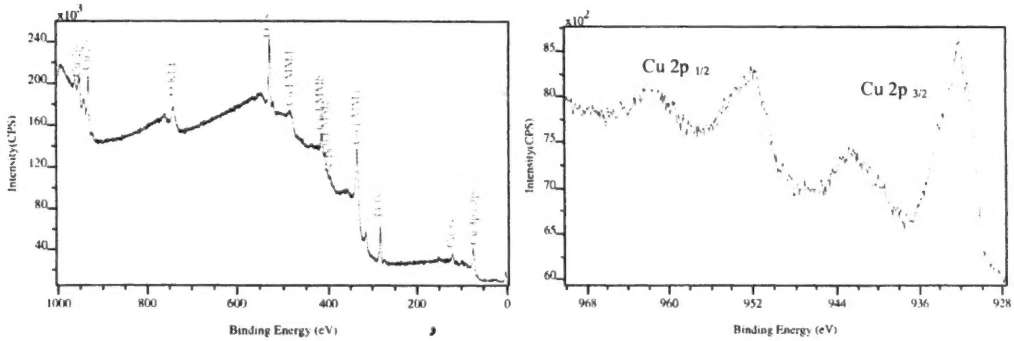

Figure A.4.a Survey scan of Cu coated with 10 vol% propylamine and b Narrow scan of Cu 2p.

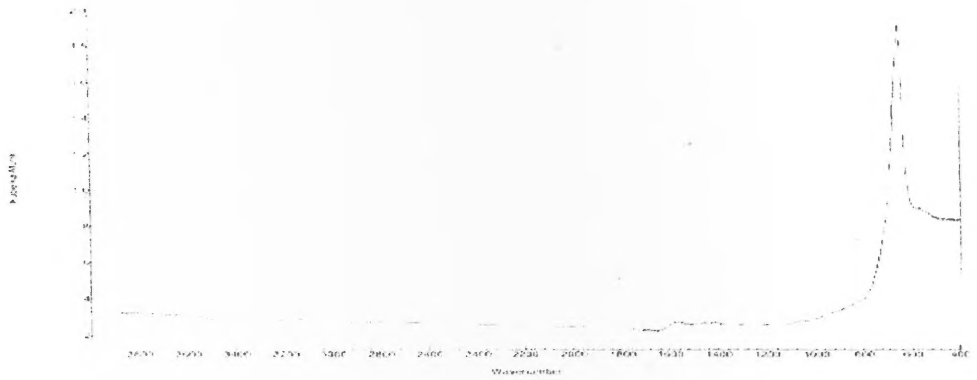

Figure A.5 IR spectrum of the copper control

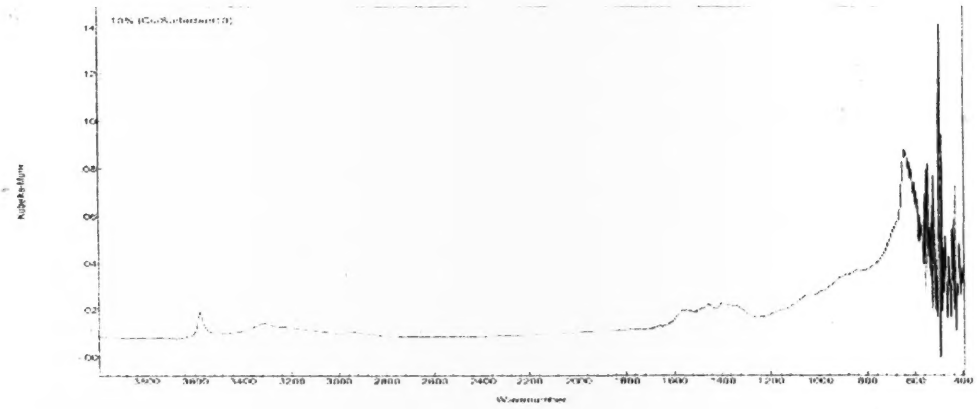

Figure A.6 IR spectrum of copper coated with 10 vol% propylamine

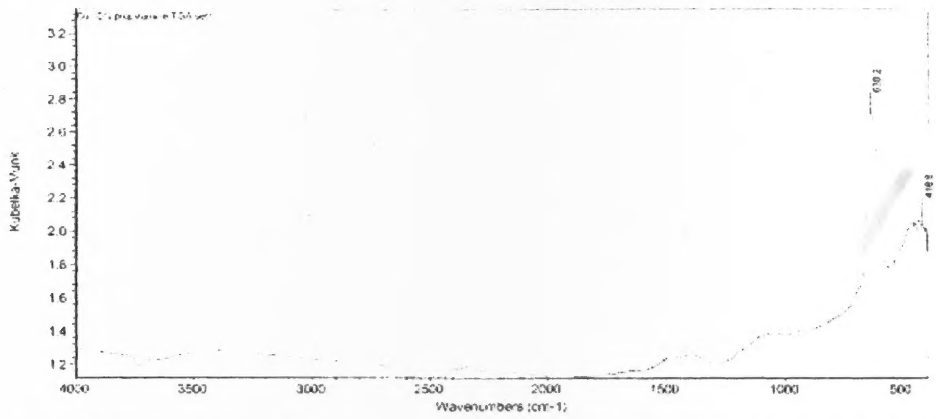

Figure A.7 IR spectrum of copper coated with 10 vol% propylamine after TGA analysis

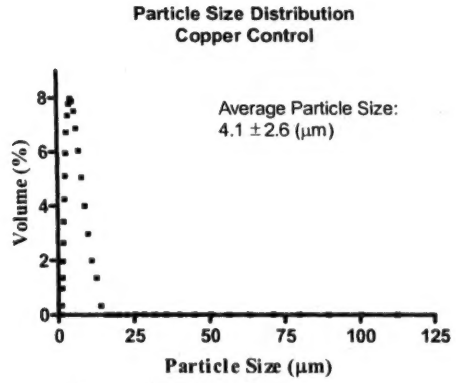

Figure A.8 Particle size distribution for the copper control

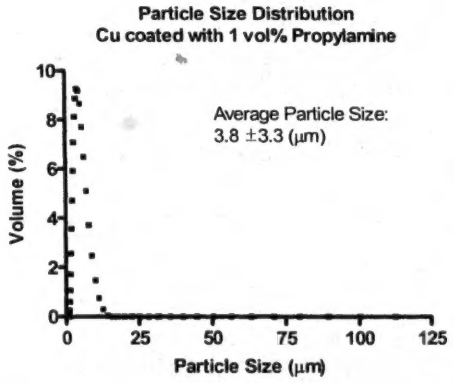

Figure A.9 Particle size distribution for copper-1 vol% propylamine

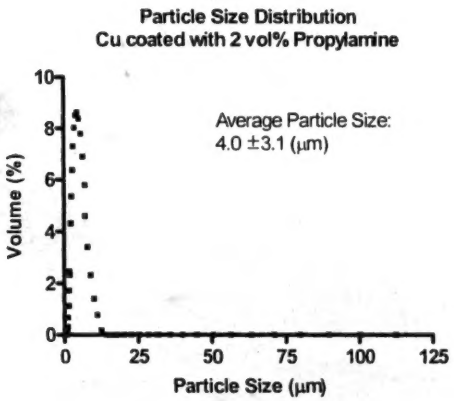

Figure A.10 Particle size distribution for copper-2 vol% propylamine

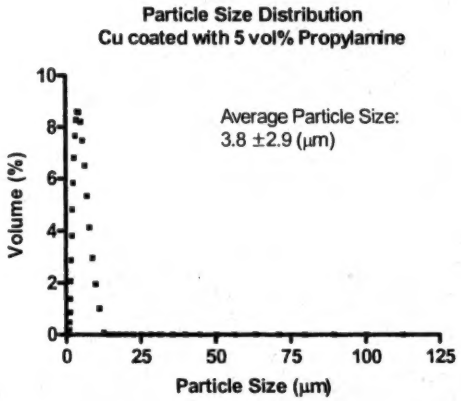

Figure A.11 Particle size distribution for copper-5 vol% propylamine

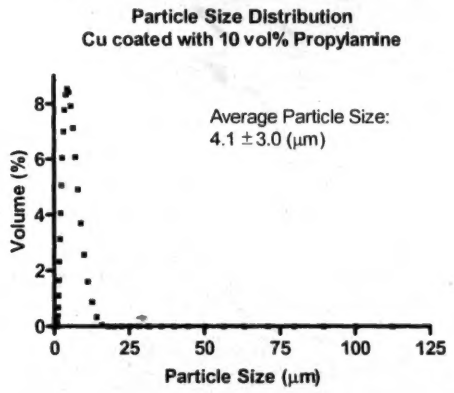

Figure A.12 Particle size distribution for copper-10 vol% propylamine

A.3 Copper coated with Butylamine

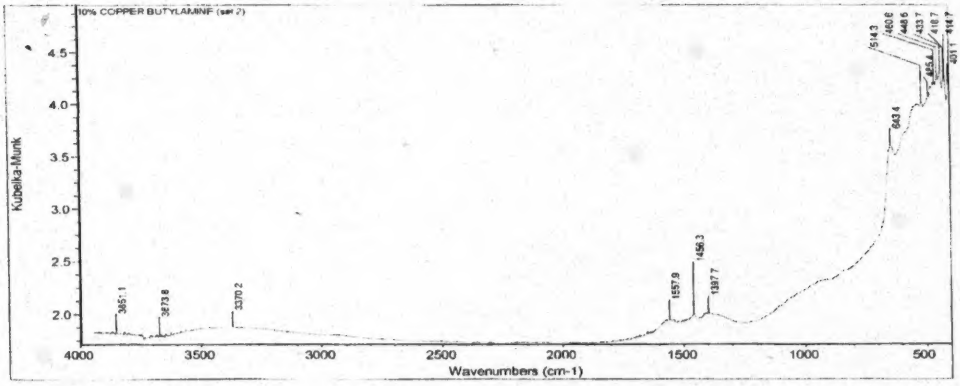

Figure A.13 IR spectrum of copper coated with 10 vol% butylamine

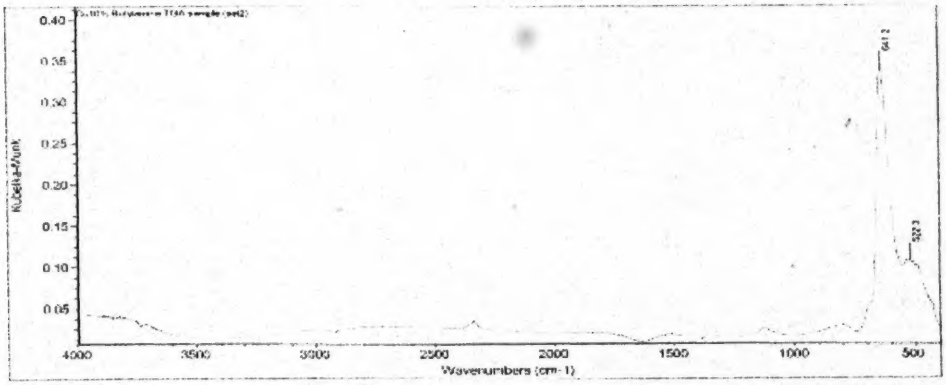

Figure A.14 IR spectrum of copper coated with 10 vol% butylamine after TGA analysis

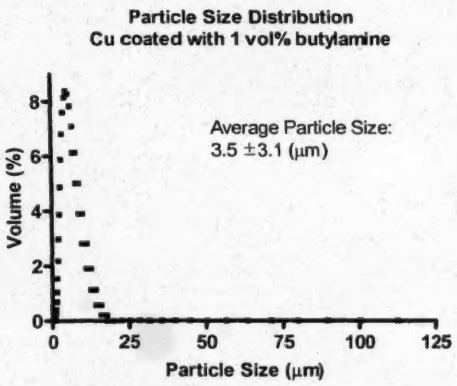

Figure A.15 Particle size distribution for copper-1 vol% butylamine

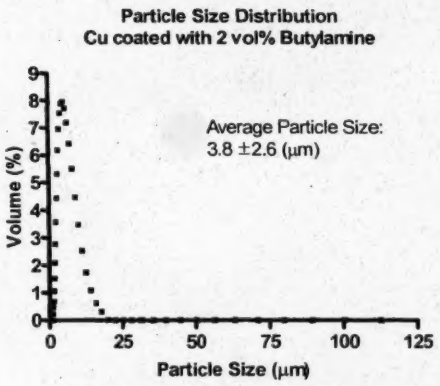

Figure A.16 Particle size distribution for copper-2 vol% butylamine

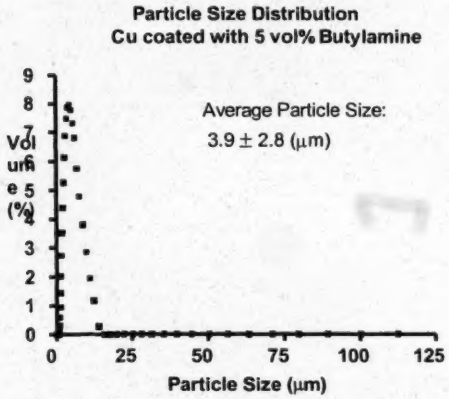

Figure A.17 Particle size distribution for copper-5 vol% butylamine

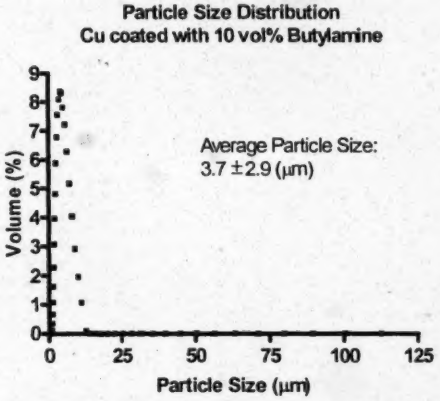

Figure A.18 Particle size distribution for copper-10 vol% butylamine

A.3 Copper coated with Benzenethiol

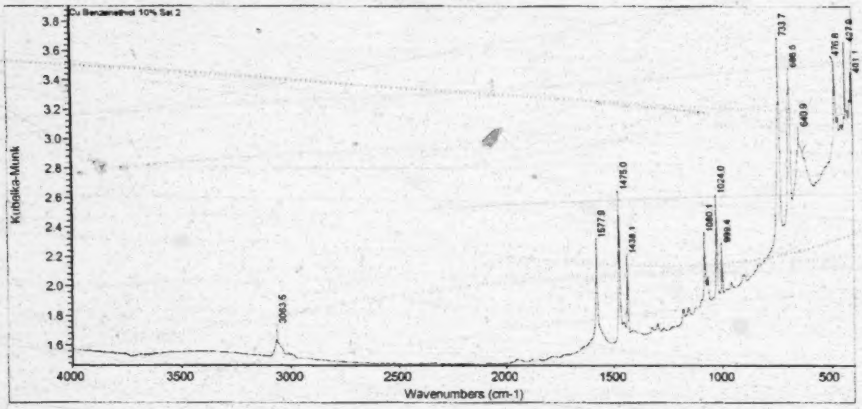

Figure A.19 IR spectrum of copper coated with 10 vol% benzenethiol

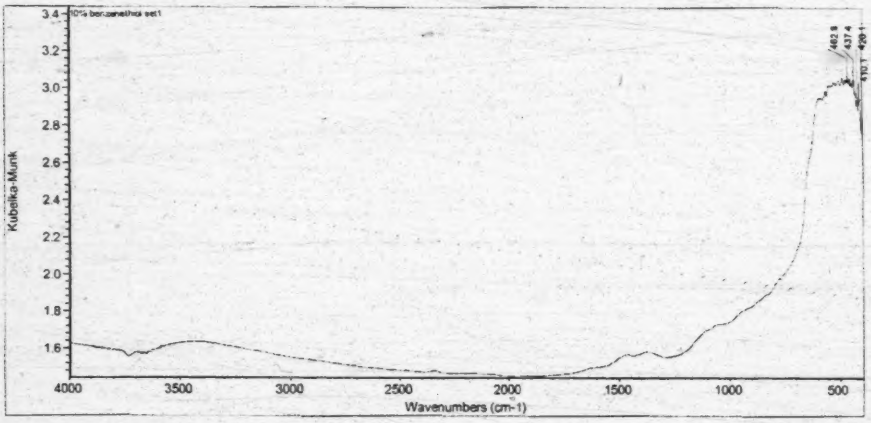

Figure A.20 IR spectrum of copper coated with 10 vol% benzenethiol (post-TGA analysis)

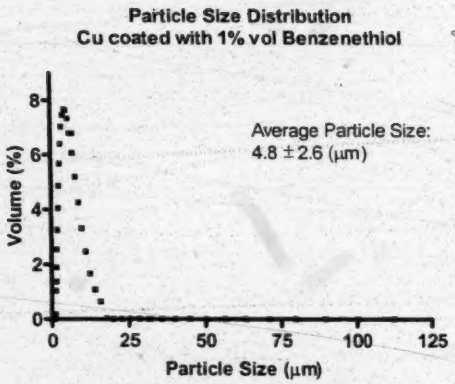

Figure A.21 Particle size distribution for copper-1 vol% benzenethiol

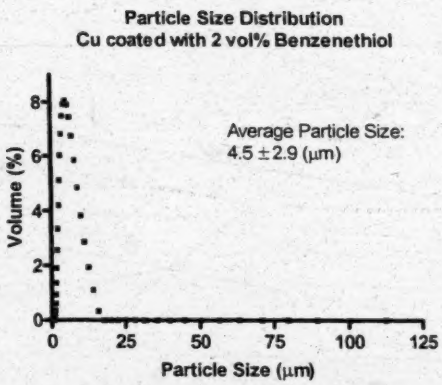

Figure A.22 Particle size distribution for copper-2 vol% benzenethiol

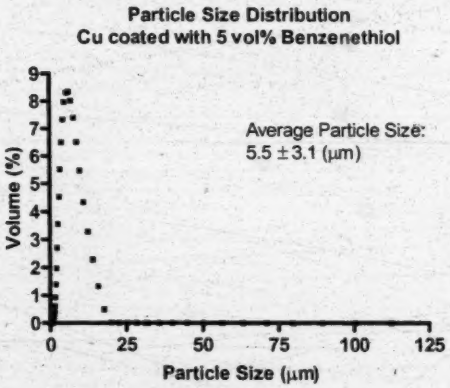

Figure A.23 Particle size distribution for copper-5 vol% benzenethiol

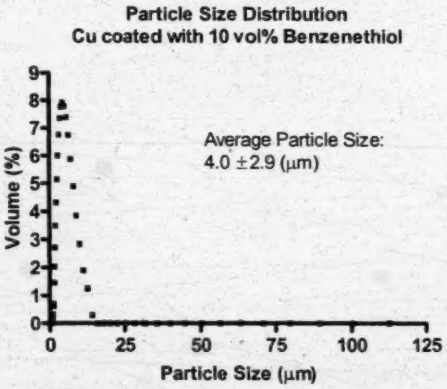

Figure A.24 Particle size distribution for copper-10 vol% benzenethiol

A.4 Copper coated with Polyacrylic acid

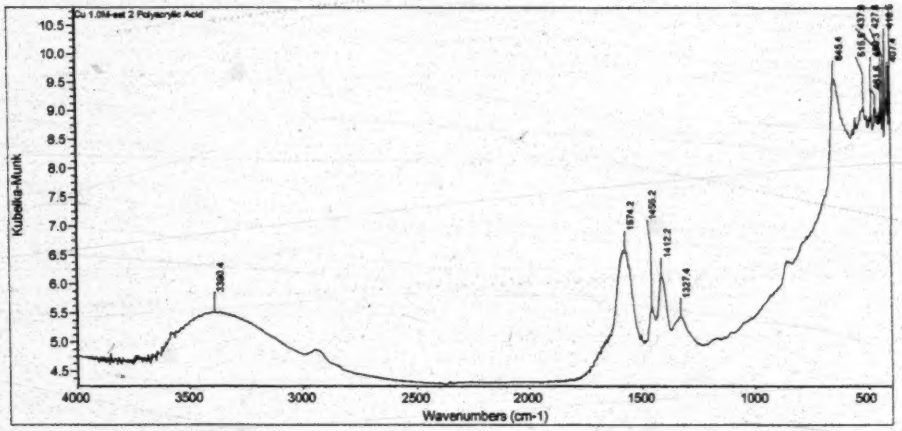

Figure A.25 IR spectrum of copper coated with 1.0 M polyacrylic acid

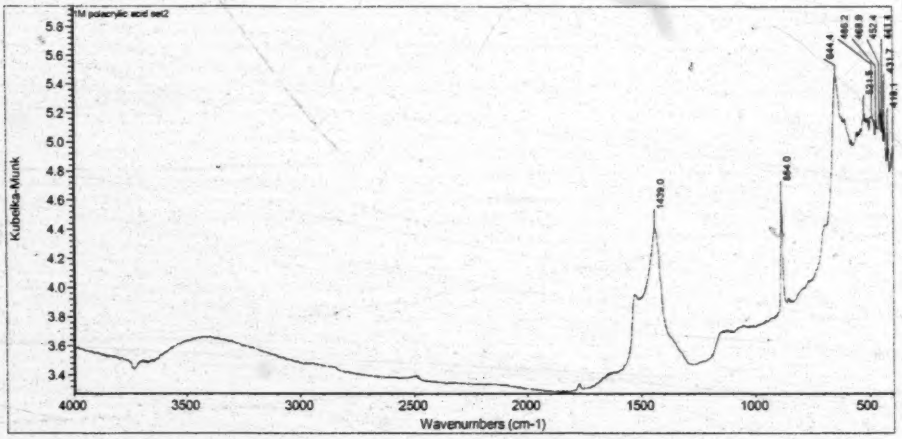

Figure A.26 IR spectrum of copper coated with 1.0 M polyacrylic acid after TGA analysis

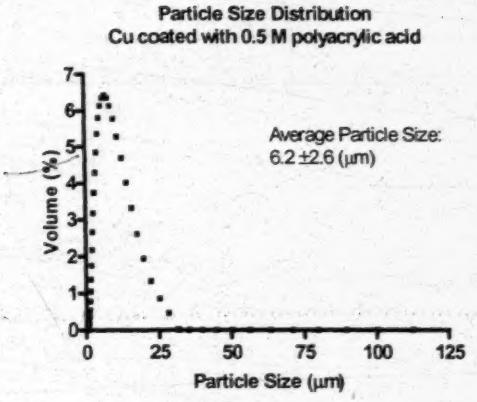

Figure A.27 Particle size distribution for copper coated with 0.5M polyacrylic acid

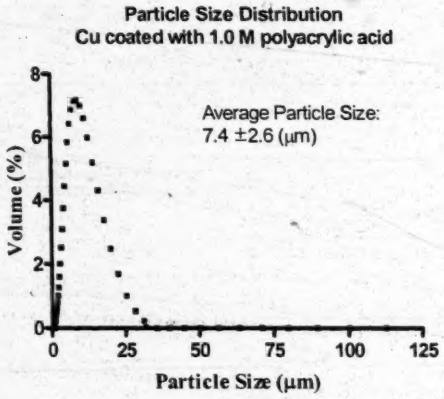

Figure A.28 Particle size distribution for copper coated with 1M polyacrylic acid

A.5 Preliminary Future Work

A.5.1 Nickel Standards

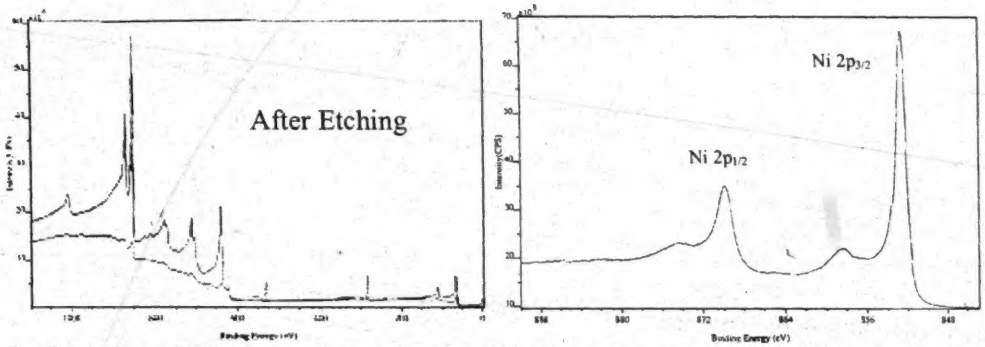

Figure A.29 a Survey Scan for Ni^0 and A.29 b Narrow Scan for Ni^0

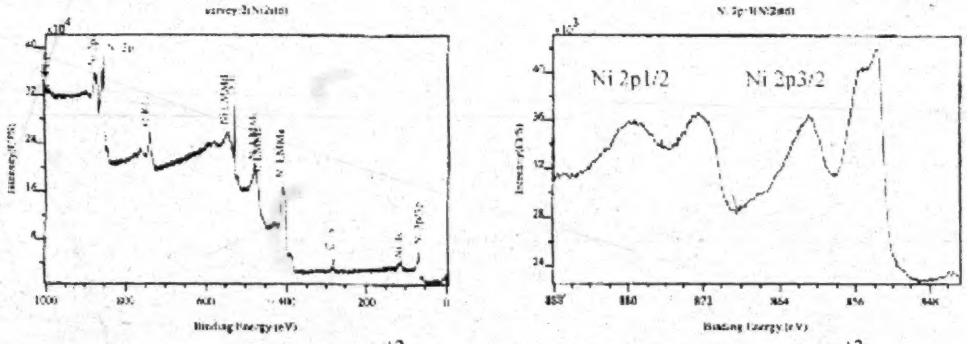

Figure A.30.a Survey Scan for Ni^{+2} and Figure A.30.b Narrow scan of Ni^{+2}

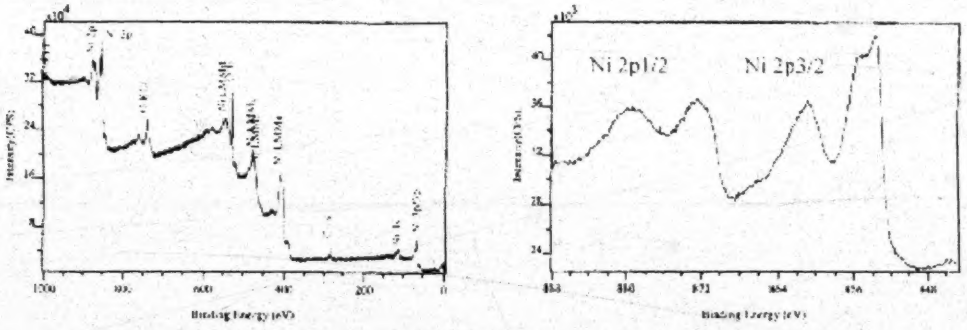

Figure A.31.a Survey Scan for Ni Black (contains Ni^{+3}) and Figure A.31.b Narrow scan of Ni Black (contains Ni^{+3})

Table A.1 Summary of spectral features obtained by XPS (Nickel process samples)

	Element / Transition	Binding Energy (eV)	FWHM (ev)
Ni LOT #2005-01-20-1	Ni 2p3/2'	854.2 (855.3)	2.66
2/2/2005	Ni 2p3/2"	855.8 (856.9)	3.07
After Drying	Ni 2p3/2"'	859.8 (860.9)	2.72
	Ni 2p3/2""	861.8 (862.9)	3.38
	Ni 2p1/2'	871.6(872.6)	2.41
	Ni 2p1/2"	873.4 (874.4)	2.77
	Ni 2p1/2"'	876.7 (877.8)	2.80
	Ni 2p1/2""	879.2 (880.3)	2.85
Ni LOT #2005-01-20-2	Ni 2p3/2'	852.48 (853.57)	3.50
2/2/2005	Ni 2p3/2"	855.12 (856.21)	3.42
After Washing	Ni 2p3/2"'	859.4 (860.49)	3.29
	Ni 2p3/2""	861.63 (862.72)	3.30
	Ni 2p1/2'	871.34 (872.43)	2.29
	Ni 2p1/2"	873.29 (874.38)	3.00
	Ni 2p1/2"'	877.52 (878.61)	2.99
	Ni 2p1/2""	880.11 (881.2)	3.06
Ni LOT #2005-01-20-3	Ni 2p3/2'	852.4 (853.6)	3.47
2/2/2005	Ni 2p3/2"	855.1 (856.3)	3.57
After Classification	Ni 2p3/2"'	859.9 (861.1)	3.20
Medium Fraction	Ni 2p3/2""	862.3 (863.5)	3.18
	Ni 2p1/2'	871.8 (873.0)	3.32
	Ni 2p1/2"	873.2 (874.4)	3.15
	Ni 2p1/2"'	877.6 (878.8)	3.26
	Ni 2p1/2""	880.2 (881.4)	3.21
Ni LOT #2005-01-20-4	Ni 2p3/2'	853.8 (855.3)	1.90
2/2/2005	Ni 2p3/2"	855.1 (856.6)	1.85
After Classification	Ni 2p3/2"'	859.2 (860.7)	2.01
Medium Fraction	Ni 2p3/2""	860.9 (862.4)	2.05
	Ni 2p1/2'	871.4 (872.9)	1.90
	Ni 2p1/2"	872.8 (874.3)	1.85
	Ni 2p1/2"'	876.9 (878.0)	1.93
	Ni 2p1/2""	879.0 (880.5)	1.95
Ni LOT #2005-01-20-5	Ni 2p3/2'	853.6 (855.1)	2.29
2/3/2005	Ni 2p3/2"	855.1 (856.5)	2.21
After Classification	Ni 2p3/2"'	857.6 (859.0)	1.90
Fine Fraction	Ni 2p3/2""	860.0 (861.5)	2.20
	Ni 2p1/2'	871.5 (872.9)	2.06
	Ni 2p1/2"	873.4 (874.8)	2.41
	Ni 2p1/2"'	876.7(878.2)	2.30
	Ni 2p1/2""	879.4 (880.9)	2.50
Ni LOT #2005-01-20-6	Ni 2p3/2'	853.9 (855.5)	2.01
2/3/2005	Ni 2p3/2"	855.2 (856.9)	2.23
Coarse Fraction	Ni 2p3/2"'	859.4 (861.1)	2.32
	Ni 2p3/2""	861.3 (862.9)	2.22
	Ni 2p1/2'	871.9 (873.5)	2.41
	Ni 2p1/2"	874.4 (876.1)	2.60
	Ni 2p1/2"'	877.6 (879.2)	2.42
	Ni 2p1/2""	879.7 (881.3)	2.50
Ni LOT #2005-01-20-7	Ni 2p3/2'	854.1 (855.5)	2.09
2/3/2005	Ni 2p3/2"	855.7 (857.1)	2.15
After Reaction	Ni 2p3/2"'	859.3 (860.6)	2.08
	Ni 2p3/2""	861.4 (862.7)	2.10
	Ni 2p1/2'	871.9 (873.2)	2.51
	Ni 2p1/2"	873.9 (875.3)	2.60
	Ni 2p1/2"'	877.4 (878.7)	2.58
	Ni 2p1/2""	880.1 (881.5)	2.50

Table A.2 Composition of the nickel samples in various stages in the production process

Nickel Samples	C 1s	O 1s	Ni 2p
After reaction	30.0	35.7	34.3
After washing	36.7	34.5	28.8
After drying	22.3	45.2	32.5
After classification - fine fraction	32.9	38.8	28.3
Coarse fraction	29.6	43.2	27.3
After classification (FC1) medium fraction	21.3	41.9	37.2
After classification (FC2) medium fraction	36.4	42.5	21.1